Theoretical Study of van der Waals Complexes at Surface Sites in Comparison with the Experiment

J. Sauer,*,† P. Ugliengo,‡ E. Garrone,‡ and V. R. Saunders§

Max-Planck-Gesellschaft, Arbeitsgruppe Quantenchemie an der Humboldt-Universität, Jägerstrasse 10/11, D-10117 Berlin, Germany, Dipartimento di Chimica Inorganica, Chimica Fisica e Chimica dei Materiali, Università di Torino, via P. Giuria 7, I-10125 Torino, Italy, and SERC, Daresbury Laboratory, Daresbury, Warrington WA4 4AD, Cheshire

Received February 18, 1994 (Revised Manuscript Received July 31, 1994)

Contents

I. Introduction 2095
II. Experimental Techniques 2098
A. Introduction 2098
B. Calorimetry and Adsorption Isotherms 2099
C. Infrared Data 2099
1. General Aspects 2099
2. Stretching Mode of Adsorbed CO 2100
3. Terminal and Bridging Surface Silanol Groups, SiOH and SiO(H)Al 2101
D. NMR Techniques 2102
III. Theoretical Methods 2102
A. Introduction 2102
B. Methods for Computing Intermolecular Interactions 2103
1. General Requirements and Basis Set Superposition Error 2103
2. Hartree–Fock plus Electron Correlation 2104
3. Density Functional Theory 2105
C. Computational Approaches to Adsorption 2106
1. Periodic Treatment 2106
2. Finite Clusters of Atoms 2107
3. Embedding Techniques 2108
4. Merits and Limits of Each Approach 2109
D. Cluster Approach 2110
1. Ionic Solids 2110
2. Metals 2111
3. Covalent Solids 2112
4. Thermodynamic Functions within the Rigid Cluster Model 2113
IV. Interaction of Molecules with Surfaces of Ionic Materials 2113
A. MgO—A Case Study 2113
B. Other Oxides 2118
C. Periodic Calculations Using the CRYSTAL Code 2120
D. Perturbed Cluster Method in Weak Adsorption 2120
V. Interaction of Molecules with Metal Cations in Zeolites 2121
VI. Interaction of Molecules with Amorphous Silica Surfaces 2122
A. Introduction 2122
B. Surface Species with Adsorbate 2124
1. Models for Isolated Silanol Groups 2124
2. Models for Geminal Species 2126
3. Models for Interacting Silanol Groups 2126
C. Interaction with H-Acceptor/H-Donor Molecules 2126
1. Interaction with NH_3 2126
2. Interaction with H_2O 2128
3. Interaction with CH_3OH 2130
D. Interaction with H-Acceptor Molecules 2131
1. Molecules with Free Lone Pairs 2131
2. Molecules with σ and π Bonds 2132
E. Validation of Cluster Models 2132
1. General Comments 2132
2. Comparison of Different Cluster Models 2133
3. Comparison between Data Calculated for Models and Observed for Real Surfaces: H-Bond Formation and Acidity 2134
VII. Interaction of Molecules with Surface Hydroxyls in Zeolites, SiO(H)Al 2136
A. Introduction 2136
B. Surface Hydroxyls without Adsorbate 2136
C. Interaction with H-Acceptor/H-Donor Molecules 2139
1. Interaction with NH_3 2139
2. Vibrational Spectra and Potential Surfaces of Adsorbed H_2O and CH_3OH 2143
3. CH Stretch Bands of Adsorbed Methanol 2145
4. Heats of Adsorption for H_2O, CH_3OH, and NH_3 2146
D. Interaction with Hydrocarbons and CO 2146
E. Effects of Including an External Crystal Potential in Cluster Calculations on Silica and Zeolites 2148
VIII. Summary and Conclusions 2149
IX. Acknowledgments 2153
X. Abbreviations 2153
XI. Basis Sets Description 2154

I. Introduction

This issue collects reviews on van der Waals (vdW) molecules. Our classification of the adsorption of molecules on different types of surfaces follows that for vdW systems in the gas phase[1,2] because it is based on the nature of the interaction instead of the magnitude of the interaction energy and the same types of interaction are responsible for both phenomena. A correspondence exists between vdW gas-phase molecules and vdW interactions with surfaces for which Figure 1 shows a few examples. As with vdW molecules, the stabilization energies observed

† Arbeitsgruppe Quantenchemie an der Humboldt-Universität.
‡ Università di Torino.
§ Daresbury Laboratory.

0009-2665/94/0794-2095$14.00/0

Joachim Sauer (born in 1949) graduated from the Department of Chemistry of the Humboldt University in Berlin and received the Dr. rer. nat. degree (equivalent to Ph.D.) in 1974. He joined the Central Institute of Physical Chemistry of the (former) Academy of Sciences in Berlin in 1977, receiving the Dr. sc. nat. degree from the Academy in 1985. He worked as a postdoctoral fellow with Professor R. Zahradnik at the Heyrovsky Institute in Prague, Czechoslovakia, and Professor R. Ahlrichs at the University of Karlsruhe. He was awarded the Friedrich Wöhler Prize of the Chemical Society of the (former) GDR and, in 1991, the Chemistry Award of the Academy of Sciences at Göttingen. He was deputy technical director of the catalysis and sorption project of BIOSYM Technologies, Inc. in San Diego, CA, from October 1990 until his appointment as head of the Quantum Chemistry Group at the Humboldt University in Berlin by the Max Planck Society in 1992. He also holds the position of a Professor of Physical and Theoretical Chemistry at this university. Dr. Sauer's research has explored the application of quantum chemical methods in chemistry, with emphasis on intermolecular interactions and surface science, particularly adsorption and catalysis. He has published more than 100 research papers, notably in the area of modeling the structure and reactivity of zeolites.

Piero Uglieugo was born in Cuneo, Italy, in 1957. In 1981 he obtained his degree (Laurea) in chemistry from the University of Torino. In 1983 he entered the University of Torino as a researcher, and since 1992 he has been working there as an Associate Professor of Structural Chemistry. He spent short periods working with Dr. V. R. Saunders at the Daresbury Laboratory (U.K.) doing theoretical calculations on surface/adsorbate systems. His main scientific interest is on modeling H-bond interactions between molecules and active sites at the surface of silica and zeolites by means of *ab-initio* techniques. He is also involved in the structural determination of H-bonded molecular crystals and in the development of a molecular graphics program.

Edoardo Garroue was born in Torino, Italy, in 1942. He received his degree (Laurea) from the University of Torino in 1966 and has worked since then in the same University, where he is an Associate Professor of Physical Chemistry. He spent one year (1977) with Professor F. S. Stone in Bath working on the surface chemistry of MgO. His interests have always been in the field of surface phenomena and cover different aspects ranging from physisorption over chemisorption to surface reactivity. The solids concerned have always been oxides of catalytic interest, acting as models for proper catalysts (amorphous silica, magnesium oxide, silica supported Cr ions). His activity is both in the field of experiment (mainly classical spectroscopies and thermodynamics) and of calculus (*ab-initio* computations of cluster models for surface sites).

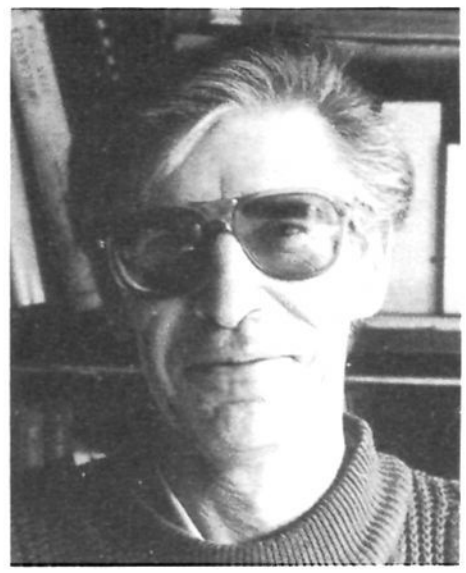

Victor R. Saunders was born in Birkenhead, U.K., in 1943. In 1969 he obtained his Ph.D. at the University of Sussex. He then spent three years working as a Postdoctoral Fellow at the University of Manchester with Dr. I. H. Hillier, and in 1972 he became senior scientific officer at the Rutherford Laboratory. In 1977 he entered the Daresbury Laboratory, where he is presently the head of the computational science group. His research interests span a wide range, always in the field of computational and theoretical chemistry. He developed highly sophisticated computational codes for calculating well-correlated molecular wave functions. He made substantial theoretical contributions to the efficient evaluation of molecular integrals for Gaussian basis functions, as well as to the implementation of a full CI computer code on vector and parallel computers. His current research interest is on the application of Hartree–Fock theory to the calculation of the electronic structure and properties of periodic systems. In this respect, he is actively involved in the development of the CRYSTAL computer code as a joint project with the theoretical chemistry group of the University of Torino.

for different types of systems cover a broad range, from 1 to more than 100 kJ/mol. We are dealing here with the whole range. The real weak and nonspecific interactions among them are traditionally named "physisorption". Typical cases of intermediate strength are H-bonded complexes with surface hydroxyl groups and ion–molecule complexes with surface ions of ionic crystals. In the limiting case of strong H-bonds, a proton may be transferred onto a base molecule. Although this is an elementary chemical step, the surface ion pairs so formed are also stabilized by vdW forces and, therefore, are within the scope of this review. We exclude phenomena connected with the making of covalent bonds between the surface and the ad-species such as the reaction

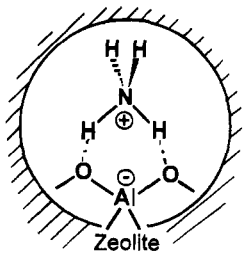

$[(CH_3)_3 NH^+ J^-]^b$

$(NH_4^+X^-)(NH_3)_n$

80 ± 20 calcd.[a]
100 - 150 obsd.[a]

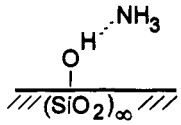

$HF - NH_3$

55 calcd.[e]

$(H_2O)_2$

28 calcd.[c]
25 - 37 obsd.[d]

24 calcd.[f]
23 ± 3 obsd.[f]

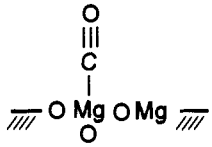

$Mg^{2+} - CO$

23 calcd.[g]
13 - 22 obsd.[g]

150 calcd.[g]

$H_2O - H_2O - H_2O$

Cu

~ 34 obsd.[h]

$H_2O - Cu$

20 - 34 calcd.[j]

$|(\Delta E_{Cu-H_2O}| < |\Delta E_{H_2O-H_2O}|$[c]

$H_2O - Ni$

12 - 45; 20 calcd.[j,k]

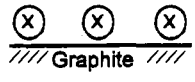

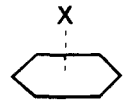

X = He 1.2 obsd.[l]
X = Kr 12 obsd.[l]

X = Ne 1.8 calcd.[m]
X = Ar 6.6 calcd.[m]

Figure 1. Correspondence between different types of van der Waals (vdW) interactions on surfaces and in the gas phase. The numbers are typical binding energies in kJ/mol. Key: a, see Table 26, the binding energy refers to the *neutral* separated systems, *i.e.* NH_3 and the bridging hydroxyl site in zeolites. b, ref 5. c, see Table 10. d, see Table 12. e, ref 6. f, see Table 1. g, see Table 6. h, ref 7. i, ref 4. j, ref 8. k, ref 9. l, ref 3. m, ref 10.

of H or F atoms with the dangling bonds of a silicon surface and reserve for them the traditional term "chemisorption".

Since specific vdW interactions are connected with characteristic changes of the properties of both the surface sites and the ad-molecule, spectroscopic techniques can be used to identify vdW complexes and to monitor their formation. As far as the distribution of surface sites is concerned, two types may be distinguished: irregularly distributed sites which, at low concentration, may become isolated (e.g. surface hydroxyls at outgassed amorphous silica) and regular arrays of sites (e.g. the Mg^{2+} ions at the (100) surface of MgO). Within the quantum mechanical treatment a small cluster of atoms can be used to deal with isolated irregularly distributed sites, while periodic *ab initio* methods, when feasible, are the choice for studying regular arrays of active sites.

We share the presumption that the idea of (surface) site–ad-atom or ad-molecule complexes is a good first approximation for many adsorption phenomena, even when calculating periodic adsorption potentials for rare gases and small nonpolar molecules on rather homogenous surfaces such as graphite. Such classical physisorption systems have been recently reviewed in this journal by Steele[3] and are not within our scope.

Of course, molecules adsorbed on isolated specific sites can also extend interactions with neighboring sites and "feel" the potential of large parts of the solid. The extent to which this is the case depends on the shape of the surface. A special case are zeolites which have micropores of molecular dimension. Quantum chemical *ab-initio* calculations of realistically shaped surfaces with many surface sites are still not feasible. However, use can be made of the results obtained by computations of the interaction of ad-molecules with individual surface sites to set up site–site potentials which describe the interaction of the ad-molecule with the whole solid. Site–site potentials can also be parametrized on the basis of observed data. Neither approach is discussed here, although we stress that such potentials are needed in molecular dynamics and Monte Carlo simulations of adsorption systems or in theoretical studies of the scattering of atoms on surfaces.

Adsorption depends not only on the forces between ad-molecules and the surface but also on the forces between the ad-molecules themselves. When the number of molecules adsorbed per surface area increases, lateral interactions start to play a role. The formation of a regular monomolecular layer will only be observed if the lateral molecule–molecule interactions are less attractive then the interaction between the molecules and the surface. For example, on defect-free Cu surfaces, H_2O molecules form a monomolecular layer, while clustering (aggregates of multimolecular layers) is observed on surfaces with defects. Note that this self-aggregation takes place also if the coverage is well below that corresponding to a monomolecular layer (see, *e.g.* ref 4). Even in such a difficult case some understanding of the observed phenomena may be achieved by combining theoretical information on the binding energy between a single transition metal atom and a H_2O molecule and on that of a H_2O dimer. The interaction of molecules on metal surfaces is frequently in the vdW realm but is not covered comprehensively in this article, in which only a brief account of the methodology is given.

We focus on *adsorption on surface sites of oxidic systems* for which a wealth of both experimental and quantum chemical *ab-initio* results has become available in recent years. After a survey of experimental techniques, most of which have been available for a

long time (section II), we consider in detail the cluster and periodic approaches to theoretical studies of surface complexes (sections III.C–D). A short account of the theoretical methods suitable for treating intermolecular interactions is given in section III.B, which deals with both conventional *ab-initio* and the rapidly spreading density functional methods. Separate sections are devoted to the interaction of molecules with ions on oxidic surfaces (IV), with silanol groups on silica surfaces (VI), and with acidic hydroxyl groups in zeolites (VII). Cationic sites in zeolites (section V) have not been studied to the same extent.

The interactions discussed in this review are of fundamental interest with respect to separation (chromatography, microporous materials), catalysis (formation of vdW molecules frequently precedes the reactive step), and molecular recognition (shape selective catalysis in micropores, separation in controlled silica mesopores). Interactions between molecules and oxidic surfaces also play a role in colloid chemistry, material science, and nanotechnology.

II. Experimental Techniques

A. Introduction

Surface vdW complexes may be compared, on the one hand, with adducts in the gas phase, and, on the other hand, with species trapped in inert matrices at low temperature. There are, however, marked differences as far as the experimental techniques available in the different fields and the related observable quantities are concerned. Gas-phase molecular complexes are studied by means of sophisticated techniques developed recently, such as the Fourier transform microwave spectroscopy,[13] which basically yield information on the *type of structure* and *some details of it* and, to a lesser extent, on the internal motions of the complex. No means is however available for determining the energy of formation of the complex or related data. Similarly, the most important spectroscopic feature of H-bonded complexes, the frequency shift of the donor group, is not accessible. For both matrix-isolated species and surface complexes, classical spectroscopic techniques are widely used, in particular the vibrational ones. Information is gained on the *structure type* of adducts but not on surface details such as intermolecular distances.

The gas–solid interaction (adsorption) is studied in all types of spectroscopic techniques, and the list of related acronyms lengthens every day (see ref 14 for an excellent description of modern techniques in surface science). The vast majority of them, however, deal with either ordering in adsorbed layers (like low-energy electron diffraction, LEED) or chemisorbed species. Spectroscopies based on electronic transitions like X-ray and ultraviolet photoelectron spectroscopies (XPS and UPS, respectively) have been recently applied by Klekamp *et al.*[15] to investigate the kinetic and electronic properties of SF_6, XE, and CO_2 on ultrathin epitaxial NaCl(100) films on Ge(100). Henzler *et al.*[16] have used UPS and electron energy loss spectroscopy (EELS) to characterize the adsorption of water vapor on epitaxial thin films of NaCl and KCl on Ge(100). They showed that on perfect NaCl surfaces, H_2O forms a well-ordered 2D-phase with a superstructure.

Freund *et al.*[17] have used angle-resolved ultraviolet photoelectron spectroscopy (ARUPS), high-resolution electron-energy-loss spectroscopy (HREELS), and near-edge X-ray-adsorption fine structure (NEXAFS) to characterize the bonding of NO, CO, and H_2O on clean and modified surfaces of NiO, Cr_2O_3, and Al_2O_3. Very recently, by means of polarization-dependent surface-extended X-ray-adsorption fine structure (SEXAFS), Pangher *et al.*[18] were able to show that water adsorbs on Ni(100) via the O atom in atop sites with a nearest-neighbor O–Ni bond length of 2.06 ± 0.03 Å. Corresponding NEXAFS data suggest that the HOH plane is tilted to the surface normal. That work is very important, because it is the first *structural analysis* of water adsorbed on a metal surface. Jacobi[19] has studied the adsorption of D_2O, NO, CH_3OH, C_6H_6, and Xe on low-index surfaces of ZnO by means of ARUPS, LEED, and thermal desorption (TDS). For the benzene molecule, an ordered monolayer of a complicated orientational order was reported.

In connection with UV–vis spectroscopy, it is known that the HOMO (highest occupied molecular orbital)–LUMO (lowest unoccupied molecular orbital) transition in a molecule is strongly affected by the solvation. Some of us[20] have recently observed a similar effect on solids, *e.g.* the $\pi \rightarrow \pi^*$ transition of acetone falls at lower frequencies on MgO or hydrotalcite than in the free molecule. Moreover, the values observed for the two solids are slightly different because of the different surface fields. NMR spectroscopy is most useful for chemisorption studies, but its use in the field of vdW interactions is just beginning. Electron spin resonance has been used only in one case to study the low-temperature adsorption of NO on MgO.[21] The isolated NO molecule is paramagnetic and yields an ESR spectrum when adsorbed, the dimer N_2O_2, stable at low temperatures, does not, and as a consequence, it has been possible to measure the equilibrium constant by following the intensity of the ESR signal. The vast majority of data comes from the classical vibrational spectroscopies. The Raman technique, however, has so far proved rather useless in surface studies, probably because of the overwhelming presence of diffuse scattering. The only field of success is surface-enhanced Raman spectroscopy (SERS), but this is limited to studies of pyridine (or daughter molecules) on silver. This means that infrared spectroscopy (IR) dominates the field. Tunnel-effect microscopy may become important to the study of vdW complexes in the future. This technique even allowed the observation of single physisorbed atoms on metals,[22] or of arrays of them. At the moment, however, applications in the field of vdW adsorption are less relevant with respect to the above techniques. One of the reasons is the difficulty in assigning the measured signals to a specific surface species.

In spite of the paucity of detailed structural data, there are, however, definite advantages when studying adsorption. First, it is rather easy to carry out direct calorimetric measurements and, therefore, to

measure the energy of interaction. Moreover, adsorption leading to vdW surface complexes is an equilibrium phenomenon. The related thermodynamic functions may be measured in principle very simply by determining the adsorption isotherm,

$$\theta = \theta(p)$$

where θ is the surface coverage and p the gas pressure. More complex schemes apply when a reactive step is involved, as, for example, in the case of proton transfer.

The ease of carrying out spectroscopic, calorimetric, and thermodynamic measurements basically depends on the specific surface area of the sample. This is large (sometimes very large) with powders or microporous solids such as zeolites. Unfortunately, such types of solids often exhibit different sites for adsorption (*intrinsic* or *structural heterogeneity*), and the results may be blurred by the coexistence of concurrent processes. Spectroscopic and thermodynamic measurements are much more difficult on well-defined samples such as monocrystals, the surface of which is only a few cm^2. Powders prepared in the form of nearly perfect microcrystals of, for example, NiO, MgO, or α-Cr_2O_3, as shown by high-resolution electron microscopy,[23] represent an interesting compromise. They offer the double advantage of high surface area and well-defined surface structures.

In the following, energetic, IR, and NMR data are reviewed separately. We note, however, that the joint use of different types of data proved very helpful in many studies. References 24–27 are examples of a combination of IR and energetic data.

B. Calorimetry and Adsorption Isotherms

Adsorption calorimetry on high-area samples is a well-established technique, in particular after the flow microcalorimeters of the Calvet type became available. Good reviews describe[28,29] how data are obtained and processed. Usually a dose-by-dose procedure is assumed, but continuous-flow techniques have also been developed.[30] Both yield the differential heat of adsorption $\Delta_a H$ as a function of coverage, the latter in a direct manner. Most Calvet calorimeters operate at room temperature or higher, where too weakly bound adsorbates are not observed. This sets a lower limit on the range of interactions which can be measured, for example, around 20 kJ/mol for CO. Recently low-temperature Calvet-type calorimeters have become commercially available that may work, for example, at 77 K. They are therefore apt for studying weak interactions, but only limited data have been published.[30]

The heat of adsorption, $\Delta_a H$, usually decreases with the coverage because of phenomena such as structural heterogeneity or repulsive interactions among adsorbates. An example for a seldom observed increase is the phase transition in the layer of N_2 molecules adsorbed on graphite.[30] A detailed exploitation of $\Delta_a H$ data is, however, only possible in simple cases. In ideal systems, where a single species is present without mutual interactions, the value of $\Delta_a H$ is constant with coverage. Moreover, the isotherm has a Langmuir shape,

$$\theta = p/(p + p_{1/2})$$

where $p_{1/2}$ is the gas pressure corresponding to half coverage. IR evidence must support the model by showing one species, the features of which are independent of the coverage.[25] Such requirements are rather strict, and really ideal systems are seldom encountered. When this is the case, a full thermodynamic characterization is possible, because $p_{1/2}$ is related to $\Delta_a G°$, the standard change of the Gibbs free energy, and, consequently, $\Delta_a S°$, the corresponding entropy change, is also readily evaluated:

$$p_{1/2} = \exp(\Delta_a G°/RT) = \exp(\Delta_a H°/RT)\exp(-\Delta_a S°/R)$$

This has been done, for example, for CO adsorbed on a few oxidic systems.[25]

When two species are present, even in nearly ideal systems, e.g. in the adsorption of CO on aluminas, the $\Delta_a H$ values are not fully meaningful *per se*: only the joint use of IR and calorimetry allows for characterization of the system thoroughly.[26]

With nonideal systems, $\Delta_a H$ values are most meaningful in the limit of vanishing coverage (Henry region), where ideal behavior is a consequence of the low adsorbate concentration (low coverage). Under the same conditions, it is also possible to measure the *equilibrium constant* for surface reactions. For instance, two of us[31] have recently determined such values for the interaction of a family of hydrocarbon molecules M with the isolated hydroxyl group on amorphous silica

$$\text{Si–OH} + \text{M} \rightleftharpoons \text{Si–OH}\cdots\text{M}$$

in the Henry region by simply monitoring the equilibrium pressure and the intensity of the vibration of the free hydroxyl group.

On samples with small surface area (monocrystals), direct calorimetry is not possible, and the (isosteric) heat of adsorption, q_a, is determined *via* the old Clausius–Clapeyron relationship

$$(\mathrm{d}(\ln p)/\mathrm{d}T)_\theta = q_a/RT^2$$

applied to a set of isotherms measured at slightly different temperatures. However, very recently a device has been constructed which determines the heats of adsorption on monocrystals by measuring the energy released upon adsorption as radiation.[32] Though brilliant, such an instrument is not yet sensitive enough to be used for weak interactions.

C. Infrared Data

1. General Aspects

When dealing with high surface area samples, it is rather easy to carry out IR measurements using widely available instruments. Their last generation makes use of the Fourier transform (FT) of the signal, which allows very satisfactory spectral resolutions and requires only short scanning times (down to 0.1

s). This opens the possibility of time-resolved spectroscopic measurements. For example, when the interaction of acetylenes with the acidic hydroxyl groups in H-ZSM5 zeolites was followed,[33] it was possible to observe first the formation of the H-bonded complexes and then to see how they were converted into protonated species (cf. section VII.D). The propensity for this conversion increased from acetylene to 1-butyne. The spectra of the H-bonded species were accurate enough to allow the measurement of all parameters of interest (shift of the stretching modes of the O−H, C≡C, ≡C−H bonds, etc.). The spectra were taken in this case at room temperature in a standard cell. Similar experiments were recently carried out by the same group to study the interaction of ethene and propene with H-ZSM5 zeolite.[34] For ethene, a value of 38 kJ/mol for the heat of adsorption in zeolite-Y (where no proton transfer from the zeolite to the molecule takes place) has been reported in the past.[35] For weak interactions, low-temperature cells are available, usually operating at a nominal temperature of 77 K. Variable-temperature cells have also been constructed,[36] which work down to the He boiling point. For monocrystals, more sophisticated techniques such as attenuated total reflection (ATR) or electron energy loss spectroscopy (EELS) are used, which yield, however, the same type of information. For particularly opaque samples, such as charcoals, an appropriate version of vibrational spectroscopy is the photoacoustic one.

Polarized high-resolution FTIR spectra were recorded by Heidberg *et al.*[37] to study the collective vibrations and ordering of CO, CO_2, H_2, CH_4, and H_2O on NaCl(100) and MgO(100) surfaces, prepared by cleaving the crystal *in situ* under ultrahigh-vacuum conditions (UHV). For the CO_2/MgO(100) system, spot profile analyses of low-energy electron diffraction (SPA-LEED) were also carried out. Orientational phase transitions were detected as well as dynamic processes due to resonant desorption by selective vibrational excitation of the adsorbate.

Elegant experiments were carried out recently by Ewing[38] dealing with the IR spectroscopy of ordered molecular adlayers of CO_2 on the (100) face of a clean NaCl crystal. The richness and sharpness of the bands has been interpreted by exciton theory, which can also reveal the temperature dependency of the geometry of the adlayer as well as the size of the formed domains.

Upon formation of vdW surface complexes, six degrees of freedom (three translational and three rotational) of the adsorbate are transformed into intermolecular modes, which fall in the far infrared (FIR) region and are difficult to observe. In a few cases, information on intermolecular modes is available, e.g. concerning water on silica.[39] This is unfortunate because undoubtedly such modes are most sensitive to the nature of the interaction. In the case of the rather strong adsorption of CO on metals,[40] the metal−carbon stretching mode is observed. In contrast, no direct observation of such modes has ever been made on oxidic systems: a weak combination band of the fundamental CO stretch with a librational mode of CO has been observed sometimes.[41] The situation is probably about to change because intense sources of radiation in the far infrared are becoming available.[42]

The observables are thus the changes in the vibrational features of (i) the surface or solid, if occurring, and (ii) the adsorbate molecule. As an example of the latter, the stretching frequency of adsorbed CO will be considered in the next section. The surface field may also reduce the symmetry of the adsorbed molecule, so that IR modes inactive in the free molecule may become active in the adsorbed one. Examples are the ν_1 mode of CO_2 adsorbed linearly on Lewis sites and the ν_1 mode of methane interacting with Na^+ cations in zeolite cavities.[43] Another example is the activation in IR of the C≡C and C=C symmetrical stretching modes of acetylene and ethene adsorbed on H-ZSM5.[33,34] Examples for case (i) are the changes in the vibrational modes of an acidic hydroxyl engaged in an H-bond (see section VII), the perturbation of surface vibrational states in highly ionic systems such as LiF induced by CO adsorption,[44] and the adsorption induced changes of the skeletal vibrations of cationic zeolites.[45]

2. Stretching Mode of Adsorbed CO

In the case of weak interactions, the CO molecule is bound to a surface site mainly by electrostatic and dispersive interactions. This invariably means that the frequency of the fundamental transition, ν_{CO}, is *higher* than that of the free molecule (2143 cm^{-1}). A value of ν_{CO} lower than that of the free gas-phase molecule is usually observed when a proper bond is established. This implies donation of electronic charge from the 5σ orbital of the CO molecule and back-donation of electronic charge from d orbitals of a metal atom to the π^* orbital, as is usual with transition-metal carbonyls or CO adsorbed on metallic surfaces. In a few cases, frequencies lower than the gas-phase value have been observed with oxidic systems and have been interpreted as due to CO molecules interacting with both ends with surface cations in a suitable arrangement.[46,47] For CO adsorption in the absence of back-donation, relationships have been suggested between ν_{CO} and the heat of adsorption alone.[24,48] as well as between ν_{CO} and both the heat of adsorption and the presumed electrostatic field at the adsorption site.[49]

Though with modern FTIR instruments it is easy to measure the first overtone, $\nu_{2,CO}$, no data have been published yet. Preliminary observations made in Torino, concerning *e.g.* CO on α-alumina, indicate that the frequency value is not less than twice that of the fundamental transition ν_{CO}. This implies a *decrease in anharmonicity* of the CO stretch in the adsorbed state, which is probably worthy of being studied.

Two methods of measuring the intensity of the stretching mode of adsorbed CO are possible. One uses the molar extinction coefficient ϵ, the other the *vibrational polarizability* α_v. Both quantities are related to $(\partial\mu/\partial Q)^2$, the square of the change of the dipole moment of the adsorbed molecule due to change of the normal coordinate Q, in this case the elongation of the C−O bond. The relation between the two quantities is

$$\epsilon = 4\pi^3\alpha_v\nu^2$$

in which ν is the frequency of the band center.[50] The measurement of ϵ is simple in principle, as it is based on the well-known Beer–Lambert law. Nevertheless, few reliable data are available because such measurements require the determination of both the absorbance of the sample carrying the adsorbate with respect to the bare one and the amount adsorbed. This is done simultaneously only exceptionally.[36] It is more common to do separate experiments, which can lead to errors, e.g. because the temperatures may be different in the two experiments. Pioneering data by Angell and Schaeffer[51] indicate that ϵ first decreases with ν_{CO}, then increases, and could even vanish in between. These results, though largely quoted in the literature, probably have to be considered with caution, as more recent work, *e.g.* on CO adsorbed on various titania phases,[24] suggests a moderate, monotonic increase of ϵ with ν_{CO}. It is possible that relatively strong interactions, characterized by large values of ν_{CO} (e.g. 2240 cm^{-1}) may cause a further decrease in ϵ.[36]

Instead, vibrational polarizability, α_v, may be measured through an entirely spectroscopic method for a regular array of sites. In such a case, the frequency ν_{CO} corresponds to a collective oscillation, and two mechanisms, static and dynamic interactions, determine its value. The dynamic contribution to the shift with respect to free CO is given by

$$\Delta\nu/\nu = (\alpha_v T)/(1 + \alpha_e/T)$$

where α_e is the electronic polarizability and T is a Madelung-like sum over the lattice of the inverse third powers of distances from a given site. On well-defined surfaces of oxides in microcrystalline form, CO adsorbs in regular arrays,[23] which are dictated by the exposed planes. Use of $^{12}CO/^{13}CO$ isotopic mixtures allows the determination of the dynamic shift, which in turn allows the calculation of α_v through the above formula. Results[20,23] are in agreement with those from the measurement of ϵ and confirm a moderate increase of $(\partial\mu/\partial Q)^2$ with increasing stretching frequency.

3. Terminal and Bridging Surface Silanol Groups, SiOH and SiO(H)Al

Two examples of surface hydroxyls with acidic properties have been extensively studied and may serve to illustrate the type of information on intermolecular interactions gained by IR techniques. One is the isolated hydroxyl group on the surface of amorphous silica, hereafter denoted SiOH (see Figure 5). It is moderately acidic and forms H-bonds with basic molecules, but it does not take part in proton-transfer reactions. To neutralize this group, extremely strong bases are required, such as NaOH. Accordingly, its pK_a is evaluated to be around 7.[52] The other species is the bridging OH group in zeolites, hereafter denoted SiO(H)Al, which is a strong acid (see Figure 14). As a consequence, it forms H-bonds even with very weakly basic molecules, and a variety of proton-transfer reactions are observed. Its ability to protonate even hydrocarbons is the key to the use of protonic zeolites as acidic catalysts. In both isolated and bridging surface hydroxyl groups, the proton gives rise to three vibrational modes: (i) OH valence stretch, ν_{OH}, (ii) SiOH in-plane deformation, δ_{SiOH}, and (iii) SiOH out-of-plane deformation, γ_{SiOH}. Only the OH stretching mode is easily observed. It occurs at 3744 cm^{-1} and in the region of 3520 and 3630 cm^{-1} for the SiOH and SiO(H)Al groups, respectively. Actually, Kazansky and co-workers have studied several overtones and found that in both cases a Morse potential profile accounts for the spacings among energy levels and that anharmonicity is small and nearly equal in the two cases.[53] The in-plane and out-of-plane bending modes occur for SiOH at 760 cm^{-1} (ref 54) and around 100 cm^{-1}, respectively, and for the SiO(H)Al sites at about 1100 and 400 cm^{-1}, respectively. They are hidden by framework vibrations and can only be observed as combination modes with the OH stretching mode in the near infrared region.[55–57] For instance, the combination mode of the out-of-plane bending of the SiOH group with the O–H stretching appears as a weak satellite band at 3850 cm^{-1}.[36] A selective means for studying vibrations involving motions of a proton is inelastic neutron scattering (INS).[57–59] Note that the out-of-plane bending mode is a hindered torsion of the proton about the Si–O axes in the SiOH group and becomes a true out-of-plane bending in the SiO(H)Al group. Consequently the frequency of this mode is much higher for the SiO(H)Al group than for the SiOH group. In the case of the interaction with CO, the frequency of the SiOH torsional transition assumes a value of 380 cm^{-1}.[60]

The vast literature on H-bonding in solution shows that, when an acidic hydroxyl group characterized by a bending, a torsion, and a stretching mode undergoes interaction, all three bands shift: the bending and the torsion mode to higher frequencies and the stretching mode to lower values.[61] In the case of surface species, the fate of the former two bands is not of much interest because they are difficult to observe. The red shift of the stretching mode is instead readily measured and constitutes one of the best studied topics in IR spectroscopy.[62] One reason is that it may be considered a measure of the acidity of the hydroxyl itself. Other features typical of the IR spectra of H-bonded hydroxyl species are the broadening of the O–H stretch and the increase of its intensity with respect to the unperturbed species. The three features are interrelated, in that the larger the $\Delta\nu_{OH}$, the broader and the more intense the band.

Two features have emerged in more recent work. Kazansky and co-workers[53] have shown, by measuring sets of overtones, that the anharmonicity of the O–H motion increases upon coordination. An alternative means for measuring the anharmonicity is the comparison between the shifts for a hydroxyl species and its deuterated counterpart, caused by H-bonding with the same molecule. In the interaction of CO with SiOH/SiOD and SiO(H)Al/SiO(D)Al species, respectively, it is found that the weak interaction with the silica hydroxyl does not change the anharmonicity of its OH stretch, while the stronger inter-

action with the more acidic zeolite species increases the anharmonicity.[31]

Actually the value of $\Delta\nu_{OH}$ is rather temperature dependent. The reason is the coupling of the pure O−H stretch mode with the low-frequency, strongly anharmonic intermolecular modes, which also explains the broadness of related bands. For example, in the comparatively strong interaction of ammonia with SiOH, a value of *ca.* -650 cm^{-1} is measured for $\Delta\nu_{OH}$ at room temperature,[35,63-67] which becomes -950 cm^{-1} at 4 K.[68] The latter two points (role of anharmonicity and temperature dependence) are rather crucial when comparing calculations on a model system with experiment because frequencies are usually computed within the harmonic approximation and correspond to absolute zero temperature.

It is appropriate to recall that, for extremely strong H-bonds such as those occurring in acidic solid phosphates, the ν_{OH} band is structured into more than one component, very often three (A, B, C bands). Such a behavior originates from the overlap of the ν_{OH} band, particularly broad and shifted to lower frequencies, and overtones, *e.g.* of the bending mode, also particularly shifted, but to higher frequencies. A Fermi resonance between the two types of modes causes intensity transfer and the appearance of pseudo-bands.[69,70] Even in such cases, however, it is possible to determine the hypothetical location of the ν_{OH} band. Recently, interpretation of the IR spectra observed on adsorption of H_2O, CH_3OH, and other proton acceptor molecules on SiO(H)Al sites in terms of such an A−B−C triplet has been suggested (cf. section VII.C.2).[70-72]

Classical work has shown that, in the interaction of an acid AH and a base B, the $\Delta\nu_{OH}$ value may be factorized as the product of two factors, one depending on AH, the other on B. As a consequence, if one considers the interaction of two acidic species A_1H and A_2H with a family of base molecules, plots of the $\Delta\nu_{OH}$ values for the two sets of data yield a straight line. This is called a Bellamy−Hallam−William (BHW) plot.[61] The slope is a measure of the relative acidity of A_1H and A_2H: this is a powerful method for measuring relative acidities of hydroxyls in an entirely spectroscopic way (see also section VI.E.3).

The literature on H-bonding interaction of surface hydroxyls up to 1976 has been reviewed by H. Knözinger.[62] No other extensive review has appeared, though the field has been continuously investigated. Correlations have been proposed, on the one hand, between $\Delta\nu_{OH}$ and the heat of adsorption and, on the other hand, between $\Delta\nu_{OH}$ and some other measure of acidity of the hydroxyl species.[62] Curthoys *et al.*[73] have proposed a linear relationship between $(\Delta\nu_{OH})^{1/2}$ and the heat of adsorption.

Both the pK_a of the hydroxyl species[74] and its gas-phase acidity (GPA)[75] have been proposed as independent parameters which measure the OH acidity. Note that the pK_a of surface hydroxyls can be measured directly (by titration) in a few cases, e.g. the SiOH species at the silica surface. Obviously, the GPA for surface species cannot be measured at all, but it can be calculated for the corresponding cluster models. The procedure by which both pK_a and GPA values for surface OH species are estimated is the following. Sets of data measured in solution for the interaction A−H···B of acidic hydroxyls with basic molecules plotted according to BHW yield slopes which are interpreted on the basis of the pK_a or GPA of the acid A−H and the corresponding values of the conjugated acid B−H$^+$. The same interpretation is then applied to BHW data concerning surface species, which allows the determination of pK_a or GPA (see also section VI.E.3). The use of GPA has become popular,[76] and the procedure is now used to calculate the GPA of surface hydroxyl species.

D. NMR Techniques

Since magic angle spinning (MAS) made high-resolution NMR techniques available for analyzing solids, these techniques have been spectacularly succesful for structure determination of adsorbents and catalysts and also proved useful for the identification of surface species and for monitoring adsorption phenomena. Reviews are available for NMR studies of simple molecules on metal surfaces[77] and on silica and zeolite surfaces.[78,79] Of course, vdW interactions will not change in a significant way the chemical shift of the nuclei. Nevertheless, species which form vdW complexes with surface sites may show a characteristic shift pattern. An example is the ^{13}C shifts of the allyl cation discussed in section VII.D. Typical probe species are the ^{129}Xe atom[80,81] and the CO (^{13}C) and N_2O (^{15}N) molecules.[79] The latter has been used to identify Lewis acidic sites in zeolites by a stronger ^{15}N NMR shift than that observed for vdW complexes with Brønsted sites or for an unspecific interaction with the zeolite.[82] The use of pyridine as a probe molecule has been reviewed by Pfeifer.[79] Due to its size, it can strongly interact only with Brønsted sites which are sterically easily accessible. At such sites it forms pyridinium cations, which are easily detected by ^1H-MAS NMR spectroscopy. ^{15}N-MAS NMR of pyridine has been used to study its adsorption on alumina, silica-alumina, and zeolite surfaces.

The formation of H-bonded complexes on surface hydroxyl groups and the possible transformation of protonated species such as NH_4^+, H_3O^+, and $CH_3OH_2^+$ has been studied by ^1H-MAS NMR spectroscopy (see section VII.C). Due to rapid exchange, only an average signal is observed for all protons involved, which complicates the interpretation of the results.[83]

III. Theoretical Methods

A. Introduction

In quantum mechanical studies of the interaction of molecules with surfaces, the following problems arise: (i) The infinite surface can not be directly treated by quantum mechanical techniques. A way has to be found to reduce the system to a tractable size. (ii) A quantum chemical level of approximation has to be selected that yields a reliable description of intermolecular interactions. (iii) The quantum chemical data obtained need proper corrections in order to relate them to observed quantities. For example, the zero point energy (ZPE) correction and the partition functions have to be evaluated before

the calculated interaction energy can be related to thermodynamic functions of adsorption.

Computational limitations require finding a good balance between optimum solutions for problems (i) and (ii), i.e. between the size of the system and the level of computation. The possibilities of dealing with the surface problem are considered in section III.C, while a special section, III.D, is devoted to the cluster approach which is presently the most widely used. The methodological aspects of calculating intermolecular interactions have been repeatedly reviewed[1,2,84,85] and only those with particular relevance to adsorption problems are discussed in section III.B. In connection with item (iii) above, we only mention briefly the so-called "rigid cluster model" [86,87] at the end of section III.D. In general the standard procedures as described, for example, in ref 88 are used. Throughout this review we also use the standard nomenclature of the quantum chemical techniques[88] with minor but obvious modifications, e.g.

MP2//SCF/DZP

describes an energy calculation within the second-order Møller–Plesset perturbation theory (MP2) approximation at the Hartree–Fock (SCF) equilibrium geometry. In both cases the basis set was a double-ζ polarization (DZP) set.

B. Methods for Computing Intermolecular Interactions

1. General Requirements and Basis Set Superposition Error

The interaction energy between an ad-molecule M and a surface site S within a surface complex, M–S, is obtained by calculating the total energies of the three systems involved and taking the difference according to

$$\Delta E = E(\mathrm{M{-}S//M{-}S}) - E(\mathrm{M//M}) - E(\mathrm{S//S})$$

The double slant denotes that all energies are evaluated at the respective equilibrium geometries. This scheme is sometimes called the "supermolecule approach". When adsorption layers are treated by periodic methods, more specific definitions apply, which are given in section III.C. By definition, the interaction energy is negative for attractive interactions. Sometimes the term "binding energy" will be used, which is defined as the negative interaction energy.

The basis sets commonly used to calculate the energies in the above equation are far from being saturated and, hence, in any complex (gas phase or surface) each subsystem will tend to use the basis functions of the other subsystem to lower its energy. This gives nonphysical, stabilizing contributions to the energy of the complex, E(M–S), and may also lead to artificial charge transfer if the basis set description of the subsystems is unbalanced. Hence, there is an error of the interaction energy which is connected with the superposition of the orbitals of the subsystems. The stability of the results with respect to this basis set superposition error (BSSE) can be checked by the so-called function counterpoise (CP) method.[89] To the basis sets of each subsystem are added all basis functions of the other subsystem without its electrons and nuclei (ghost functions). The energies obtained at the equilibrium geometry of the complex for each subsystem, e.g. E(M{S}//M–S), are lower than the energies calculated at the same geometry with the basis functions of the respective subsystem alone, e.g. E(M//M–S), and the difference is defined as the BSSE:

$$\epsilon(\mathrm{M}) = E(\mathrm{M//M{-}S}) - E(\mathrm{M\{S\}//M{-}S})$$

$$\epsilon(\mathrm{S}) = E(\mathrm{S//M{-}S}) - E(\mathrm{S\{M\}//M{-}S})$$

The BSSE values ϵ(M) and ϵ(S) are used to define a counterpoise corrected (CPC) interaction energy,

$$\Delta E^{\mathrm{c}} = \Delta E + \epsilon(\mathrm{M}) + \epsilon(\mathrm{S})$$

which, by comparison with perturbation theory, has been shown to converge to the BSSE free correct value.[90] The BSSE values should always be calculated as a check of the quality and balance of the basis set. This is important not only for vdW interactions between the ad-molecules and the surface but also for the description of ionic materials themselves. If the size and the quality of the chosen basis sets do not take into account the different requirements for cations and anions, the electrons on the anions may tend to use the basis functions available on the cations to improve their energy. As far as the possibilities to eliminate the BSSE are concerned, their is a long lasting debate in the scientific community (see refs 1, 2, 84, 85, and 90 for the original reference). Some people demand that the basis set should be improved until the CP values indicate that the BSSE is sufficiently small. Other people claim that CP-corrected values are the best approximation to the correct interaction energy. This view gets support from the observation that the ΔE^{c} values are less basis set dependent than the uncorrected ones, provided that the BSSE is within tolerable limits and there are no major errors in the description of the charge distribution. There is a third group of people who suggest alternative schemes for removing the BSSE. It is argued that only part of the CPC values should be used for corrections because in the real complex not all of the ghost functions would be available. For example, in a recent paper it is claimed that the full CPC correction is justified at the SCF level but that it overcorrects at the MP2 level (where the CPC values are much larger than at the SCF level).[91]

In the limit of large intermolecular distances, interaction energies can be approximated by perturbation theory[84,92] and a Taylor series expansion of the intermolecular distance can be made.[93,94] This shows that the interaction energy depends on the electric moments and the polarizability of the subsystems. For example, a good description of the polarizability is needed to account for dispersive interactions.

Hence, the requirements of quantum chemical methods in order to get reliable results for intermolecular interactions are well understood (cf. refs 1, 2, 84, and 85) and can be summarized as follows: control over the BSSE and proper description of the

electric moments and the polarizability of the subsystems.

2. Hartree–Fock plus Electron Correlation

For ion–molecule or H-bonded complexes, the lowest level of approximation fulfilling the above requirements are SCF calculations using split-valence or double-ζ basis sets with polarization functions (SVP or DZP). A special but widely used example is the 6-31G* basis sets from the Pople group which use polarization functions on the non-hydrogen atoms only. Inclusion of dynamical electron correlation is mandatory if the dispersion energy is significant for the problem studied, but it also improves the description of the Hartree–Fock electric moments and polarizabilities. The simplest method, MP2, is sufficient unless very accurate results are aimed at. Note that basis set requirements are higher than for SCF calculations, but already for basis sets of DZP or similar quality the results can be improved by a special choice of the orbital exponents for the polarization functions and by adding diffuse s,p functions.[1,85] For really weak interactions such as those found in rare gas dimers or rare gas–benzene complexes, dispersion forces are the largest fraction of the binding, so that very large basis sets are necessary to reach convergence.[10] Note also that usually the BSSE is substantially larger at the correlated level than at the SCF level, e.g. about 30% instead of 10% of the total binding energy (see refs 1 and 85 for the original references, ref 91 and Table 1 provide specific examples).

Changes in the vibrational spectra on complex formation can only be reliably predicted when both intermolecular forces and intramolecular frequencies are reliable. While sound values of interaction energies can be obtained using either observed or theoretical equilibrium geometries of the partner molecules, the prediction of frequency shifts on complex formation—as do all frequency calculations—requires first determination of the equilibrium structures at the respective computational level. Normally, frequency calculations start from the harmonic approximation. Intramolecular harmonic frequencies obtained at the SCF/DZP level are known to be too large due to neglect of electron correlation and basis set dependence. As the deviations from accurate frequencies have been found to be systematic, the concept of the scaled force field has been suggested and frequently used with success.[95,96] The idea is to multiply the computed harmonic force constants using a small set of scale factors which are transferable among different molecules and have values slightly smaller than one. The MP2 approximation yields accurate harmonic frequencies provided that sufficiently large basis sets are used.[97]

As observed frequencies are affected by anharmonicities which are large for X–H bonds, accurate predictions have to account for these effects. Anharmonicity corrections can be obtained (i) from perturbation theory, (ii) from variational calculations which expand the vibrational wavefunctions in a basis set, e.g. of harmonic oscillator functions, or (iii) from numerical solution of the Schrödinger equation. The latter two approaches are limited to a few degrees of freedom (two to three, exceptionally four). For molecules with as many degrees of freedom as models of adsorption systems may have, full anharmonic treatments have not come to our attention so far. Fortunately, the OH stretching mode of surface hydroxyl groups is well separated from all other modes, and a solution of the one-dimensional problem by numerical integration is possible (see, e.g. refs 98 and 99). Sometimes, a crude, but very efficient procedure is used which scales selected or all calculated harmonic frequencies by a common factor which is around 0.9 for SCF/6-31G* and SCF/DZP calculations (cf. ref 88). This multiplier is derived from a comparison of computed wavenumbers with a sufficiently large set of *observed* wavenumbers. Therefore, it efficiently accounts both for neglected anharmonicity effects and systematic erros of the quantum chemical method.

Table 1. Performance of Different Methods for Water and Its Dimer Complex[a]

	monomer		dimer		
method	μ	R_{OH}	ΔR_{OH}	$R_{O\cdots O}$	$-\Delta E^b$
obsd[c]	1.86[c]	95.7[c]		298 ± 1[d]	22.8 ± 2.9[c]
MP4/[5s,3p,2d,1f/3s,2p]		96.2	0.56	291	23.7 (19.3)
MP2/[5s,3p,2d,1f/3s,2p]	2.03	96.0	0.71	290	24.0 (19.6)
MP2/DZP[e]	2.12	96.7	0.64	292	25.4 (19.3)
SCF/DZP[e]	2.14	94.8	0.45	300	20.6 (18.2)
SCF/MINI-1[f]	2.10	101.1	0.6	288	28.1 (20.1)
SCF/3-21G	2.39	96.7	0.6	280	45.9 (28.0)
DFT-VWN (local)	2.03	97.8	1.9	271	38.3 (36.6)
DFT-PERDEW (nonlocal)	1.94	98.0	1.0	288	25.1 (23.4)
DFT-BP (nonlocal)	2.00	97.8	1.2	289	18.9 (17.4)

[a] SCF and MPi results from ref 196. DFT results from Ref 118. Dipole moment, μ, in D, bond distances and their changes, R and ΔR, in pm, and interaction energies, ΔE, in kJ/mol. [b] Values CP corrected for BSSE in parentheses. [c] See ref 118 for the original references to observed data. [d] References 197. [e] Double-zeta plus polarization basis set on all atoms except on oxygen for which a valence triple-zeta basis set is used. [f] Reference 101.

In conclusion, major computational errors can only be avoided if at least split-valence basis sets with polarization functions are used and—when dispersion dominates—MP2 calculations are performed using specifically designed or large basis sets (cf. the review by Hobza et al. in this issue). Of course the above statements are only true for systems for which a one-determinant description is appropriate. Otherwise, a multireference treatment should be used.

This is not the place for an exhaustive coverage of the relevant original literature which is provided by other contributions to this issue and which has been provided previously.[1,2,84,85,95] The data on the H_2O dimer in Tables 1–3 and on the CO and SiH_3OH molecules in Tables 4 and 5 are given merely as an illustration.

In view of computational limitations, the level of approximation necessary to properly describe intermolecular interactions in adsorption studies is frequently in conflict with the need for a periodic treatment of the solid or for large cluster models. Hence, many researchers could not resist the temptation to use the small 3-21G basis set, which is known to provide sound molecular structures and, after applying a uniform scale factor of about 0.9, to yield reasonable vibrational frequencies at low com-

Table 2. Wavenumbers (cm^{-1}) of the Intermolecular Vibrational Modes of the Water Dimer Obtained with Different Methods[a]

mode	obsd[b]	DFT-BP grad corr	DFT-VWN local	MP4/ [5,3,2,1/3,2]	MP2/ [5,3,2,1/3,2]	MP2/ TZ(O)DZP[c]	SCF/ TZ(O)DZP[c]	SCF/ MINI1[d]	SCF/ 3-21G
A″ HOH twist (A)/H wag	520	663	785	641	649	646	593	683	832
A′ HOH twist (A and D)	320	393	464	367	368	365	323	403	491
A′ O···O stretch	243	205	271	190	190	179	162	261	245
A″ HOH rock (A and D)		159	174	157	142	132	138	217	204
A′ HOH twist (A and D)	155	154	163	160	155	158	143	197	203
A″ HOH twist (A and D)		137	151	149	136	145	131	109	152

[a] DFT-type results from ref 118 and MPi and SCF results from ref 196. [b] See ref 118 for the reference to the original paper and for the assignment. [c] Double-ζ plus polarization basis set on all atoms except on oxygen for which a valence triple-ζ basis set is used. [d] Results from ref 101.

Table 3.[a] Observed[b-e] and Calculated OH Frequency Shifts (cm^{-1}) in the Water Dimer

method	H_2O $(\nu_s + \nu_{as})/2$	$(H_2O)_2$ ν_{OH}	$\Delta\nu_{OH}$
N_2 matrix, 11 K[b]	3681[b]	3550[b]	−131[b]
gas phase[d,e]	3706[d]	3600[d]	−106
		(3545)[e]	(−161)
	normal modes (GF)		
	harmonic		
MP4/[5s,3p,2d,1f/3s,2p]	3861	3740	−121
MP2/[5s,3p,2d,1f/3s,2p]	3903	3749	−154
MP2/TZ(O)DZP	3907	3772	−135
SCF/TZ(O)DZP	4154	4057	−97
SCF/TZ(O)DZP-scaled (0.9)	(3739)	(3651)	(−88)
SCF/MINI-1[g]	4012[g]	3843[g]	−169[g]
SCF/3-21G	3879	3728	−151
SCF/3-21G-scaled(0.954)[f]	(3700)	(3556)	(−144)
DFT-VWN (local)	3757	3394	−363
DFT-PERDEW (grad corr)	3703	3498	−205
DFT-BP (grad corr)	3733	3496	−237

[a] SCF and MPi results from ref 196 DFT results from ref 118. [b] Reference 198. [c] Reference 199. [d] Reference 200, reassignment of the spectra of ref 201. [e] Reference 201. [f] Special scale factor for OH bonds, ref 202. [g] Reference 101.

Table 4. Predictions for the CO Molecule by Different Methods: Equilibrium Bond Distance, R_{CO}, in pm, Harmonic Vibrational Frequency, ν^0_{CO}, in cm^{-1}, and Dipole Moment, μ, in D[a]

method	R_{CO}	ν^0_{CO}	μ[b]
obsd	113	2170	−0.11
MP2/TZ2P	114	2123	−0.26
MP2/6-31G*	115	2125	−0.19
SCF/6-31G*	111	2440	0.26
SCF/3-21G	113	2312	0.39
DFT-BP/TZ2P	113	2188	−0.20
DFT-VWN/6-31G*	114	2169	−0.19

[a] Results from ref 203. [b] The negative sign means the direction $^-CO^+$.

putational cost. However, the 3-21G basis set violates all of the above criteria for intermolecular interactions as exemplified in Table 1 for the H_2O dimer. It heavily overestimates the binding energy due to a large BSSE and a too large dipole moment of water. Moreover, it is unable to describe the dipole polarizability to any extent. Using this basis set in MP2 calculations will only increase the BSSE. Hence, the use of the 3-21G basis set in MP2 calculations (see, for example, ref 100) should be avoided. This is, of course, also true for any basis set not containing polarization functions. There are, however, other small basis sets which are suited for studying the structure and energetics of intermolecular complexes

Table 5. Predictions for the Silanol Molecule by Different Methods: Energy of Deprotonation, ΔE_{DP} (kJ/mol), Harmonic Vibrational Frequencies, ν^0_{OH} (cm^{-1}), and Selected Bond Lengths and Angles (pm, degree)

method	ΔE_{DP}	ν^0_{OH}	R_{OH}	R_{SiO}	∠SiOH	ref
CPF/[8s,5p,3d,1f/4s,2p][a]	1531		95.8	165	117.7	204
MP2[5s,3p,2d,1f/3s,2p]		3916	95.9	165	117.6	196
MP2/DZ(2d,p)	1543	3960	96.0	166	117.3	205
MP2/TZ(O)DZP[b]	1550	3870	96.6	167	116.9	196
SCF/TZ(O)DZP[b]	1576	4176	94.6	165	120.5	206
SCF/3-21G	1637	3995	96.0	168	126.9	202
DFT-BH/DNP+[c]	1482	3780 ± 20	97.0	166	116.7	205

[a] Coupled pair functional calculations. [b] Double-ζ plus polarization basis set on all atoms except oxygen for which a valence triple-ζ set has been used. [c] DFT calculation with numerical basis set (Dmol code).

at the SCF level only. An example is the MINI-1 basis set[101,102] which was designed to yield a small BSSE and which also gives dipole moments and vibrational frequencies[101-103] almost as good as the 6-31G* basis set. Examples will be given in the following sections. However, as expected for a low cost method, there are also limitations: bond distances are too long.

3. Density Functional Theory

Only recently could methods based on density functional theory (DFT)[104-106] be considered for describing interactions of molecules with surfaces. While these methods emerged from solid state physics and always played a role in describing bulk solids and surfaces, encouraging results for molecules have been reported only after exchange and correlation functionals including gradient corrections have been set up, and efficient and numerically stable codes are being developed. The analytical evaluation of derivatives of the energy with respect to displacements of the nuclei is also an important aspect of the recent developments. Moreover, in addition to the developments on existing DFT codes, these techniques have been implemented in widespread *ab initio* codes such as GAUSSIAN 92,[107] CADPACK,[108] and TURBOMOLE.[109] We will use the acronym LDA to refer to the local density approximation in general, while we use DFT-VWN and DFT-BH to refer to the particular Vosko–Wilk–Nusair[110] and Barth–Hedin[111] (local) functionals, respectively. Reference is made to the gradient corrected density functionals in the same way, e.g. DFT-BP for the Becke and Perdew corrections to the exchange[112] and correlation energy,[113] respectively.

The use of the DFT-type methods as a practical tool in molecular energetics and dynamics was reviewed some years ago in this journal by Ziegler.[114] When he compared the dissociation energies observed for the first metal–carbonyl bond in the $Ni(CO)_4$, $Mo(CO)_6$, $Cr(CO)_6$, and $W(CO)_6$ molecules (104, 126, 162, 166 kJ/mol) with the results of LDF calculations, he found that the results obtained with local functionals are almost twice as large (192, 226, 276, 249 kJ/mol), while those obtained with gradient corrections are in reasonable agreement with the experiment. This is in agreement with the results of Sosa et al.[115] who reached a similar conclusion for metal–carbonyl complexes. Substantial overbinding has also been reported for DFT studies of adsorption of CO on the Cu(100) surface (for both slab and cluster in the order of magnitude of 100%)[116] and on various sites including impurities on MgO surfaces.[117] The results for the CO molecule itself, which is an important probe molecule, cf. section II.C.2, do not differ much between DFT calculations without and with gradient corrections. Table 4 shows the equilibrium distance, the harmonic vibrational frequency, and the dipole moment for the CO molecule. The DFT-type methods almost exactly reproduce the experimental harmonic frequencies, and in this respect they appear superior to even MP2.

The H_2O dimer (Table 2) is the simplest H-bonded system which shows that gradient-corrected functionals are necessary to obtain reasonable values for intermolecular interaction energies. In addition, it has been noted that special care is necessary with numerical integrations which are used in DFT methods for evaluating the total energy.[118] Similar observations have been made for more strongly bonded complexes. While for the dative bond in $H_3B\cdots NH_3$ the local density approximation (DFT-BH/DNP) yields a binding energy as high as 197 kJ/mol, the result with gradient corrections (DFT-B-LYP/DNP), 115 kJ/mol,[119] is close to the best *ab initio* value (MP4/6-311++G(3df,2p)//MP3/6-31G*) of 119 kJ/mol.[120] In this study a numerical double-ζ basis set with polarization functions (DNP) was used.

As far as the *intermolecular* vibrational modes of the H_2O dimer (Table 2) and of the $H_3B\cdots NH_3$ adduct[119] are concerned, the DFT approach performs as well as the MP2 method, provided that gradient corrections are present. Table 2 shows for the H_2O dimer that the remaining deviation from the observed wavenumbers persists even when passing to the MP4(SDTQ) level and using an extended basis set consisting of [5s,3p,2d,1f/3s,2p] contracted functions on O/H. It seems that this deviation is due to anharmonicity effects which are not accounted for by the calculations. The local functional (DFT-VWN) and the SCF/3-21G approach yield too large frequencies in accord with the overbinding given by these methods.

A very important characteristic of the H-bond formation is the frequency shift of the stretch mode of the donor OH group. Due to the coupling between its two OH oscillators, this shift is more easily defined in the partially deuterated complex, $DOH\cdots OHD$, than in the all-hydrogen dimer. The data presented in Table 3 use the following definition of the shift

$$\Delta\nu_{OH} = (\nu_s + \nu_{as})/2 \text{ (free } H_2O) - \nu_{OH} \text{ (donor, } H_2O \text{ dimer)}$$

The DFT methods even with gradient-corrected functionals predict shifts that are almost twice as large as those observed (Table 3) and elongations of the OH bond also about twice as large as the accurate theoretical value, MP4/[5s,3p,2d,1f/3s,2p] (Table 1). That gradient-corrected DFT methods have a problem with the description of the potential curve for the OH bond is already seen for the free H_2O: the OH bond is 0.02 Å too long and the predicted *harmonic* frequency matches the observed *anharmonic* one which means that it is about 160 cm^{-1} too low. The intramolecular H-bond in malonaldehyde is another example for this feature of the DFT method.[118] It seems, however, that this weakness is peculiar to OH bonds and that, for example, NH and CH bonds are much better described. This is unfortunate because the hydroxyl group is an important and abundant surface species.

There are other types of interactions for which DFT-type methods have not been succesful so far. These include charge-transfer complexes such as the ethene–halogen molecule complexes[121] and really weak interactions dominated by the dispersion energy.

C. Computational Approaches to Adsorption

1. Periodic Treatment

Ideally, one would like to include the whole solid behind a well-defined crystal surface, then to add the layer of molecules adsorbed on the surface, and treat such a semiinfinite system with an *ab-initio* all-electron method inclusive of electron correlation. By means of well-defined quantum-mechanical methods, one would then calculate relevant quantities amenable to experiments, such as (i) the binding energies of the adsorbate at different coverages and on different crystal surfaces; (ii) IR and Raman spectra of the adsorbed molecules; and (iii) data about the structure of the adduct, which are not easily obtained by experiments.

The above procedure will probably remain a dream for several years to come, but enormous progress has been made with the treatment of perfect crystalline solids by means of a well-defined crystal orbital *ab-initio* Hartree–Fock approach, coded in the computer program CRYSTAL.[122–126] The program is the result of a joint project involving the laboratory of theoretical chemistry of Torino University and the computational group at Daresbury Laboratory.

CRYSTAL provides a self-consistent field solution to the Hartree–Fock–Roothaan equations subject to periodic boundary conditions. The method exploits the long-range order present in crystalline systems by formally incorporating the full symmetry of the corresponding space group into the theoretical scheme. This *a priori* avoids the approximations inherent to the cluster approach described in the other paragraphs. The quantum mechanical solution is obtained by means of a multistep process. It starts with an atomic orbital basis and evaluates the one- and two-electron integrals required to construct the Fock

matrix in direct space. This Fock matrix and its associated overlap matrix are then Fourier transformed into reciprocal space where they become block diagonal. The solutions of the corresponding matrix equations yield a set of eigenvalues and eigenvectors at points in the reciprocal space. These are then used to construct a new density matrix that will be Fourier transformed back into direct space and used to redefine a new Fock matrix. This cycle continues until the total energy converges to a specified tolerance threshold. The physical properties of the solid are then computed using the converged SCF wave function.

When dealing with adsorption problems, a surface is defined by selecting a slab of the crystal which consists of a number of layers large enough to ensure, for instance, convergence of the electric potential in the binding region. Similarly, adsorption of regular arrays of molecules can be studied by considering a bidimensional cell consisting of a portion of the surface plus a number of guest molecules. The content and shape of the selected cell depends on both the coverage and the geometrical features of surface sites one intends to simulate. Vanishing coverage is treated by considering very large surface unit cells, in which the interaction between the adsorbed molecules is progressively reduced (supercell approach).

A number of calculations are needed to compute the binding energy per unit cell per adsorbate molecule, each of them giving an energy value defined per unit cell as (i) E(slab/ads), the energy of a crystal slab plus the interacting periodic array of adsorbed molecules; (ii) E(slab), the energy of the clean crystal slab, (iii) E(ads), the energy of the periodic array of adsorbed molecules without the underneath solid surface, and (iv) E(mol), the energy of one isolated adsorbate molecule.

From these quantities we can calculate the binding energy per unit cell between the whole adsorbate layer and the surface as

$$\Delta E^{uc}(\text{slab/ads}) = E(\text{slab/ads}) - E(\text{slab}) - E(\text{ads})$$

We can also define the interaction energy per unit cell between the adsorbate molecules themselves, i.e. without any surface underneath, as

$$\Delta E_L(\text{ads}) = E(\text{ads}) - N \cdot E(\text{mol})$$

This definition assumes that the unit cell contains N molecules. ΔE_L(ads) is also known as *lateral interaction energy* and can be either positive (repulsion) or negative (attraction) depending on the nature of the molecules. In the limit of very low coverages, i.e. large distances between adsorbate molecules, ΔE_L(ads) will tend toward zero.

The observed energy of adsorption, ΔE_{exp}, corresponds to the process in which the molecules move from an ideal gas state onto the host surface, where they will stick due to favorable interactions,

$$\Delta E_{exp} = E(\text{slab/ads}) - E(\text{slab}) - N \cdot E(\text{mol})$$

Again, N molecules per unit cell are considered. If use of the previous formulas is made, a link between the computed ΔE^{uc} and the experimental one, ΔE_{exp}, can be established:

$$\Delta E_{exp} = \Delta E^{uc}(\text{slab/ads}) + \Delta E_L(\text{ads})$$

If a supercell methodology is adopted for low coverages it holds that

$$\Delta E_L(\text{ads}) \approx 0$$

so that

$$\Delta E_{exp} \approx \Delta E^{uc}(\text{slab/ads})$$

Almost all systems reported in section IV belong to the category in which lateral interactions are zero, but a few examples will be discussed in which this assumption is no longer justified.

BSSE estimates may be carried out following the recipes for molecular complexes, in which the electrons belonging either to the slab or to the adsorbate are omitted and the nuclear charges of the corresponding atoms are set to zero, leaving, however, the basis functions on these atoms unaltered.

A number of applications using the CRYSTAL code have already been published. The properties of thin slabs of a given crystal, which are models of bare crystallographic surfaces, have also been computed.

2. Finite Clusters of Atoms

A more straightforward and naive approach is to consider a limited number of atoms around the active site and apply the quantum-mechanical description to such a piece of the solid, referred to as a *cluster*. Of course, the crude procedure of cutting out the cluster from the solid inevitably creates spurious electronic states at the border of the cluster, which must be handled in some way to avoid artifacts in the subsequent calculation. Various strategies have been developed so far to cure this problem, which depend largely on the type of solid considered.

Ionic solids are characterized by electrons highly localized around nuclei, so that the cutting procedure is in principle less severe here than when applied to other systems. The long-range potential due to the infinite array of ions is considered the main source of errors in the cluster approach to ionic solids. It is clear that the error is smallest when the cluster of ions is neutral. Moreover, when designing clusters for adsorption studies, one should also make sure that the individual layers of ions are neutral since they are in the semiinfinite crystal. However, frequently clusters are used which build shells of ions around a central ion which represents the binding site, e.g. the $(MgO_5)^{8-}$ is used as a model for the 5-fold-coordinated Mg site on the MgO(001) surface (see section IV). It is hoped that the unrealistic electric properties of such clusters can be corrected by embedding them in an array of point charges (vide infra). Similar problems arise when the cluster method is adopted for partially covalent and partially ionic solids such as silica and zeolites and the bonds are cut heterolytically. Highly charged clusters are obtained which are, as such, useless for studying vdW interactions. Another problem of such clusters is that they do not have the stoichiometry of the bulk and

hence may have unrealistic acid–base properties. For example, due to its large number of oxygen anions the $(MgO_5)^{8-}$ cluster will be much more basic than the MgO(001) surface. Another example is the highly charged $H-Al(OSiO_3^{3-})_4$ model used in a study of the interaction of CH_3OH with the bridging hydroxyl site in zeolites.[127] This model turns out to behave as a strong base and not as a strong acid, which is the reason for the strange result that a proton was abstracted from the CH_3 group of the CH_3OH molecule instead of a protonation of CH_3OH (cf. section VII.C.). The strong electrostatic field artificially created will inevitably bias the delicate energetics of physisorption. The reader is referred to section VII for more details on possible drawbacks of using such charged clusters.

For solids with electron pairs localized in well-defined chemical bonds, the homolytic cut results in a cluster with dangling bonds containing unpaired electrons. The use of such high-spin-state clusters in chemisorption studies is not recommended, both because of problems in getting SCF convergence and of the undesirable coupling with the electronic states of the incoming adsorbate. The easiest and chemically best defined procedure for making a cluster neutral is to saturate the dangling bonds resulting from an homolytic cut, with monovalent atoms, normally hydrogen. By this procedure, the cluster becomes a molecule and the surface complex becomes a molecular complex. To calculate the various properties of such "molecular" models, standard and well-documented *ab-initio* packages for molecules such as HONDO,[128] CADPAC,[108] GAMESS,[129] TURBOMOLE,[109] or GAUSSIAN[107] may be used. Furthermore, electron correlation can be included in a straightforward way and geometry optimizations as well as frequency calculations can be carried out. The relevant intermolecular features of the surface complex are easily calculated within the supermolecule approach[1] (cf. section III.B).

3. Embedding Techniques

Embedding techniques at various levels have been suggested to close the gap between the cluster approach and the periodic treatment. They are considered not only because the cluster models need corrections for neglected interactions with their surroundings but also because they are a promising alternative to the use of supercells in periodic calculations. In this approach interactions between the adsorbate species may give undesired effects, unless the supercells become prohibitively large. Embedding techniques should also properly take into account the perturbation caused by the adsorbate on the electronic states of the underlaying infinite solid. These are the ideas behind the perturbed cluster approach which have been implemented into the EMBED code.[130–135] Mathematical details have been recently reported in the original literature, so only a qualitative description is given here. A cluster containing the active site is defined and the corresponding wave function is calculated in such a way that a smooth link is attained with the wave function of the surrounding crystal. Then a solution of the unperturbed crystal has to be obtained by the CRYSTAL code. An iterative procedure is carried out to match the two solutions in a self-consistent way.

When dealing with the adsorption of molecules on metal surfaces in a cluster approach, serious problems arise. The requisite of electron localization at atoms or in bonds, which allows for treatment of ionic or covalent materials in a well-defined way, is no longer valid for metals. For such systems an embedded cluster theory which does not require periodic solutions was proposed by Whitten in the early 1980s.[136,137] This method, which has been recently summarized,[138] divides the model of the metal/adsorbate system into an interior part (surface sites plus adsorbate) and an exterior part as the embedding medium. A localization transformation of the molecular orbitals of the whole model is used to define the electronic subspace of the interior part. Compared with other proposals, it has the advantage that both SCF and CI calculations of molecular quality may be performed on a portion of the lattice/adsorbate system in a straightforward way. We note, however, that the method required to perform an *ab-initio* calculation of the whole *embedding* part and computational benefits are only achieved when calculations of higher quality (better basis set, inclusion of electron correlation) are made for the *embedded* part.

A hybrid method is the basis of the ICECAP code.[139,140] It treats the region in which the adsorption takes place quantum-mechanically and embeds it in the infinite host crystal, which is described by a semiclassical model. Madelung plus polarization fields are taken into account, and polarization corrections are self-consistently included up to infinite distance. To our knowledge, ICECAP has been applied to the study of vacancies or impurities in ionic crystals, but not to calculations of vdW interactions on surfaces.

Many attempts have been made and are being made to improve the cluster model by including corrections for the external long-range potential, $V_{ext}(\mathbf{r})$, into the calculation (see, *e.g.*, ref 141). This leads to terms such as

$$F_{\mu\nu} = F^{0}_{\mu\nu} + \langle \mu(\mathbf{r}) | V_{ext}(\mathbf{r}) | \nu(\mathbf{r}) \rangle$$

in the Fock matrix elements $F_{\mu\nu}$. The fixed external potential V_{ext} may be defined according to Hermann[142] as represented by a superposition of contributions $V_i(\mathbf{r})$ centered at substrate atom sites $\mathbf{R}_i$,

$$V_{ext}(\mathbf{r}) = \sum_i V_i(\mathbf{r} - \mathbf{R}_i)$$

Each V_i is given by a multipolar expansion, envisaging multipole moments q_{LM} and spherical harmonics $Y_{LM}(\mathbf{r})$,

$$V_i(\mathbf{r}) = \sum_{LM} (q_{iLM}/r^{L+1}) Y_{LM}(\mathbf{r})$$

It is, however, very common to restrict the multipoles to point charges or, at most, to charges plus dipoles. From a computational point of view, the increase in computer time due to inclusion of the external potential in an SCF procedure is very modest, because only extra one-electron integrals are needed and virtually all quantum mechanical packages allow

for the addition of an array of charges in a straightforward way.

The different embedding schemes differ by the way the multipoles q_{iLM} are determined and the one-electron integrals $\langle\mu(\mathbf{r})|V_{ext}(\mathbf{r})|\nu(\mathbf{r})\rangle$ are evaluated.

(1) A CRYSTAL calculation of the substrate is performed and the nonexpanded electrostatic potential, $V^{crystal}(\mathbf{r})$, is derived from the periodic wave function in the region where adsorption takes place. A cluster model is chosen, adopting the same structure, and the molecular electrostatic potential, $V^{cluster}(\mathbf{r})$, is evaluated from the cluster wave function in the same region. (1a) The difference of the values of these two potentials is then least-square-fitted to the classical electrostatic potential of a finite number of point charges, located, e.g., at substrate ion positions (point ion cluster, PIC) outside the quantum mechanical cluster

$$V^{ext}(\mathbf{r}) = V^{crystal}(\mathbf{r}) - V^{cluster}(\mathbf{r}) = \sum_i^{PIC} q_i/(\mathbf{r} - \mathbf{R}_i)$$

The best fit is obtained by varying the values of the charges, keeping their location fixed. An example is the scheme of Greatbanks et al.[143] (1b) The charge density of the crystal and the cluster are partitioned according to a generalized Mulliken scheme which allows for expression of the electrostatic potentials of the crystal and the cluster, respectively, in terms of atomic multipole contributions. The external potential is obtained as the difference of the two potentials:

$$V^{ext}(\mathbf{r}) = \sum_i^{crystal} \sum_{LM} (q_{iLM}{}^{crystal}/r^{L+1}) Y_{LM}(\mathbf{r} - \mathbf{R}_i) - \sum_i^{cluster} \sum_{LM} (q_{iLM}{}^{cluster}/r^{L+1}) Y_{LM}(\mathbf{r} - \mathbf{R}_i)$$

i.e., no fitting is involved. However, to avoid numerical errors, the summation does not include the atoms of a well-defined inner zone of the cluster and the crystal (in which the adsorption takes place). It is assumed that the charge distributions of the cluster and the periodic crystal do not differ in this zone. Similarly, the correction term $\langle\mu(\mathbf{r})|V_{ext}(\mathbf{r})|\nu(\mathbf{r})\rangle$ is only added to the Fock matrix if both atomic orbitals, μ and ν, are centered on nuclei belonging to the inner zone. This scheme suggested by Teunissen et al.[144] offers a solution to two important problems: (i) It reduces the artificial polarization of the charge distribution by the external potential in the outer zone of the cluster where Pauli repulsion is not preventing such effects. (ii) It eliminates contributions to the calculated binding energy of the adsorbed species which are due to the terminating atoms introduced to saturate dangling bonds but are not present in the real crystal.

(2) Simpler schemes start from the Madelung potential for the bulk crystal using charges estimated from population analysis of cluster calculations or from chemical considerations. For example, full ion charges may be used for MgO, while half ionic charges may be chosen for partially ionic solids such as SiO_2. The value of the embedding charges may even be treated as free parameters in order to assess the sensitivity of the results to different Madelung potentials. There are two ways to include point charges into a Fock operator: (2a) as an Ewald sum, consisting of a direct space term (from which the charges of the cluster atoms should be subtracted) plus a reciprocal space term,[145] and (2b) as a finite number of point charges (PIC). The charge value and/or the positions of some of these charges may be adjusted to reproduce the exact Madelung potential. The former approach needs special one-electron integrals while the latter requires trival modifications of existing codes only. Scheme 2b has also been used to embed clusters with saturating atoms, but the choice of the PIC was not trival.[146] The saturating atoms themselves contribute to the potential felt by the interior atoms of the cluster and, to avoid exceedingly large polarization, embedding point ions should not be placed very close to the bordering atoms.

A number of problems arise when embedding a cluster in an external potential, in particular in a point ion potential. (i) No compensation for the interrupted charge transfer at the border is included, e.g. between Si^{4+} and O^{2-} ions in siliceous materials. (ii) At the periphery of the cluster, due to the absence of Pauli repulsion with the electrons of the surrounding, spurious and large charge polarization may result, unless special precautions are taken such as in scheme 1b above. Such polarization effects can spoil calculated adsorption energies. (iii) No geometry optimization is possible for those degrees of freedom which involve a quantum mechanically moiety and point charges. If this were done, collapse of the two parts would occur, because no Pauli repulsion between the two moieties exists. For such reasons, extreme care must be taken when the adsorption process is localized on atoms which are at the border of the cluster: the presence of unscreened nearby charges may introduce spurious attractions, particularly if the adsorption step involves incipient bond breaking.[127]

4. Merits and Limits of Each Approach

Of all the approaches described above, none is completely satisfactory. A list of features are reported in the following: (a) Though CRYSTAL is a very efficient code, the computing burden rises steeply when dealing with large cells at low coverage (supercell approach) and large basis sets, in particular with double-ζ plus polarization basis sets. (b) CRYSTAL does not handle electron correlation; therefore quantitative predictions are biased in cases in which such a feature is mandatory in the description of binding. This is the case when dispersion makes a significant contribution to the binding of the adsorbate. In a number of cases[147-151] the *a posteriori* evaluation of correlation functions based on the final self-consistent-field (SCF) charge densities adopting various density functionals[11,113,152,153] has been shown to improve structural and energetic data dramatically. Causà *et al.*[154] have recently obtained encouraging results in a study assessing the performance of a number of different density functionals in order to calculate structural and thermochemical data for a large number of covalent and ionic crystals; work is in progress to assess the merit of such functions when dealing with weakly-bound systems.[155] (c)

CRYSTAL does not allow for calculation of gradients of the energy with respect to the positions of the nuclei analytically and does not handle automatically geometry optimization and frequency calculations. (d) EMBED is a powerful code but requires further development in order to be of general use for the chemical community. The computational burden involved may be very large depending on the size of the cluster initially chosen and on the kind of problem studied.[156] There is some genuine hope of success in the application of EMBED to the class of problems involving weak interactions between a molecule and the surface, where no bond-breaking or charge separation is involved. (e) The *cluster* approach is very popular in that (i) electron correlation, both nondynamic and dynamic, as well as geometry optimization and frequencies calculations, can be computed in a straightforward way and (ii) the geometrical definition of the cluster is simple and the cut from the underlying solid usually takes into account the features of the active site which one wishes to model; this is particularly relevant when modeling the acidic sites of zeolites in which a number of different topologies can occur. (f) Whereas the perturbed cluster and the periodic approaches are formally correct, the *cluster* approach is theoretically not satisfactory, being based on an arbitrary cut of an infinite solid. Indeed, no theorem ensures that the properties computed with a cluster of a given size and topology will converge to those properly computed with a perturbed cluster approach on the same system. In other words, the only way to study the dependence of various properties on the cluster size is to repeat the calculation on a cluster with a larger number of atoms in different ways. Different strategies in the termination of the cluster also alter the final properties of the site to be modeled. It is obvious that, due to finite computer resources and to the rapid increase in the number of atoms, one is forced to limit the checking of various results to medium sized clusters. This is particularly true if the level of calculations (basis sets, electron correlation) is to be kept constantly high across the different clusters. The same holds for the supercell kind of calculations. (g) There is no unique way to saturate the dangling bonds at the border of the cluster. Results should be checked against different strategies and solutions, but this has rarely been done so far. (h) Even in the presence of a perfect embedding technique, the cluster approach is of great relevance if one wishes to assess which forces are relevant to the electronic properties of the adsorbed molecule and, in particular, which component is due to the long-range response of the crystal.

Indeed the cluster approach has been widely used for studying the interaction of molecules with all types of solids, i.e. ionic, covalent, and metallic. It will be discussed in detail in the next section.

D. Cluster Approach

1. Ionic Solids

The inclusion of the external Madelung potential seems to be essential to ensure that the atoms of the cluster have the same charge they would have in the periodic surface. Otherwise their charge would be too low, indicating a more covalent bond. The effect of the lattice potential may be appreciated when considering the extreme case of O^{2-} present in ionic solids such as MgO. It is stable when embedded in the lattice but dissociates in O^- plus one electron in the gas phase.

This suggests that the reduction in Madelung potential at the ionic surface with respect to the bulk may cause an increase in covalency of the cluster itself, and even a consequent change in the geometrical features. This fact poses a problem because, to our knowledge, none of the calculations reported so far take into account that the magnitude and position of the charges may change near the surface. As far as the (100) surface of the rock salt structure is concerned, there is evidence, however, that reconstruction phenomena such as rumpling are negligible, because the decrease in Madelung potential is only some 5%.[157] Low-coordinated structures lead instead to a definite increase in covalency.[158,159]

The vast majority of computational work has dealt with the unrelaxed (100) face of rock salt crystals of light atoms, such as LiF and MgO. When considering weak adsorption on such a plane, it is of paramount importance to know the electrical potential and its derivatives (field, field gradient) outside the crystal. The computation of the electric field outside a point array of charges is straightforward. Very recently Causà *et al.*[160] have derived rigorous procedures for obtaining the Madelung potential outside the surface of an ionic material. By means of the program CRYSTAL, the electrostatic potential outside the (001) LiF surface was calculated. An infinite slab of ten layers parallel to the (001) plane was considered, and the contributions of net charges of ± 1 e assigned to each site of the remaining planes were summed up to infinity. Convergence of the potential as a function of the number of layers in the slab was observed after the inclusion of the fifth layer. This potential was then fitted using a cluster made of two layers with 89 point charges. In each layer the 20 charges at border points were treated as varying parameters in a best fitting procedure, while the other 69 point charges were kept fixed to the value of ± 1 e. Electrical neutrality was also enforced within each layer. The quality of the fit was within 8.9×10^{-5} au in the region above the surface, where adsorption takes place. Recently, the same author has extended the procedure in the following way:[155] starting from a three-layer slab of a LiF(001) surface, the *ab-initio* electrostatic potential in the region where adsorption takes place (from 2 to 5 Å, above the surface, respectively) was computed with the CRYSTAL code. A cluster of few atoms to be treated quantum mechanically was then defined. This cluster was embedded in an array of point charges, which were determined such that the quantum mechanical electrostatic potential of the cluster plus the embedding charges computed in the same van der Waals region matches the corresponding values obtained by the full CRYSTAL calculation. At this stage the interaction of CO was studied on both the embedded cluster and the periodic surface in the supercell

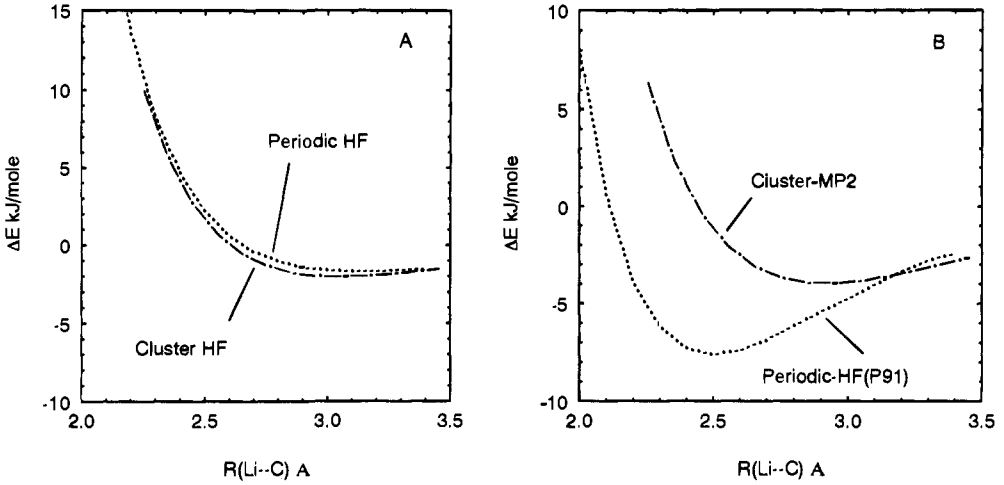

Figure 2. Binding energy curves for a CO molecule adsorbed C-down on a Li ion at the (100) LiF surface. Basis sets are 6-311G* (CO), 6-2G (Li), and 7-311G (F). All data are uncorrected for BSSE. (A) Short dashed line refers to a fully periodic Hartree–Fock *ab-initio* calculation; long dashed curve refers to *ab-initio* SCF calculation on a LiF cluster embedded in an array of potential-derived charges (see section III.D.1 for details). (B) same as (A) except that binding energies were computed by means of the Perdew correlation density functional[11] method for the periodic calculation and by the MP2 method for the cluster calculation.

approach. The results (Figure 2a) show very good agreement between the two procedures. The periodic calculation has also been carried out by including electron correlation effects by means of the post-SCF correlation density functional of Perdew.[11] For the cluster, the standard MP2 method has been adopted. As clearly shown from Figure 2b, the two methods give very different results for both intermolecular separation and values of the binding energy. Much work is obviously needed to assess merits and drawbacks of density functional methods in the field of intermolecular interactions.

2. Metals

The common phenomenon on metal surfaces is chemisorption. Of course, really weak interactions can also occur, i.e. for rare gases. Even for admolecules such as H_2O, NH_3, and CO, a discussion in terms of vdW interactions is fruitful. In this respect, an excellent source of references on many aspects of water adsorption on metals has been published.[161] Quite a number of calculations dealing with metal cluster/molecule adsorption have been reported, and the field is so wide that a specific review would be needed. For the description of various embedding cluster methodologies, the reader should refer to the comprehensive review of Sauer[162] and to references 163–165 for recent work. Here, a brief account of the problems arising from the cluster approach with respect to adsorption is given by referring to selected studies. For methodological reasons, some of them are included although they deal with classical chemisorption systems.

In a fundamental paper, Hermann *et al.*[166] have studied the dependence of CO adsorption on the size of Cu clusters mimicking the (100) crystal face of metallic copper. The clusters considered were $Cu_1\cdots CO$, $Cu_5\cdots CO$, $Cu_{10}\cdots CO$, $Cu_{14}\cdots CO$, and $Cu_{34}\cdots CO$. The SCF method was used: for the central Cu atom, where adsorption takes place, a full [14s,11p,6d]/(8s,6p,4d) basis set was adopted, whereas for the surrounding atoms only the 4sp electrons contributing to the conduction band were explicitly included in the SCF procedure and all other electrons were replaced by a pseudopotential. For CO, a DZ basis set was chosen. The binding energy showed a strong oscillation as a function of the cluster size: −54, +44, −39, +27, and −54 kJ/mol for Cu_1, Cu_5, Cu_{10}, Cu_{14}, and Cu_{34}, respectively. The reason for this behavior are variations of the electrostatic charge superposition and substrate polarization, which strongly depend on cluster size and geometry (through symmetry restrictions) and are reflected in the substrate cluster electronic energy levels. Similar calculations have recently been reported by Baerends *et al.*[116] for the adsorption of CO on Cu(100). They compared a periodic 2D slab calculation with calculations on clusters involving models of up to 37 copper atoms. Both kinds of calculations were based on the local density functional (LDF) approximation and used the Vosko–Wilk–Nusair (VWN) exchange-correlation expression.[110] While the binding energies for the clusters varied widely as a function of the cluster size for both adsorption sites considered (top and 4-hollow), the stabilization energy computed for the periodic 2D system converged smoothly with the number of layers in the slab. The hollow site was the preferred one, even if the difference in the binding energies with respect to the top site decreases with the number of layers, in agreement with experimental findings. It is worth noting that the absolute value of the binding energy is overestimated by the LDA method by about a factor 2. Gradient corrections for exchange[112] and correlation[113,167,168] may perhaps improve the result, but no systematic studies are available at the moment.

Siegbahn *et al.*[169] were the first to propose a prescription for calculating an accurate chemisorption energy using the cluster model. In the case of hydrogen adsorption they noted that, in order to get steady chemisorption energies as a function of the cluster size, those electronic states of the clusters should be considered which have one singly occupied orbital of the same symmetry as the hydrogen 1s

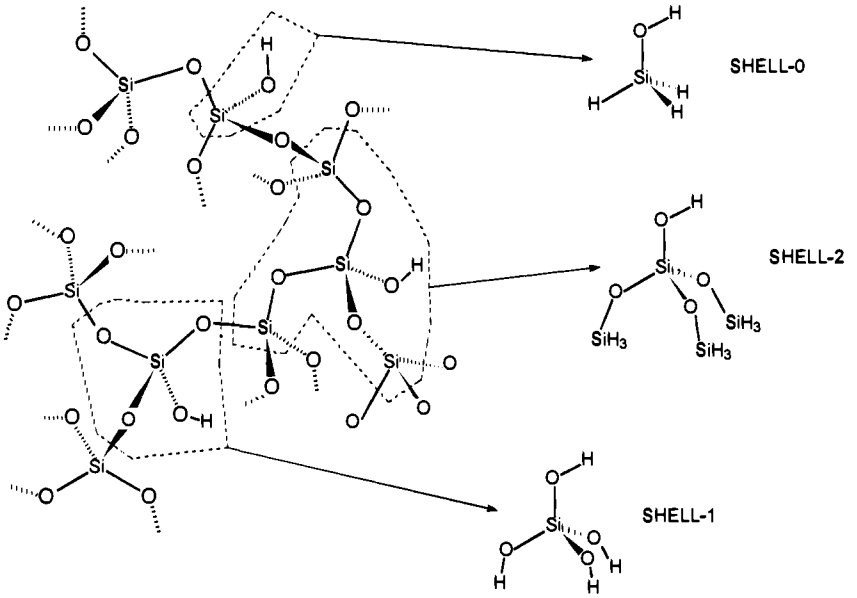

Figure 3. Models of different size for isolated surface silanol groups.

orbital. The same method was applied to the adsorbed methyl radical.[170] The adsorption of CO on Cu clusters was also re-examined by the same authors.[169] In that case, however, it was much less clear how to prepare the substrate electronic states in such a way as to render the cluster ready to accept the incoming electron density contained in the 5σ orbital of the CO molecule. An a_1 cluster orbital should be initially empty: such a requirement, however, can be met only by charging the cluster or by pushing electrons in a very diffuse orbital. A series of calculations inclusive of electron correlation on small Cu clusters showed that geometry relaxation is relatively important in decreasing the oscillations in the binding energy, probably due to a better balance between bonding and nonbonding ability of a site with respect to those found for the fixed bulk geometry. The justification for selecting such a "bond prepared state" is that in a real metal all states are energetically so close to each other that localization of such a bond prepared state can be achieved at no energetic cost.

It is clear that application of the cluster method to metal systems is still quite critical, particularly when dealing with weak intermolecular interactions, where a "bond prepared state" is difficult to define. This is certainly a field where efficient embedding techniques are urgently needed, even though electron correlation, which is essential for the description of such systems, will increase even more the complexity of the actual codes and the cost of the calculations.

The reader interested in application of the Whitten embedding method may refer to a number of recent studies in which the adsorption energies and adsorbate structures as a function of surface adsorption were computed, namely: hydrogen on Ti(0001) and Cu(100) and Ni(111)[171-177] adsorption of CH, CH_2, CH_3, NH_3, H_2O, OH, CO, CH_3O, OHC, O, and C_6H_6 on Ni(111).[178-186]

3. Covalent Solids

The easiest and chemically best defined procedure for making a cluster neutral is to saturate the dangling bonds resulting from a homolytic cut with monovalent atoms, normally hydrogen. Considering silica, two kinds of termination are possible as shown in Figure 3, which leaves either an Si or O atom with unsaturated valencies. Hydrogen atoms may replace either the missing oxygen or silicon atoms. The electronegativity of hydrogen is intermediate between that of oxygen and silicon. This means that, when oxygen linked to silicon is substituted by H, the Si–H bonds is polarized in the same direction as Si–O, though to a lesser extent. Analogous considerations hold when H is linked to oxygen as a substitute of silicon. But this approach is also not without problems. For example, the presence of terminal OH groups free to rotate may result in spurious intramolecular H-bonds, which, in turn, may alter the acidity of such models (see section VII for details). Problems also arise when attempts are made to embed such an H-saturated cluster into a finite or infinite array of point charges.[187] The distance of a saturating H atom to the nearest point charge is small, and therefore polarization effects which are not properly compensated by Pauli repulsion are particularly large. Moreover, the presence of the saturating atom must somehow be taken into account when fixing the magnitude of the point charges.

Fluorine atoms can also serve as saturating atoms on Si, for instance, in trifluorosilanol as a model for the isolated hydroxyls of silica. This has already been done by Geerlings *et al.*[188] and in the context of zeolite models by Datka *et al.*[189,190] New results for F_3SiOH as a free model and in the complex with an ammonia molecule are also reported in the present review. A third possibility is the use of pseudoatoms as terminators. Such a procedure was popular years ago in semiempirical calculations,[191] but it is also possible in an *ab-initio* approach. The *ab-initio* study of chemisorption on Si surfaces is a recent example.[192] Sauer[162] has given further examples and a full description of the approach, and there is no need to repeat this discussion here. One of the limitations of this approach is that difficulties immediately arise when either improvement of the basis set or inclusion

of electron correlation is desired. Therefore, we recommend working with defined molecules to which well-established methodologies may be applied. The hope of restoring the electronic effect of the infinite solid, the knowledge of which is already limited, by means of oversimplified methods is rather weak.

There are previous reviews[162,193-195] on cluster models of silica and zeolites which cover the studies published up to 1987.

4. Thermodynamic Functions within the Rigid Cluster Model

The cluster approach provides data on the formation of a localized surface complex, M−S, as a result of the interaction of an isolated molecule, M, with an adsorption site, S. From the calculated structures, vibrational frequencies, and energies of these species, the enthalpy and entropy of formation, ΔH^C and ΔS^C, and the equilibrium constant K^C can be calculated using the standard rigid rotor−harmonic oscillator−ideal gas approximation (see, e.g., ref 88). For the formation of surface complexes, a modification has been suggested[86,87] which takes into account that the adsorption site S and the surface complex S−M are part of the solid which has no rotational or translational degrees of freedom. Hence, on complex formation the three rotational and three translational degrees of freedom of the molecule in the gas phase are converted into the six low-frequency modes for the vibrations of the adsorbed molecule relative to the surface. When the interaction is weak the additional assumption can be made that the intramolecular modes and the lattice modes of the solid do not change. For the equilibrium constant, K^C, this leads then to the expression

$$K^C = \frac{p_0 V_Q}{kT} \frac{Q^{vib}_{(6)}}{Q^{rot}_{(3)}} \exp - \frac{\Delta E}{kT}$$

in which Q are the partition functions, p_0 is the standard pressure, and V_Q is the quantum volume. With the assumption that there is no interaction between neighboring sorption complexes, the Langmuir isotherm is obtained,

$$\theta/(1-\theta) = K^C p$$

which can be used to calculate the pressure at which a certain coverage is obtained. For the differential enthalpy and entropy of adsorption, $\Delta_a H$ and $\Delta_a S$, we have

$$\Delta_a H = \Delta H^C$$

$$\Delta_a S = \Delta S^{0,C} - R \ln(p/p_0) + R \ln(1-\theta/\theta)$$

A convenient standard state which does not make reference to a particular concentration of surface species is half coverage, $\theta = 1/2$. If we insert $\theta = 1/2$ in the Langmuir isotherm we get

$$K^C = 1/p_{1/2}.$$

The pressure at which half coverage is achieved is $p_{1/2}$.

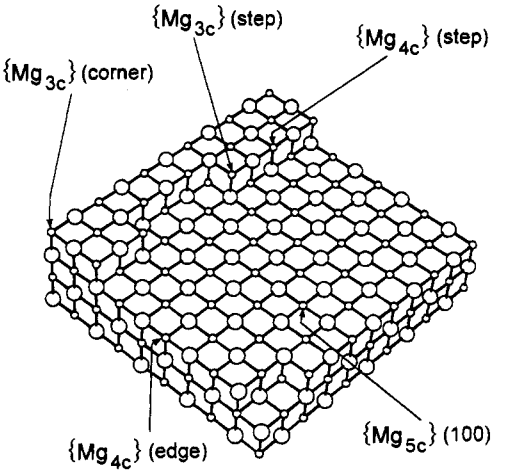

Figure 4. Ball-and-stick representation of a piece of MgO crystal; Mg^{2+} ions as small spheres, O^{2-} as large spheres. Also shown are coordination number and description of the topology of each cation site. The Madelung constants computed[12] for those sites are 1.681 {Mg_{5c}}(100); 1.591 {Mg_{4c}}(edge); 1.566 {Mg_{4c}}(step); 1.344 {Mg_{3c}}(corner), 0.873 {Mg_{3c}}(step). The Madelung constant for a bulk {Mg_{6c}} is 1.747.

IV. Interaction of Molecules with the Surface of Ionic Materials

A. MgO—A Case Study

Magnesium oxide is the lightest binary oxide with strongly basic properties and definite ionic character: the even lighter BeO prefers a hexagonal structure and has a partially covalent nature.[207] This view is supported by the net charges obtained in periodic *ab-initio*[208] calculations on MgO and the MgO(001) surface.[209] For such reasons, MgO has attracted much interest from the theoretical point of view. MgO is known to act as a catalyst for some base-catalyzed reaction such as the isomerization of olefins and the Cannizzaro disproportionation.[210] It is definitely more interesting, however, as a model oxide. Depending on the preparation route, it may be obtained either as high surface area material, made up of irregularly shaped particles, or as low surface area material, made up of nearly perfect cubelets.[211] High-resolution transmission electron microscopy (HR-TEM) shows that also in the former case the building blocks of irregular particles are tiny cubes.

As a consequence, a cubic morphology such as that reported in Figure 4 may always be assumed. This figure also illustrates some of the possible coordinative situations for Mg^{2+} and O^{2-} ions occurring at the surface. Besides the (100) faces, at which 5-fold coordinated ions occur, some 4-fold coordinated species are visible at edges and steps, and even 3-fold coordinated ions at vertices and kinks. The actual occurrence of such types of coordinative situations is documented by experiments. For the whole family of alkaline earth oxides, measurements in the UV−vis region by means of diffuse reflectance spectroscopy have long ago shown that *three* electronic transitions are present at energies lower than that of the excitations,[212] related to bulk oxygen ions. They correspond to surface states involving 5-, 4- and 3-coordinated oxygen anions.[158]

Table 6. Interaction of CO and NO with Surface Sites of Ionic Materials Computed within the Cluster Approach. Interaction Energy, ΔE (kJ/mol), Shift of the CO or NO Stretch Frequency, $\Delta\nu$ (cm^{-1}), Distance between the Surface Site and the Closest Atom of the Ad-molecule, R(S−C) (Å), and Intermolecular Stretch Frequency, ν(S−C) (cm^{-1}). Column C Shows the Coordination of the Site Where Adsorption Takes Place

model[a]	C	method	$-\Delta E^{b,c}$	$\Delta\nu^{d}$	R(S−C)	ν(S−C)[d]	ref
CO/Mg^{2+} (free ion)	0	DZ	161				265
CO/Mg^{2+}	1		92				
$CO/Mg^{2+}\}^{P}$	3		60		2.38		
$CO/Mg^{2+}\}^{P}$	4		39				
$CO/Mg^{2+}\}^{P}$	5		38		2.48		
$CO/Mg^{2+}\}^{P}$	5	3-21G	36		2.44		222
	5	VTZ	22				
$CO/(MgO)_3\}^{P}$	3	3-21+G	4[e]				237
	5	3-21+G	173[f]				237
$CO/(MgO_5)^{8-}\}^{P}$	5	[4s,3p]/DZ/TZ[g]	23	31	2.58	103	223
$CO/(MgO_5)^{8-}\}^{P}$	5	[4s,3p]/TZ/TZ[g]	23 [16]	31	2.59		229
$CO/(MgO)_{13}\}^{P}$	5	[4s,3p]/TZ/TZ(DZ)[g]	16 [8]	17	2.59		
$CO/(MgO)_9\}^{P}$	5	[4s,3p]/TZ/TZ(SZ)[g]	22 [7]	19	2.66		
$CO/(MgO)_{13}\}^{P}$	5		39[7]	7	2.60		
$CO/(MgO)_{21}\}^{P}$	5		51 [8]	4	2.60		
$CO/(MgO_5)^{8-}\}^{P}$	5	DFT-Xα/	116	67			229
$CO/(MgO_5)^{8-}\}^{P}$	5	[7s4p1d]/TZP/TZP[g]	109	48			
$CO/(MgO)_9\}^{P}$	5		94	47			
$CO/(MgO)_{13}\}^{P}$	5		47	23			
$CO/(MgO_3)^{4-}\}^{P}$	3	TZ (CI-SD/TZ)[c]	57 (81)[c]	97 (73)[c]	2.36		234
$CO/(MgO_4)^{6-}\}^{P}$	4		32 (48)[c]	55 (55)[c]	2.44		
$CO/(MgO_5)^{8-}\}^{P}$	5		22 (31)[c]	31 (43)[c]	2.6		
CO/Mg^{2+}	0	TZ/DZP/TZ[g]	152	195	2.24	232	266
$CO/(MgO_5)^{8-}\}^{P}$	5		23	31	2.58	103	
$CO/Mg^{2+}\}^{P}$	5		19	15	2.43	120	
$CO/(MgO)_9\}^{P}$	5	DFT-Xα/GTO[h]	94	54	2.22	183	267
$CO/(MgO)_6\}^{P}$	4		99	56	2.18	198	
$CO/(MgO)_4\}^{P}$	3		103	85	2.23	197	
$CO/(MgO)_{13}\}^{P}$	5		[36]	30			268
$CO/(MgO)_9\}^{P}$	5		[54]	54			269
$CO/(MgO)_9\}^{P}$	5	DFT-VWN/GTO[h]	105	60	2.18	221	117
$CO/Mg^{2+}\}^{P}$	5	[4s4p1d]/MIDI-3++/[4s4p1d]	20 [16]		2.46 [2.47]		232
$CO/(MgO_5)^{8-}\}^{P}$	5	[4s4p1d]/MIDI-3++/[4s4p1d]	46 [17]		2.40 [2.58]		
$CO/(Mg^{2+})/AIMP(O_5)^{8-}\}^{P}$	5	[4s4p1d]/MIDI-3++/[4s4p1d]	17 [12]		2.61 [2.62]		
$CO/(MgO_5)^{8-}+Mg^{2+}{}_{13}\}^{P}$	5	[4s4p1d]/MIDI-3++/[4s4p1d]	16 [2]		2.73 [3.16]		
$CO/(NiO_5)^{8-}\}^{P}$	5	[4s,3p]/DZ/TZ[g]	24	38	2.48	108	223
$CO/Ni^{2+}(H_2O)_3(OH^-)_2$	5	TZP	8.8 [7.2]		2.25	[52]	244
		CEPA/TZP	[9.6 ± 4.5]		[2.85]		
$CO/(NiMg_8O_9)\}^{P}$	5	LDF-TXα/GTO	160	45	1.88	327	117
$CO/(NiMg_8O_9)\}^{P}$	5	DFT-VWN/GTO	175	46	1.86	342	
$CO/(CoMg_8O_9)\}^{P}$	5	DFT-Xα/GTO	175	46	1.89	333	
$CO/(CuMg_8O_9)\}^{P}$	5	DFT-Xα/GTO		60	1.85	342	
$NO/(NiO_5)^{8-}\}^{P}$	5	MC-CEPA/TZP	10 ± 5				254
$NO/(NiO_5)^{8-}\}^{P}$	5	CI-TZP	18				252
$NO/Ni^{2+}\}^{PR}{}_{strong}$	5	SCF/SDZC[i]	29 [14]				253
$NO/Ni^{2+}\}^{PR}{}_{strong}$	5	IC-ACPF	43 [22]				
$NO/Ni^{2+}\}^{PR}{}_{weak}$	5	SCF/SDZC[i]	62 [46]	50			
$NO/Ni^{2+}\}^{PR}{}_{weak}$	5	IC-ACPF	77 [55]				
$NO/O^{1-}\}^{PR}{}_{strong}$	5	SCF/SDZC[i]	37 [24]	−85			
$NO/O^{1-}\}^{PR}{}_{strong}$	5	IC-ACPF	76 [51]				
$NO/O^{1-}\}^{PR}{}_{weak}$	5	SCF/SDZC[i]	119 [110]	−197			
$NO/O^{1-}\}^{PR}{}_{weak}$	5	IC-ACPF	157 [130]				
MgO/CO powder		adsorption techniques (isosteric heats)	13−22				48, 49, 225, 226, 228

Table 6. (Continued)

model[a]	C	method	$-\Delta E^{b,c}$	$\Delta\nu^{d}$	R(S−C)	ν(S−C)[d]	ref
MgO/CO ultra thin film	5	adsorption techniques (isosteric heat); IRAS	42	35			224
MgO/CO single crystal	5	molecular beams technique and kinetic model	25−30				227
MgO/CO powder	5	FTIR		14			217
MgO/CO powder	4			27			47
MgO/CO powder	3				60		218
NiO/CO sintered microcrystals	5	FTIR	30	7			245−248
NiO(10%)MgO/CO solid solution	5	FTIR		13			235
NiO/NO in vacuo cleaved	5	TDS; HREELS	50	−76			252
NiO/NO sintered microcrystals	5	adsorption techniques (microcalorimetry); FTIR	83	−71			250, 251, 255, 270

[a] $\}^{P}$ represents a point charge array surrounding the all-electron cluster. $\}^{PR}$ represent a point charge array plus a repulsive exchange operator with a strong or a weak field of surrounding point charges. [b] Entries enclosed in brackets are corrected for BSSE. [c] CI-SD results in parentheses. [d] Harmonic approximation. [e] vdW complex. [f] Chemisorption complex. [g] Basis set for CO/Mg/O (outer ions of the cluster). [h] Gaussian-type orbitals. The basis sets were Mg^{2+} (13s,8p,3d)/[7s,4p,1d]; O^{2-} (11s,7p,1d)/[6s,4p,1d]; CO (9s,5p,1d)/[7s,4p,1d]. [i] Ni SDZC extended with two diffuse p and one diffuse d functions; N, O [4s,3p] plus diffuse p and d functions.

The oxygen dianion, O^{2-}, is unstable in the gas phase—it decays to O^{-}—and only exists in the solid because of the stabilization by the Madelung field. As a consequence, it is the less stable the lower its coordination in the solid. Three-coordinated anions and the vast majority of four-coordinated ones react readily with practically all molecules, including methane,[213] pyridine,[214] and CO, the latter two giving rise to a quite uncommon chemistry.[215] This means that it is not easy to get information on the types of cations exposed, because the usual probe molecules for cations are exceedingly reactive. An uncommon probe for surface cations turns out to be the superoxide O_2^{-} species which can be generated at the surface by the reaction of molecular oxygen with e.g. hydrocarbons.[12] These species show electron spin resonance (ESR) signals which are sensitive to the electric field of the underlying solid. In this way at least five different cationic sites can be identified.[12]

At the (100) plane, the Madelung constant is reduced by some 5% only,[158] and the features of the surface ions are accordingly similar to those of the bulk, although they have lost one ligand out of six. For instance, reconstruction or rumpling of the (100) plane seems to be very limited,[216] and so are changes of the Madelung potential.[158] Such surface cations are chemically rather inert and thus appear as ideal candidates for the formation of weakly bound vdW complexes, which are described below.

The system most studied is CO on MgO, both experimentally[47,217] and computationally (see Tables 6 and 7 for references). Most experimental information is gained through IR spectroscopy. At room temperature, a complex chemistry involving highly uncoordinated O^{2-} anions is observed, leading to CO_2^{2-}, $C_3O_4^{2-}$ (ketenic structure), and even more complicated species[218] which are outside the scope of this review. A small fraction of CO sitting on low-coordinated Mg^{2+} cations gives rise to an IR band at 2202 cm^{-1}, which is attributed to three-coordinated species.[47] Adsorption at a nominal temperature of 77 K takes place both on edge sites (four coordinated), with a CO band at 2159 cm^{-1}, and on the (100) faces. This latter phenomenon is best studied on particular samples (MgO smoke) obtained by combustion of Mg ribbons[217] and not through the usual procedure of decomposing magnesium hydroxide, as they are made up of rather large microcrystals in the shape of practically perfect cubelets with a negligible concentration of three- and four-coordinated sites. Adsorption on the (100) faces occurs by the building up of an ordered array of CO oscillators. The CO peak shifts with coverage from 2156.0 cm^{-1} ($\theta = 0$) to 2148.1 cm^{-1} at higher coverage. $^{13}CO/^{12}CO$ mixtures reveal that such a shift arises from the counteraction of static and dynamic interactions between CO oscillators (−11.3 and 3.1 cm^{-1}, respectively). From the latter value, the dynamic polarizability α_v is evaluatd to be 0.0306 Å^3. No definite value is available for the heats of adsorption for the different Mg^{2+}/CO complexes. However, as shown by data in Table 6, heats of adsorption ranging from 13 to 42 kJ/mol have been measured, depending on the sample preparation, the coverage attained, and the method of measurement.

Carbon dioxide reacts readily with MgO, mainly involving basic O^{2-} anions and forming surface carbonates. At low temperature, weakly adsorbed species are formed, of the type side-on, the structure of which resembles that of the products of CO_2 with alkali metals.[219] End-on linear species are also formed, interacting with one Mg^{2+} center, readily recognizable by relatively small perturbations of the ν_1, ν_2, and ν_3 modes of the free molecule. Actually, the ν_2 mode (which is only Raman-active in the free molecule) is rendered active by the asymmetric interaction with the surface.

Hydrogen is able to dissociate even under very mild conditions[220] (room temperature) at very low-coordinated O^{2-}/Mg^{2+} double sites, forming hydride species and hydroxyls: no study has been conducted of the physisorbed state of the H_2 molecule.

Early studies by Colbourn and Mackrodt[221] have shown that CO is bound to the Mg site and that the binding energy is around 38 kJ/mol. Pope *et al.*[222] studied interactions between MgO and a family of molecules, some of them radical species: HCO, HOC, H_2CO, HCOH, CH_3O, and CH_2OH. All of them are assumed, in a rather fanciful way, to be possible intermediates in processes such as the gasoline synthesis. In such a case comparison with experiment is virtually impossible.

In a more recent work, Pacchioni *et al.*[223] have performed a series of calculations on the interaction of CO with the (100) surface of MgO. An $(MgO_5)^{8-}$ cluster embedded in a large array of point charges of ±2 e was treated quantum-mechanically. The structure of the cluster was held fixed to that of the bulk (Mg−O distance = 2.1 Å). A TZP basis set was used and electron correlation has been included using the CISD method (configuration interaction using singly and doubly substituted configuration). A detailed partitioning into various contributions to the binding energy has also been performing using the constrained space orbital variations (CSOV) procedure. The array of charges has been carefully chosen to get a converged Madelung potential in the region where CO is bound, i.e. 2−4 Å above the MgO surface. The binding energy and the shift of the CO stretch frequency caused by adsorption were computed. Both electrostatic effects and Pauli repulsion, caused by the overlap of the CO electron density with that of surface oxygens surrounding the Mg cation, contribute to the blue shift of the CO frequency. The best estimate of the binding energy was within the range of experimental data of 13−42 kJ/mol[48,49,224-228] (see Table 6), whereas the computed blue shift of 31 cm^{-1} is much larger than the experimental value of about 14 cm^{-1}.[47,217]

Very recently, Pacchioni *et al.* compared the SCF results for CO adsorbed on a variety of MgO clusters of different size with those of a periodic calculation on a slab of three bidimensional MgO layers (CRYSTAL code, see section IV.C and Table 7).[229] The Mg^{2+} ion and its first-neighbor oxygen ions were described by a TZ basis set, all other atoms in the cluster by a DZ or SZ basis set depending on the size of the cluster. For the periodic calculation the DZ basis set was used. The CO basis set was [4s3p] in all cases. From the data reported in Table 6 it is clear that when larger and neutral $(MgO)_{13}$ and $(MgO)_{21}$ clusters were adopted the binding energy dropped dramatically to a few kJ/mol, in agreement with the value computed with the CRYSTAL code. The value of the ν_{CO} shift also decreases with the increased size of the cluster, from 31 to 4 cm^{-1}.

Cluster calculations were also carried out by Neyman and Rösch[117,230] by means of the LDF-Xα method using a TZ(d) basis set for the cluster and a [7s4p1d] basis set for CO. The perturbation of the CO stretch was computed, and some results are reported in Table 6. Clearly, the BSSE is large with the adopted basis sets and the dependence of the binding energy on the cluster size is largerly reduced if corrections are made for the BSSE. The periodic calculations (see section IV.C and Table 7) yielded values of the binding energy and of the CO frequency stretch shift close to those obtained for clusters of intermediate size. No BSSE correction was reported for the binding energy of the periodic calculation. The data in Table 6 also show that both the binding energy and the CO blue shift are overestimated when the local density functional method is used. Unfortunately, strict comparison between SCF and LDA results is biased by different basis sets used and the lack of BSSE estimates for the LDA binding energies.

Rösch *et al.*[230] have reported a study of the relevance of the Madelung field on the computed quantities. The value of the net charges in which the $(MgO)_9$ cluster was embedded was set to ±1.5 e: the blue shift in the ν_{CO} frequency was 16 cm^{-1}, compared with the value of 54 cm^{-1} obtained with the value of the net charges set to ±2 e. Obviously the Madelung field has a dramatic effect and more detailed investigations should be done in that direction.

Lakhlifi and Girardet[231] have studied the potential interaction surfaces of CO with the MgO(001) crystal face. A carefully determined semiempirical potential expression was used, and the computed binding energy was around 16 kJ/mol, whereas the CO molecule was found to be located between two Mg^{2+} ions.

Nygren *et al.*[232] have recently made a relevant investigation on the CO/MgO(001) system, in order to assess the importance of both Madelung potential and exchange forces on the capability of the Mg^{2+} site to interact with the CO molecule. To this purpose, an *ab-initio* full ion model potential (AIMP)[233] was used to embed the true cluster while the rest of the crystal was represented as point charges. The AIMP method allows one to describe the surrounding of the Mg^{2+} in such a way as to avoid the artificially high polarization of charge of the quantum-mechanically treated cluster due to the unscreened net charges at the lattice sites. Data in Table 6 clearly show the good agreement between the binding energy corrected for BSSE for an all-electron cluster, $(MgO)_5^{8-}$, and one in which the five oxygen anions were replaced by the AIMP, $(Mg^{2+})/AIMP(O_5)^{8-}$. It should be noted that BSSE is much larger for the unscreened all-electron cluster than for the one treated with the AIMP method. Enlarging the border of the cluster with a shell of second neighbors consisting of $(Mg^{2+})_{13}$ has a dramatic effect on the SCF binding energy, which is now as low as 2 kJ/mol, after the counterpoise correction (CPC) was taken into account. Inclusion of electron correlation by means of the MCPF method increases the SCF value of the binding energy to 7 kJ/mol, still much lower than any experimental estimate.

Pacchioni *et al.*[234] have extended the calculations to simulate the adsorption on edge and on corner sites of an MgO crystal. The edge site was represented by the $(MgO_4)^{6-}$ cluster, whereas the corner site was described by the $(MgO_3)^{4-}$ cluster. Both clusters were embedded in a large array of point charges, chosen such that a stable Madelung potential was obtained. The binding energy for the nondefective (100) site was 22 kJ/mol at the SCF/TZ level which increased to 31 kJ/mol at the CISD/TZ level. A single set of polarization functions was added to

Table 7. Adsorption Studies Using the CRYSTAL Code. Interaction Energy, ΔE, and Distance between the Surface Site and the Closest Atom of the Adsorbed Molecule R(S−M)

model	method[a]	coverage[b]/structure	$-\Delta E$ (kJ/mol)	R(S−M) (Å)	ref
H_2O/MgO (001)	8-51G(O)/8-61G(Mg)/6-31G* H_2O	1:4 O-down	17 (35,31,26)[c]	2.4 (2.1,2.1,2.1)	151
three layers	PHF(CS,P86,P91)[a]	1:4 H-down	23 (52,52,46)[c]	2.7 (2.4,2.4,2.4)	
H_2O/ZrO_2 (001)	PS(Zr)-11G(sp)-21G(d)/PS(O)/				260
tetragonal	41G(sp)				
two layers	6-21G H_2O AEOW		95		
	PS(O)-41G(sp) PSOW		26		
	H_2O/H_2O repuls AEOW		−37		
	H_2O/H_2O repuls PSOW		−36		
experimental[d]			90−120		262
CO/MgO (001)	8-51G(O)/8-61G(Mg)/3-21G CO	1:4 C-down	19	2.447	258
single layer	PHF[a]	1:4 O-down	18	2.306	
CO/MgO (110)	8-51G(O)/8-61G(Mg)/3-21G CO	1:1 C-down	28	2.40	257
two planes slab	PHF[a]	1:1 O-down	27	2.18	
		1:1 CO/CO rep	−15		
CO/MgO (001)	8-511G(Mg)/8-411(O),	1:2 C-down	13.9 (23.4)[c]	2.84 (2.50)	155
three layers	6-311G* CO, PHF(P91)[a]	1:2 O-down	8.4 (6.9)[c]	2.72 (2.58)	
CO/MgO (001)	DZ(Mg)/DZ(O),	1:2 C-down	30	2.60	267
three layers	[4s3p] CO, PHF[a]				
CO/Al_2O_3 (0001)	STO-3G Al, O/3-21G CO	1:1 C-down[d]	26	2.41	259
two layers	PHF[a]	1:1 O-down[d]	16	2.23	
experimental[e]			45		271
CO/LiF (001)	6-2G(Li)/7-311G(F)/6-21G* CO	1:4 C-down	6	2.94	256
three layers	PHF[a]	1:4 O-down	12	2.43	
CO/LiF (001)	6-2G(Li)7-311G(F)/6-311G* CO	1:2 C-down	1.7 (7.6)[c]	3.12 (2.50)	155
three layers	PHF (P91)[a]	1:2 O-down	1.5 (3.8)[c]	2.98 (2.42)	
N_2/LiF (001)	6-2G(Li)/7-311G(F)/6-311G* N_2				155
three layers	PHF(P91)[a]	1:2 N-down	1.6 (5.6)[c]	3.03 (2.42)	
N_2/MgO (001)	8-511G(Mg)/8-411(O),	1:2 N-down	11.2 (17)[c]	2.78 (2.47)	155
three layers	6-311G* N_2, PHF(P91)[a]				
NO/LiF (001)	6-2G(Li) 7-311G(F), 6-311G* NO	1:2 N-down	2.1 (4.9)[c]	3.08 (2.63)	155
three layers	PHF(P91)	1:2 O-down	1.6 (3.7)[c]	2.98 (2.50)	
NO/MgO (001)	8-511G(Mg), 8-411(O)	1:2 N-down	2.1 (6.9)[c]	2.92 (2.58)	155
three layers	6-311G* NO, PHF(P91)[a]	1:2 O-down	1.0 (5.1)[c]	2.78 (2.50)	
Cl_2/MgO (001)	8-51G(O)/8-61G(Mg)/6-21G* (Cl)	1:2[b]	12 (37,39,33)[c]	2.77 (2.53,2.50,2.51)	150
three layers;	PHF(CS,P86,P91)[a]	1:4[b]	16 (38,41,36)[c]	2.76 (2.52,2.49,2.50)	261
$Cl \perp O_{surf}$		1:8[b]	17 (38,43,38)[c]	2.75 (2.52,2.46,2.48)	

[a] PHF, periodic Hartree−Fock; CS, Colle−Salvetti correlation correction; P86, P91, perdew correlation correction. [b] Coverage *m:n* means *m* adsorbate molecules each *n* cationic centers. [c] The data in parentheses include correlation corrections obtained with the CS, P86, or P91 functionals, cf. footnote *a*. [d] Microcalorimetric measurements for high surface area monoclinic zirconia. [e] Calorimetric heat refers to CO adsorbed on coordinative unsaturated Al^{3+}(IV) on low index regular crystallographic faces of γ-Al_2O_3. Computed values refer to CO adsorbed on coordinative unsaturated Al^{3+}(VI) in corundum.

both carbon and oxygen atoms, whereas the TZ basis for the MgO cluster was supplemented with a set of diffuse functions.

The SCF and CISD values for the edge site were 32 kJ/mol and 48 kJ/mol, respectively, whereas the values for the corner site were definitely higher, 57 kJ/mol and 81 kJ/mol, respectively. The SCF and CISD blue shifts of the value of the CO frequency for the nondefective (100) site were 31 cm^{-1} and 43 cm^{-1}, respectively. The corresponding shifts in frequency for CO adsorbed either on the edge or on corner sites were 55 (55) cm^{-1} and 97 (73) cm^{-1}, respectively, compared with experimental values of 27 cm^{-1} and 60 cm^{-1} (see Table 6).

Neyman and Rösch[117] have also modeled the Ni^{2+}, Co^{2+}, and Cu^{2+} impurities in MgO, by means of the $NiMg_8O_9$, $CoMg_8O_9$, and $CuMg_8O_9$ clusters. The binding energy of the CO molecule adsorbed upon these clusters (see Table 6) and the ν_{CO} stretch have also been computed. IR data for solid solution of NiO (10%) in MgO interacting with CO have been reported by Scarano *et al.*:[235] the measured shift of the ν_{CO} stretching frequency was 13 cm^{-1}, much smaller than the computed value around 45 cm^{-1} (see Table 6).

Oxygen-isotope exchange between the CO adsorbate and the MgO surface has been analyzed by Huzimura *et al.*[236] using a similar approach, but due to limitation in the software only a reduced number of point charges were included. The same group[237] has carried out a study of the trapping and oxidation of CO at surface step sites of MgO, where reactivity is known to be higher than at sites of regular surfaces. They showed that the convergence of the electrostatic potential in the region where the CO molecule is bound was quite slow, charges of ±1.9 e were required at more than 500 bulk sites. The

polarization effect of this Madelung field on the quantum mechanical moiety is such that the Mulliken net charges at the Mg and O atoms of the $(MgO)_3$ cluster change from +1.15 e to +1.36 e and from −1.14 e to −1.32 e, respectively.

Sawabe *et al.*[238] have recently studied both the physisorption and chemisorption of H_2 on the MgO low-coordination site. The cluster chosen was $(MgO)_4$. Comparison was made between the results obtained for the bare cluster and for the cluster embedded both at the center of a cube consisting of 45 × 45 × 45 charges of ±2 e to mimic the bulk and at the corner of a slab consisting of 45 × 45 × 2 charges ±2 e to mimic a low-coordination site. Basis sets were in the range from 3-21G to 6-311(+)G. The Mulliken net charges of the atoms in the cluster change from ±1.09 e (bare cluster) to ±2.00 e for the cluster embedded in the bulk array of charges. When embedded at the corner of the slab of point charges, the Mulliken charges become +1.83 e and −1.90 e for the innermost Mg and O atoms, respectively. However, the most exposed atoms showed Mulliken net charges of +1.31 e and −1.09 e for Mg and O, respectively, which reveals that, although these charges are increased by the Madelung potential with respect to the bare cluster, the corner atoms still have substantially less ionic character than the bulk atoms. In agreement with the quadrupolar nature of the electrostatical field around H_2, there are two physisorption structures with about the same energy: a linear structure on the oxygen site and a T-shape structure on the Mg^{2+} site. The best estimate of the binding energy, obtained at the RMP4/6-31(+)G//Mg(6-31G);O;H (6-31(+)G**) level, is 8 kJ/mol for both types of complexes. Neither BSSE nor zero point correction (ZPE) were taken into account. The best computed value of the barrier of the H−H bond breaking is about 113 kJ/mol, very close to the value of 100 kJ/mol determined by temperature-programmed desorption.[239]

For the interaction of CO_2 with MgO, the only calculation is that reported recently by Pacchioni.[240] Both physisorption and chemisorption structures were analyzed by means of SCF, CISD, and MP2 methods using the following basis sets of DZ(d) quality: Mg^{2+}[13s8p/6s3p], O^{2-}[11s7p/5s3p], C,O-[9s5p1d/4s3p1d], d functions with exponents of 0.657 and 0.74 were added to C and O, respectively. Two sites on the (100) MgO surface were considered: a regular one in which Mg^{2+} is five-coordinated $\{Mg^{2+}\}_{5c}$ and a four-coordinated defect site $\{Mg^{2+}\}_{4c}$ which represents a cation at the crystal edges. The clusters chosen were $(MgO_5)^{8-}$ and $(MgO_4)^{6-}$, respectively, both embedded in a large array of point charges to accurately represent the Madelung potential in the chemisorption region. The CO_2 molecule is physisorbed at SCF level preferentially *via* its oxygen to the $\{Mg^{2+}\}_{5c}$ and $\{Mg^{2+}\}_{4c}$ cations by 17 and 32 kJ/mol, respectively; when corrections are made for the BSSE, these values reduce to 12 and 28 kJ/mol, respectively. The BSSE-corrected MP2 values are 23 and 37 kJ/mol, respectively. Electron correlation also decreases the SCF $Mg^{2+}\cdots O$ distance from 2.41 to 2.22 Å for the $\{Mg^{2+}\}_{5c}$ to $\{Mg^{2+}\}_{4c}$ site, respectively. Laser-induced thermal desorption techniques[241] showed that the binding energy is in the range of 30−40 kJ/mol, in semiquantitative agreement with the calculations.

The SCF harmonic shifts of the ν_1, ν_2, and ν_3 modes of CO_2 are 15 (20) cm^{-1}, −14 (−16) cm^{-1}, and 26 (39) cm^{-1} for $\{Mg^{2+}\}_{5c}$ and $\{Mg^{2+}\}_{4c}$, compared with experimental values of 42 cm^{-1}, −17 cm^{-1}, and 21 cm^{-1}.[219] A recent study based on polarized infrared spectra of CO_2 on MgO (100) single crystal surface prepared by cleaving a single crystal *in situ* under UHV conditions[242] revealed a shift of −15 cm^{-1} in the ν_3 mode, in contrast with both calculations and the experiments carried out on powdered MgO samples.

The results discussed in this and the subsequent section are summarized in Table 6.

B. Other Oxides

Among other metal oxides on which adsorption may take place, NiO has certainly been one of the most relevant. Solid NiO has rock salt structure with a Ni−O distance of 2.08 Å. It is generally accepted to be highly ionic with charges close to the ideal values of ±2 e. The NiO(100) surface is not reconstructed and shows a slight contraction of the Ni−O distance in the top layer of about 2% normal to the surface.[243]

Pöhlchen and Staemmler[244] studied the adsorption of CO on the (100) NiO surface. Two different cluster models were selected. In the first, a cluster consisting of one Ni^{2+} cation plus five adjacent O^{2-} ions was considered, and charge neutrality was ensured by adding eight protons, which yield the formally neutral molecular cluster $Ni(H_2O)_3(OH)_2$. In the second model, the same $(NiO_5)^{8-}$ unit is embedded in a lattice of point charges, which represents the semi-infinite ionic crystal. Ni^{2+} electronic configuration in NiO clusters was $3d^8$ and the cluster had a $^3B_1$ ground state symmetry. Good quality IR spectra taken at 77 K were available for the interaction of CO with polycrystalline NiO samples.[245-247] Experimental binding energy is around 30 kJ/mol.[248] Basis sets as large as TZ(d,p) have been adopted, and electron correlation has been included *via* complete active space SCF (CASSCF) and coupled electron pair approximation (CEPA). The best estimate of the binding energy was 10 ± 5 kJ/mol, in line with the experimental findings. It is worth noting that the binding energies obtained for the $(NiO_5)^{8-}$ clusters embedded in a semi-infinite lattice of point charges and for the *molecular* $Ni(H_2O)_3(OH)_2$ cluster were very similar. Indeed, the spatial extents of the fully occupied 2p shells of the Madelung stabilized O^{2-} ions and of the O atoms in H_2O and OH^- were also very similar.

Pacchioni *et al.* reported analogous calculations for the CO adsorption on the (100) surface of NiO.[223] The usual $(NiO_5)^{8-}$ cluster was embedded in a large array of ±2 e point charges, *i.e.* full ionicity was assumed also for NiO. SCF/TZ calculations yield a binding energy of 24 kJ/mol, a value which is higher than the value computed by Pöhlchen and Staemmler.[244] The reason is probably that the absence of polarization functions both causes a large BSSE and leads to exceedingly polarized molecules, which corresponds to high values of the electrostatic binding

energy. The perturbation of the electron density of CO due to the solid caused a blue shift of 38 cm^{-1} of the CO stretch at SCF/TZ level; an experimental value of 7 cm^{-1} was measured for very low CO coverages on NiO,[245-247] whereas with diluted (10%) solid solution of NiO in MgO,[235] the measured shift was 13 cm^{-1}.

Snis *et al.*[249] have recently computed the interaction of the N_2O molecule with cluster models of the CaO surface. They used a multireference externally contracted configuration interaction scheme (MR-CCI). The basis sets (exponents in parentheses) were MIDI-4 plus a diffuse p (0.07) for Ca^{2+} and [9s3p/4s3p] plus diffuse p (0.05147; 0.06368) and d functions (0.9; 1.0) for nitrogen and oxygen, respectively. An effective core potential (ECP) was used on Ca^{2+}. N_2O was found to be bound *via* its central N atom to an O^{2-} ion at the corner of a cubelet. A binding energy of 43 kJ/mol was computed, which reduced to 25 kJ/mol after corrections for the BSSE. The experimental binding energies are in the range of 15–27 kJ/mol, depending on the N_2O partial pressure.[249]

Recently, the interaction of NO with the (100) surface of NiO has been the subject of both experimental[245,246,250-252] and computational work.[252-254] Relevant data have been collected in Table 6.

Kuhlenbeck *et al.*[252] have carefully studied the adsorption of NO on NiO(100)/Ni(100) and on the *in vacuo* cleaved NiO(100) single crystal with an impressive number of different techniques. By means of XPS, angle-resolved ultraviolet photoelectron spectroscopy (ARUPS), near-edge X-ray-adsorption fine structure (NEXAFS), and high-resolution electron-energy-loss spectroscopy (HREELS), they have shown that the NiO(100) film deposited on the Ni(100) surface has similar occupied and unoccupied states as a bulk NiO(100) sample. HREELS reveals that there is only one species adsorbed on the surface, as seen from the single band at 1800 cm^{-1} due to the stretching frequency of the NO molecule. NEXAFS data on the NO/NiO(100) system showed that the molecular axis is tilted by 45° relative to the surface normal. From TDS a binding energy of about 50 kJ/mol was measured.

Escalona Platero *et al.*[246,250,251,255] measured IR spectra of the NO molecule adsorbed on highly sintered NiO samples; this material was a collection of microcrystals of cubic shape with well-developed {100} facelets, as confirmed by means of transmission electron microscopy (TEM) micrograph.[246] The IR spectra of the NO/NiO system showed a series of bands, the main feature of which was seen at 1805 cm^{-1}, *i.e.*, a band red-shifted by 71 cm^{-1} with respect to the stretch frequency of the free NO molecule (1876 cm^{-1} in gas phase), in good agreement with the value of 76 cm^{-1} obtained by Kuhlenbeck *et al.*[252] The band at 1805 cm^{-1} is the only one which survives at low NO coverage, whereas shoulders at both sides (1825 and 1770–1765 cm^{-1}) only showed up at higher NO coverage.

Microcalorimetric measurements were carried out on the same microcrystalline sample;[250] the heat of adsorption at low coverage ($\theta \approx 0.12$) was 83 kJ/mol, which decreased to 75 kJ/mol at higher coverage ($\theta \approx 0.5$). From both IR data and calorimetric measurement it is clear that lateral interactions are relevant in explaining the complexity of the data for the adsorption of NO on NiO(100) face.

All the theoretical calculations on the NO/NiO system were done by means of a cluster approach embedded in point charges of ±2 e, i.e. assuming full ionicity. Pettersson[253] has applied an embedding procedure in which Madelung potential as well as Pauli repulsion of the atoms surrounding the active site were taken into account. Ni^{2+} and an oxygen anion with a reduced charge, O^{1-}, were also studied as possible sites of adsorption. The latter site was meant to simulate reduced ionicity of anions due to the presence of the surface. A series of calculations were done in order to study the dependency of the binding energy on the value of the Madelung potential. Net charges reduced to ±1 e were used (weak potential) as well as typical values of ±2 e (strong potential). A sizeable increase in the value of the binding was obtained (see Table 6), when passing from strong to weak potential case. The calculation showed that the NO molecule does prefer a bent conformation with respect to the surface normal, the bending angle being around 45°, in good agreement with NEXAFS data.[252] The NO stretching frequency was computed at the SCF level. A *blue shift* of about 50 cm^{-1} with respect to the frequency computed for the free NO was computed for NO adsorbed on Ni^{2+} embedded in a weak potential; on the contrary, a *red shift* of about 85 cm^{-1} was computed for the adsorption on the O^{1-} ion embedded in a weak potential (see Table 6).

Staemmler[254] performed quantum mechanical calculations on a $(NiO_5)^{8-}$ cluster embedded in an array of point charges of the usual ±2 e value. The NO molecule linearly located on top of Ni^{2+} was only weakly bound (ROHF/TZP value of 10 ± 5 kJ/mol, see also Table 6). Tilting the molecular axis by about 45° resulted in a stronger binding energy because of a much favorable orbital overlap which has been analyzed in term of a CASSCF wave function with a basis set of DZ quality (see Table 6). Similar results were obtained when the molecular cluster $Ni(OH_2)_3$-(OH) 2 was adopted.

A CI/DZ of the adsorption of NO on the $(NiO_5)^{8-}$ cluster was also performed by Kuhlenbeck *et al.*,[252] resulting in a binding of 17 kJ/mol and a tilt angle of the NO axis with respect to the surface normal of about 45° (see Table 6).

In summary, experimental data show that NO is bounded to the Ni^{2+} ion of the NiO(100) surface in a bent conformation, decreasing its vibrational frequency by about 70 cm^{-1} and giving a considerable heat of adsorption of about 80 kJ/mol. Lateral interactions at high coverage are responsible for the rich features in the IR spectra. Calculations agreed on the conformation of the adsorbed structure (NO bent by about 45° and sit on top of Ni^{2+}) but the dependence of both the binding energy and the NO vibrational frequency on the Madelung potential, which is used to embed the cluster, is too large to allow any definite conclusion. The problem is still unresolved and we look forward to seeing new studies on this interesting system.

C. Periodic Calculations Using the CRYSTAL Code

Table 7 shows results published so far for vdW interactions of molecules with surfaces obtained by periodic calculations using the CRYSTAL code (cf. section III.C).

Due to its relevant role as probe molecule in IR experiments, the CO molecule is the most studied adsorbate,[256-259] but H_2O,[151,260] Cl_2,[150,261] NO,[155,256] and N_2[155] molecules have also been dealt with. Mainly the (100) surfaces of ionic crystals have been studied, namely MgO,[150,151,257,258,261] Al_2O_3(corundum),[259] and LiF.[155,256] Water on the (001) surface of tetragonal zirconia, ZrO_2, is the only example of the interaction with a partially covalent solid.[260]

Basis sets were adopted for the crystal slabs which were already optimized in early studies with respect to the description of the bulk crystal. For the adsorbates, a variety of basis sets have been selected ranging from 3-21G to 6-311G*. The study of the ZrO_2/H_2O interaction used pseudopotentials for ZrO_2. When the core electrons of the adsorbed water were replaced by the same pseudopotential, the system was found to be unbound, a result in conflict with both experiment[262] and all-electron calculations.[260]

The CO molecule was allowed to interact with the surface cation (Mg^{2+}, Al^{3+}, and Li^+) either *via* its oxygen or carbon atom. The bond axis was always kept perpendicular to the crystal plane. The SCF method gave almost the same binding energy for the C-down and O-down cases, with the exception of the Al_2O_3(0001) and MgO(001)[155,259] surfaces. In a series of calculations[155] it has been clearly shown that correlation corrections based on the Perdew density functional[11] give a clear preference for the C-down approach, in agreement with both cluster calculations and experimental evidence. A similar trend has been found for the NO molecule adsorbed on the (100) face of MgO and LiF.[155,160,256]

The analysis of the charge density maps and density of states revealed that electrostatic forces dominate the binding of CO, N_2, and NO on ionic surfaces and that very little charge transfer took place between the adsorbate and surface. The values of the binding energies show that the adsorption is very weak, as expected from the experimental estimates and cluster calculations. For this reason, relaxation of the position of the exposed surface atoms is in general not relevant for the calculation of the binding energy.

Scamehorn *et al.* carried out an extensive structural search to find out how water bonds to the (001) MgO surface.[151] The preferred conformation is one in which H_2O forms a bifurcated hydrogen bond with the oxygen ions of the MgO(001) surface. The conformation in which water was adsorbed oxygen down on top of the Mg^{2+} cation was also found to be stable. Correlation corrections using the SCF density increases the binding in all cases, with a corresponding decrease of the surface molecule distance.[151]

The coverage was always chosen such that the lateral interactions, E_L(ads) were almost negligible. Systems with a sizeable ΔE_L(ads) were Cl_2/MgO(001) with a Cl_2/Mg^{2+} ratio of 1:2, CO/MgO(110) at 1:1 coverage, and the H_2O/ZrO_2 case.

Physisorption of H_2O on a (001) MgO surface was also studied by Parrinello *et al.*[263] using the Car–Parrinello method[264] which is a DFT approach using plane waves as basis functions. In the periodic treatment a slab model consisting of three layers was adopted. A structure for the physisorbed water was found in which the H-atoms are directed toward the surface O atoms; at the same time, the O-atom of the water molecule is also in short contact (2.08 Å) with the Mg^{2+} surface ion. Substantial surface relaxation was discovered, but no chemisorption occured, even when the dynamics was run at higher temperature.

These studies show that the CRYSTAL approach in adsorption studies is very promising due to obvious advantages over the cluster method. The fast progress in hardware and software technology expected in this decade will certainly allow calculations on larger systems with very low concentration of the adsorbate in the supercell. It is also worth noting that CRYSTAL is the only code capable of estimating the lateral interactions. They may be relevant, for instance, in assessing the change of the dynamic polarizability of the adsorbate induced by the surface underneath. With the increased computer power and more tuned algorithms, it will soon be possible to carry out *ab-initio* molecular dynamics calculations inclusive of periodic boundary conditions in which both physisorption and chemisorption steps will be handled in a natural way.

D. Perturbed Cluster Method in Weak Adsorption

The perturbed cluster approach, as coded in the EMBED program, has been applied to the study of CO adsorption at a stepped LiF(001) surface.[156] This is, to our knowledge, the only published paper in which a system involving vdW interactions has been treated by means of EMBED. To reduce the computational cost, only a single layer LiF(100) face was selected to simulate the unperturbed adsorbent. A CRYSTAL calculation on this slab yields the needed unperturbed wave function. To simulate the stepped surface, two Li^+F^- ion pairs were superimposed onto the (001) slab in a square arrangement above the respective counterions. Only vertical relaxation of the ions belonging to the "tablet" was taken into account.

The CO molecule adsorbed on one of the Li atoms of the tablet is far enough from the underneath (001) surface not to experience any notable electric field. Hence, the adsorption is dominated by the local nature of the defect. The basis sets adopted were those optimized for bulk LiF, namely, 6-11G for Li^+ and 7-311G for F^-. For the CO molecule, a standard 6-21G basis was adopted. Two types of structures were chosen in which CO is adsorbed either C-down or O-down. Optimization of the intermolecular degrees of freedom as well as of the CO bond distance was carried out, keeping some obvious symmetry constraints. The binding energies and CO vibrational frequency were computed and compared with those resulting from the adsorption of CO on the regular LiF(001) face, when the same EMBED code was applied. Comparison with periodic adsorption of CO on LiF(001) was also made.

The preferred conformation was the O-down one in all cases, a well-known artifact due to both the

SCF method and too small basis sets for describing CO itself. The binding energies are 12 and 15 kJ/mol for the C-down and O-down adsorption of CO on the perfect surface, respectively. These values increase to 33 and 58 kJ/mol, respectively, for adsorption on the stepped surface. Unfortunately, due to a lack of data, comparison cannot be made with either experiments or cluster calculations. The increase of the binding energy is expected, since the exposed position of the Li^+ ion of the "tablet" increases the electrostatic field experienced by the CO molecule.

The interpretation of the vibrational stretching frequency shift of the CO molecule is more controversial. A red shift with respect to the value of the free molecule was computed for the C-down adsorbate on both unstepped and stepped surface sites (12 and 15 cm^{-1}, respectively), a result opposite to current experimental knowledge on similar systems, to results of cluster calculations on related systems and to the values obtained with the CRYSTAL code in a supercell approach with a better basis set for CO (6-21G*). At the same time, a blue shift of 25 cm^{-1} was computed for the C-down adsorbate on the unperturbed surface, whereas a red shift of 65 cm^{-1} was computed for CO adsorbed on the stepped surface. Clearly, the basis set adopted for carbon monoxide (6-21G) is too crude to give a good description of the multipole moments of this molecule (cf. the 3-21G result in Table 4). Moreover, it may also happen that small differences such as vibrational shifts are at the moment within the numerical errors inherent in the EMBED methodology. A great amount of testing, perhaps on even simpler cases, is urgently needed and we look forward to seeing new results soon.

V. Interaction of Molecules with Metal Cations in Zeolites

Acidic hydroxyls in zeolites and zeolitic systems may be replaced by cations of various types by simple manipulations. There are difficulties in obtaining a fully exchanged sample with cations other than monovalent, for the evident reason that two or more protons have to be substituted simultaneously, which is not always possible, particularly in zeolites with a low Al content. Zeolites substituted with monovalent cations are perfectly well defined systems. In particular, one may distinguish between systems with a low Si/Al ratio such as X and Y zeolites, where the concentration of M^+ sites is accordingly high, and systems with a high Si/Al ratio such as ZSM-5, showing few M^+ sites which presumably do not interact. A further important distinction concerns the nature of the cation, whether of transition series or not. In the following, only d^0 or d^{10} will be considered, to exclude chemical interactions between the cation and the probe molecule. Such a choice includes, besides alkaline and alkaline earth cations, Zn^{2+} and Cu^+. At the moment there is much interest in Cu^+-substituted zeolites as catalysts for exhaust gas treatment. Such samples are usually prepared by chemical exchange with Cu^{2+} ions and subsequent reduction. A particularly efficient route to such samples is the vapor-phase reaction with CuCl of the H-form of zeolites, causing the evolution of HCl.[272]

In conclusion, ideal candidates for the comparison of experimental and computational data are the alkaline-ion substituted zeolites with a low Al content, such as MFI or mordenite, because they provide well-defined independent sites. Of comparable interest are the data concerning low coverages of adsorbate in systems with high Al content. Unfortunately, theoretical work on alkaline-atom substituted zeolites has not been carried out recently, and results are only available at the semiempirical level or at the *ab-initio* SCF level with small basis sets. The field has been recently reviewed,[273] and we mention only briefly some problems.

The properties of free cation–molecule complexes can serve as a first approximation to rationalize the observed data on the adsorption of molecules on cation sites in zeolites, e.g. qualitative changes of the IR spectra of the adsorbed molecules. For example, an SCF/MINI-1 study of the complex of Na^+ with ethene[103] predicted a lengthening of the CC and CH bonds by 0.008 and 0.005 Å, respectively, and a corresponding shift of the CC and CH stretch modes by −40 and −50 (average) cm^{-1}, respectively. As expected, the observed frequency shifts are smaller, about 10–13 and 9–25 cm^{-1} respectively (see ref 103 for the references to the original papers). The reason is, of course, that the electric field of the cation is weakened by the ions surrounding it in the zeolite. This weakening is site specific. The next approximation should consider this effect. Many calculations have been published in the past[273] which tried to include a large number of neighboring ions by adopting models including aluminosilicate rings typical of the cation site considered, but—because of computational limitations—used semiempirical methods like CNDO/2. We mention only those of Dilmukhambetov *et al.* for the interaction of NH_3 and H_2O with Li^+ and Na^+ ions in six-membered ring models of zeolite Y[274] and Beran for the interaction of CO with models of four- or six-membered ring sites.[275,276] Over a decade ago, Sauer and Deininger showed by comparison with *ab-initio*[277] and observed gas-phase data that the CNDO/2 method overestimates binding energies of unsaturated hydrocarbon molecules by about a factor of 2, though it is able to correctly discriminate between different adsorption structures.[278] *Ab-initio* calculations on clusters embedded in point charge arrays were recommended as an alternative a decade ago.[279] Using this method Sauer et al.[279] obtained different binding energies for H_2O molecules adsorbed at different Na^+ sites of zeolite A.

Spectroscopic studies on alkaline-ion substituted zeolites were focused on molecules which primarily interact with cationic sites only, such as CO, CO_2, N_2. Classical work by Angell[51] and Egerton[280] has been supplemented recently.[281,282] The case of Na-ZSM-5 is typical: a strong band is observed at 2178 cm^{-1}, due to the CO stretching mode of the Na^+–CO species. The band is slightly asymmetrical, which indicates the presence of slightly different cation sites. A weak combination band is also seen at about 2310 cm^{-1}, from which a value of *ca.* 140 cm^{-1} is derived for the frequency of the Na–C stretching mode. A band at 2112 cm^{-1}, definitely less intense

than the principal one at 2178 cm^{-1}, is ascribed to CO molecules interacting with both ends with Lewis sites. Also observed is a rather pressure-dependent band at 2138 cm^{-1}. It is ascribed to liquid-like CO species which show hindered rotational modes. The IR spectra of CO adsorbed on NaX and NaY zeolites are slightly more complex.

The adsorption of molecular nitrogen is interesting[283] because its N−N stretching mode, IR-inactive in the free molecule, becomes active due to the asymmetry imposed by the adsorption site. *Ab-initio* calculations of the frequency shift of N_2 and H_2 on interaction with a Na^+ cation have been compared with shifts observed for these molecules in NaA zeolites.[284] The orientation of the diatomic molecules relative to the cation is determined by their quadrupole moment which interacts with the gradient of the field created by the cation (in the model) or the whole zeolite structure (in reality). The quadrupole moments of N_2 and H_2 have opposite signs, therefore N_2 orients parallelly with respect to the line connecting its center of mass with the cation, while the H_2 molecule orients perpendicularly. These structures are found in calculations which predict frequency sifts of 16 and −67 cm^{-1} (MP2/6-311G**) for the N_2-Na^+ and H_2Na^+ complexes. The shifts observed on adsorption in an NaA zeolite are 8 and −83 cm^{-1}, respectively. A more recent study of the adsorption of H_2 on Na-forms of several zeolites[285] also reports red shifts of the order of magnitude of 100 cm^{-1}. The question is raised whether it is the asymmetry of the orientation of the H_2 molecule which renders its stretching mode IR-active. One possibility for an asymmetric interaction is a dual site adsorption involving a cation and a nearby oxygen atom.

In the family of alkaline zeolites ranging from Li-substituted to Cs-substituted ones, the frequency of adsorbed N_2 decreases regularly from 2338 to 2328 cm^{-1}, whereas it is almost independent of coverage.[283] The extinction coefficient also decreases steadily by 1 order of magnitude. An estimate of the electric field at the site of adsorption may thus be made, which results in the obvious order $Li^+ > Na^+ > K^+ > Rb^+ > Cs^+$. Isosteric heats of adsorption also decrease regularly in the series.

The same authors have studied, on the same set of samples, the adsorption of methane.[286] Similar considerations hold: the ν_1 mode which is chosen for observation is IR-inactive in the gaseous molecule and becomes active because of the asymmetry imposed by the site; the shift in ν_1 decreases along the series $Li^+ \rightarrow Cs^+$, as does the heat of adsorption. Similar work conducted on mordenite and H-ZSM-5 substituted with Na^+ and alkaline-earth cations[53] shows similar features. It is noteworthy that the properties of the cationic site are sufficient to explain the results and that the basic oxygen atoms nearby seem to play no role, in contrast to the case of molecular hydrogen adsorption described above.

In a number of cases, the isosteric heat of adsorption has been evaluated through the Clausius−Clapeyron relationship from a set of isotherms at different temperatures, for instance in the case of saturated hydrocarbons on Na−X and Na−Y.[287]

In another case, the "optical isotherms" yielded by the intensity of the IR band of adsorbed CO_2 as a function of pressure have been used to compute the energy of interaction of carbon dioxide with A zeolites.[288] For CO interacting with Na-, Ca-, and Zn-exchanged Y zeolites, the energy of interaction has been directly measured by calorimetry,[46] together with the IR spectra. As observed above for N_2 and CH_4, the CO stretching frequency is a function of the energy of interaction.

A particularly neat result has been observed for the CO adsorption on Cu^+-exchanged ZSM-5[289] by varying the pressure in the 0−40 Torr range at a nominal temperature of 77 K. The IR spectra show that the cations form CO complexes with successively one, two, and three ligands. All have CO modes in the 2170−2130 cm^{-1} region, which indicates that chemical interactions are basically absent and that electrostatics dominate the interaction. Such a result is in good agreement with high-level computations on the Cu^+−CO gas-phase complex, which show negligible d−π^* back-donation, in contrast with the analogous complex involving the metallic Cu atom.[290]

There is a wealth of experimental evidence, some rather recent, which awaits support from calculations. In the absence of a computational counterpart, we refrained from giving a complete account of the experimental literature and only proposed some of the relevant data as a stimulus to future computational work.

VI. Interaction of Molecules with Amorphous Silica Surfaces

A. Introduction

The rigid tetrahedron SiO_4 is the building block of all siliceous materials, from zeolites to quartz and amorphous silica. The reason why such a relatively rigid unit is able to aggregate in many different ways is to be sought in the peculiar bond between two SiO_4 moieties. In contrast with the rigidity of the O−Si−O angle, it costs virtually no energy to change the Si−O−Si angle from 130° to 180°. This has been shown in a number of studies of the siloxane bridge, Si−O−Si.[291,292] Their main concern was to obtain reliable empirical potentials for use in molecular mechanics and dynamics studies on zeolites. A minimal H_3Si−O−SiH_3 cluster was adopted, the Si−O−Si angle corresponding to the energy minimum was 142°, and the increase in energy from 145° to 180° was only 4.2 kJ/mol at the CISD/TZ+2d level. To compress the angle to a value of 130°, the increase in energy was around 2.5 kJ/mol, illustrating the very flat nature of the siloxane bridge. A more recent study[293] of the potential energy surface of the H_3Si−O−SiH_3 model investigated the basis set dependence of the results. It turned out that the energy differences just mentioned are even too large. Considering basis sets in which the polarization space includes up to five d-functions and four f-functions, the conclusions were reached that the minimum Si−O−Si angle is larger than 145°, the barrier to linearization of this angle is smaller than 1.5 kJ/mol, and about 3 kJ/mol is necessary to strain the Si−O−Si angle to 130°.

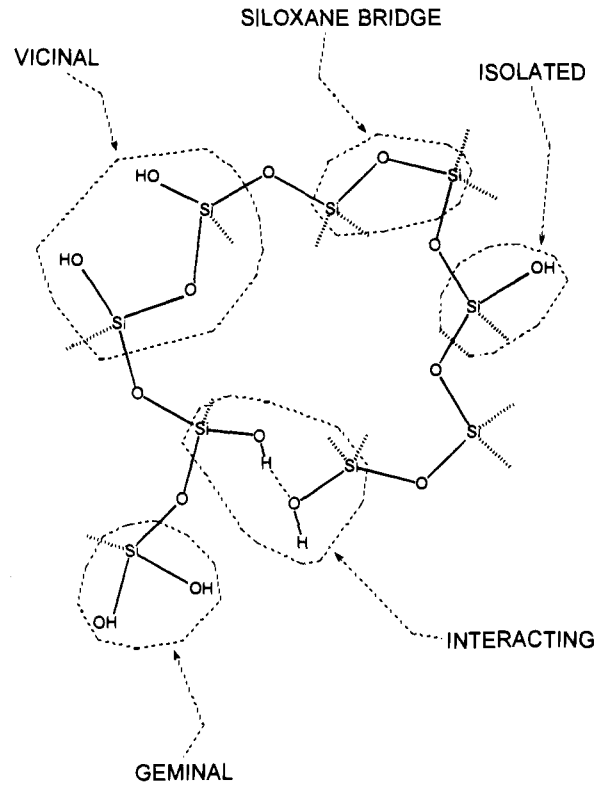

Figure 5. Structural schemes of various sites found at the hydrated amorphous silica surface.

Because of such flexibility, amorphous silica is also easily formed which consists of a network of such building blocks with a random distribution of the Si–O–Si angle centered around 140°. Peripheral SiO_4 groups carry OH groups, which terminate (this time in a physical sense) the unsaturated valencies. Figure 5 shows a structural model of amorphous silica, in which, besides the siloxane bridge, different types of surface hydroxyls have been identified. They differ either by the number of hydroxyl groups per Si atom (single and geminal) or by their spatial proximity (isolated, vicinal, and freely interacting). ^{29}Si CP/MAS NMR spectra show three silicon signals, namely that of the bulk silicon, the one due to silicon linked to one hydroxyl group, and, finally, that due to silicon carrying two hydroxyl groups.[294–297] The number of geminal species is a function of the preparation method and may reach some 15% of the whole population of isolated silanols, whereas the relative populations of isolated and vicinal sites is dependent on the thermal treatment of amorphous silica. Zhuralev[298] has shown that the number of total silanols per nm^2 is around 4.9, irrespective of both the kind of silica and the method of preparation. By increasing the temperature of treatment, the vicinal species react *via* elimination of a water molecule and form a new siloxane bond:

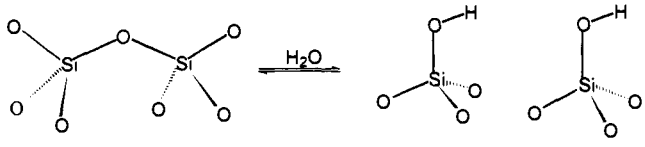

The number of surviving single silanol groups may be reduced to about 1 SiOH group per nm^2 at 973 K.

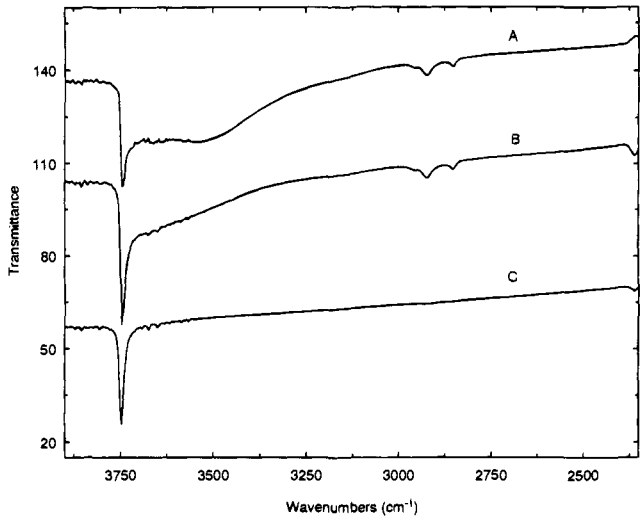

Figure 6. IR spectra of amorphous silica (Aerosil-Degussa 330 m^2/g) as a function of the temperature of treatment. Spectra recorded after heating the sample at the specified temperature for 1 h; weak bands in the 2900 cm^{-1} region are due to hydrocarbon impurities. (A) 373 K. (B) 573 K. (C) 973 K.

Such species are *isolated* as the average distance between two of them on the surface is about 10 Å.[299]

The IR spectrum of amorphous silica as a function of the temperature treatment is shown in Figure 6. H-Bonds between freely interacting species are the origin of a broad band in the OH stretch region which is typical of samples treated at low temperature. The sample dehydrated at 973 K shows only a very sharp band, attributed to the OH stretch of either isolated or geminal surface silanols. This is one of the three vibrational modes described in section II.C.3.[54,300]

As to the interaction of adsorbate molecules, as reported in section II, mainly IR spectroscopy is used. Knözinger reviewed the field[62] and reported IR spectroscopic data for more than 95 molecules; calorimetric data were also reported, when available. A more recent review is not available. The features of such interactions are those typical of hydrogen bonding. The surface hydroxyls play the role of a weak hydrogen donor and the adsorbed molecule assumes the role of the base. The well-defined peak at 3750 cm^{-1} and the transparency in the spectral region from 3700 to 2000 cm^{-1} is ideal for studying the formation and evolution of surface hydrogen bonds.

In the following we review the computational work done on the silica surface/adsorbate interaction, mainly at the *ab-initio* level within a cluster approach. The various structures resulting from the geometry optimization are gathered in Figure 7. Tables 8 and 9 provide additional information on structures and vibrational features, while Tables 10 and 11 show data related to binding energies. Observed data are in Table 12. Earlier data obtained by semiempirical methods and using cluster models terminated by pseudoatoms were reviewed by Zhidomirov and Kazansky.[191] We first review work on the surface species without any adsorbate. Section C is devoted to surface complexes of H_2O and CH_3-OH, both of which can act either as H-acceptor or H-donor with respect to surface hydroxyl groups.

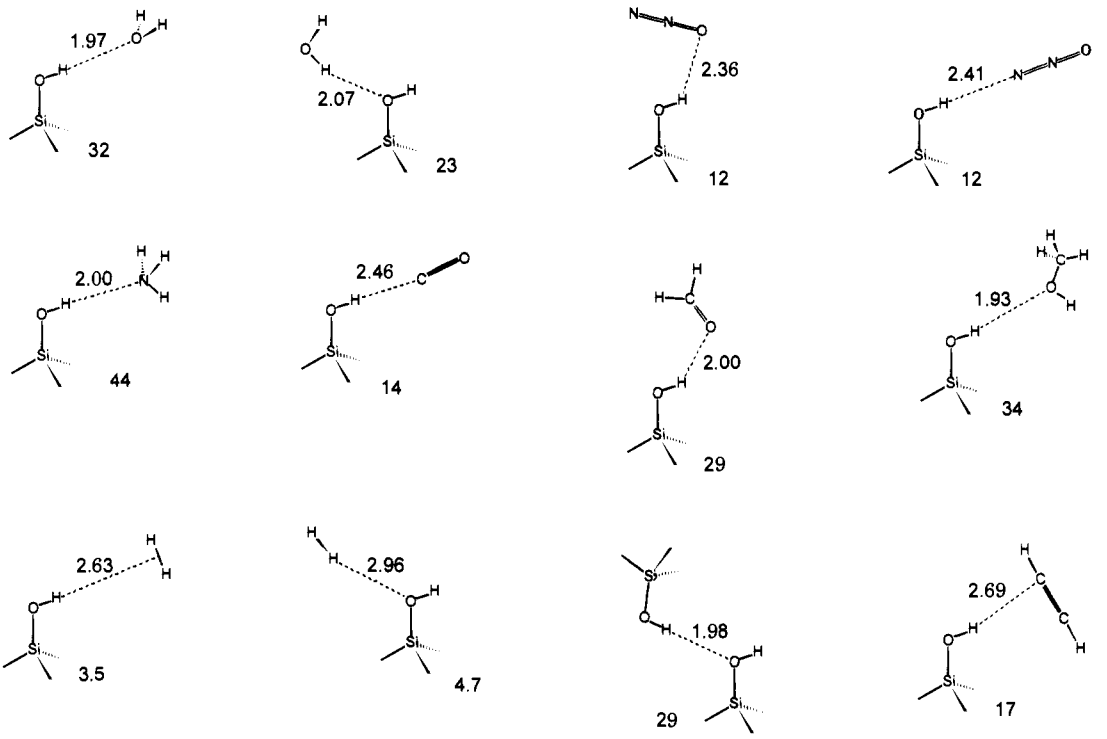

Figure 7. Structures of complexes between silanol and simple molecules. The intermolecular distances (Å) and binding energies (uncorrected for BSSE; kJ/mol) were obtained at the SCF/DZP and MP2/SCF/DZP levels. The results for H_3SiOH/H_2 refer to the DZ++(2p,2d) basis set.

Molecules which are H-bond acceptors on the silica surface are the subject of section D.

B. Surface Species without Adsorbate

Four different types of active sites have to be modeled by a properly chosen cluster: the siloxane bridge, isolated and geminal silanol groups, and hydroxyls in mutual interactions. The siloxane bridge has been studied by means of the smallest $H_3Si-O-SiH_3$ molecule, as already reported above. For the isolated and geminal hydroxyl species, three different clusters may be defined by different cutting procedures: a shell-0 cluster with dangling bonds on Si, a shell-1 cluster with dangling bonds on the oxygen atoms adjacent to Si, and finally a shell-2 cluster, where the Si atom is surrounded by three OSi groups and the outermost silicon atoms show unsaturated valencies. Virtually all calculations to date on this topic have adopted the hydrogen atom as a dangling bond saturator. For isolated silanol species, the shell-0, shell-1, and shell-2 clusters correspond to silanol (H_3SiOH), orthosilicic acid ($(HO)_3SiOH$), and trisiloxysilanol ($(H_3SiO)_3SiOH$), respectively (see Figure 3). Geminal sites are represented by corresponding molecules which carry two hydroxyl groups per Si atom: silanediol ($H_2Si(OH)_2$), again orthosilicic acid ($(HO)_2Si(OH)_2$), and disiloxysilanediol ($(SiH_3O)_2Si(OH)_2$).

Interacting surface species have not received much attention so far. If one considers the surface of hydroxylated amorphous silica, a large number of structures may be identified that bring two silanols in interaction. Such a situation is difficult to model. It is therefore interesting to examine the two extreme situations: (i) OH species sitting on adjacent Si atoms HO−Si−O−Si−OH (*vicinal* species); (ii) two SiOH groups in free contact. It appears that vicinal species are actually unable to establish a H-bond.[301] Although chains containing at least three silicon atoms such as (HO)Si−(O−Si−O)−Si(OH) can have a strong H-bonding ability, it has been preferred to study two H_3SiOH molecules in free interaction.[206,302]

The last site to be considered includes an isolated hydroxyl group and a nearby siloxane bridge. Even the simplest model, the $H_2Si(OH)-O-SiH_3$ molecule, is useful for the study of the extra stabilization gained when the adsorbate already H-bound to the OH group extends a second contact to the oxygen atom of the nearby siloxane group. Results on water adsorption will be reported in section VI.C.2. Of course, the shell-2 model may also serve that purpose, but the computational cost is much larger.

1. Models for Isolated Silanol Groups

Isolated silanol groups have been the subject of much computational work, due to their well-characterized structural and spectroscopical features. On highly dehydroxylated silica surfaces they cannot interact with each other and a molecular model may be adopted with confidence. Silanol is the simplest model: as a molecule, it is unstable with respect to condensation to disiloxane, though some features of it may be established experimentally.[303] It was thoroughly characterized from both a geometrical and a spectroscopical point of view in a series of papers[99,202,205,291,304,305] (cf. Table 5, section III.B). Anharmonicity of the OH bond has also been considered either by computing the potential energy resulting from stretching the OH bond and solving the corresponding monodimensional nuclear Schrödinger equation,[99,305] or in a perturbative approach at the SCF/6-31G* level.[306] While in the former case the OH mode was decoupled from all other normal

Table 8. Vibrational and Structural Features of Surface Complexes on Terminal Silanol Groups[a] (Wavenumbers in cm^{-1}, distances in Å)

model	method	vibrational features[a,b]		intermolecular features		ref
H_3SiOH/H_2O	DZP	$\Delta\delta$(HOH) $\Delta\nu(OH)_s$ $\Delta\nu(OH)_a$ ν(O···O)	$+21^D/0^A$ $-33^D/-2^A$ $-19^D/-5^A$ 104^A	SiOH···OH_2	1.97	98
H_3SiOH/H_2O	3-21G			SiOH···OH_2	1.74	188
$(HO)_3SiOH/H_2O$	6-31G*	$\Delta(\nu(OH)_s+\delta(HOH))$ $\Delta(\nu(OH)_s+\delta(OH)_{as})$	-17 -14	SiOH···OH_2	1.93	318
$(HO)_3SiOH/CH_3OH$	3-21G	$\nu'(CH_3)_{as}$ $\nu''(CH_3)_{as}$ $\nu(CH_3)_s$	$3023^A\ 2977^D$ $2977^A\ 2895^D$ $2869^A\ 2816^D$	SiOH···O(H)Me MeOH···O(H)Si	1.67 1.84	317
H_3SiOH/CH_3OH	6-31G**			SiOH···O(H)Me MeOH···O(H)Si	1.94 2.05	206
	DZP[c]	$\Delta\nu$(SiOH) $\Delta\delta$(COH) $\Delta\nu$(SiO) $\Delta\nu$(CO)	$+3^A\ +128^D$ $+55^A\ +44^D$ $-13^A\ +14^D$ $-27^A\ +10^D$	SiOH···O(H)Me MeOH···O(H)Si	1.93 2.06	
H_3SiOH/H_3SiOH	6-31G**			SiOH···O(H)Si	1.98	206
	DZP[c]	$\Delta\delta$(SiOH) $\Delta\nu$(SiO)	$+72^A\ +113^D$ $-32^A\ +10^D$	SiOH···O(H)Si	1.98	
H_3SiOH/NH_3	DZP	$\Delta\delta(NH_3)_s$ +98 $\Delta\delta(NH)_s$ −10	$\Delta\delta(NH_3)_a$ −1 $\Delta\nu(NH)_a$ −17	SiOH···NH_3 H_2NH···O(H)Si	2.00 2.39	328
F_3SiOH/NH_3	DZP	$\Delta\delta(NH_3)_s$ +134 $\Delta\nu(NH)_s$ −13	$\Delta\delta(NH_3)_a$ −2 $\Delta\nu(NH)_a$ −21	SiOH···NH_3	1.88	360
H_3SiOH/H_2CO	DZP	$\Delta\delta(CH_2)_s$ −2 $\Delta\nu(CH_2)_s$ +27	$\Delta\delta(CH_2)_a$ +39 $\Delta\nu$(CO) −17	SiOH···OCH_2	2.00	341
H_3SiOH/CO C-bound, O-bound	DZP	$\Delta\delta$(SiOH) $+21^C$ $\Delta\nu$(CO) $+25^C$	$\Delta\delta$(SiOH) $+16^O$ $\Delta\nu$(CO) -7^O	SiOH···CO SiOH···OC	2.46 2.26	345
H_3SiOH/CO C-bound, O-bound	6-31G*	$\Delta\nu$(CO) $+22^C$	$\Delta\nu$(CO) -13^O	SiOH···CO SiOH···OC	2.46 2.30	346
H_3SiOH/N_2O N-bound, O-bound	DZP	$\Delta\nu_3$ $+5^N$ $\Delta\nu_3$ $+20^O$	$\Delta\nu_1$ $+23^N$ $\Delta\nu_1$ -22^O	SiOH···ONN SiOH···NNO	2.36 2.41	351
H_3SiOH/H_2 T-shaped, F-shaped	6-31G**	$\Delta\nu$(H-H) $\Delta\delta$(SiOH)	$-12^T\ -10^F$ $+39^T\ +91^F$	SiOH···H_2^T H_2···O(H)Si^F	2.78 2.80	355
H_3SiOH/H_2 T-shaped, F-shaped	3-21G	$\Delta\nu$(H−H)	-21^T	SiOH···H_2^T H_2···O(H)Si^F	3.90^T 2.41^F	357
	6-31G**	$\Delta\nu$(H−H)	-14^F	SiOH···H_2^T H_2···O(H)Si^F	4.40^T 2.80^F	356
	MP2/6-31G**			SiOH···H_2^T H_2···O(H)Si^F	3.99^T 2.57^F	
H_3SiOH/C_2H_2	DZP MP2/DZP	$\Delta\nu$(CC) −4 $\Delta\nu$(CC) −4	$\Delta\nu$(CH) −7 $\Delta\nu$(CH) −11	SiOH···C SiOH···C	2.69 2.38	367

[a] Superscripts A and D identify the adsorbed molecule as H-acceptor or H-donor with respect to the surface OH group. [b] Shifts of the harmonic vibrational frequencies relative to those computed for the isolated molecules. [c] On the O-atoms a value triple-ζ basis set was employed.

modes, in the latter coupling with the Si−O stretch and Si−O−H bend was included. Both methods yield results around 80 cm^{-1}, in excellent agreement with the experimental value of 90 ± 15 cm^{-1}.[53,55,307] The rotation barrier around the Si−O bond has been measured to be 3.8 ± 0.3 kJ/mol,[300] a value very close to 2.4 kJ/mol computed at MP2/DZP//SCF/DZP.[305]

The GPA of silanol has been the target of a number of papers.[204,308,309] The best value obtained so far is 1531 kJ/mol, obtained using a high computational level (Coupled Electrons Pairs Approximation) and with a large [6s,5p,2d,1f/8s,5p,3d,1f/3s,2p] basis set for Si/O/H atoms, respectively.[204] The computed GPA is in excellent agreement with the recent experimental measurement of 1502 ± 21 kJ/mol by Damrauer *et al.*[303]

The shell-1 model $Si(OH)_4$ has been also used in the past[86,188,304,310−315] by a number of authors and more recently by Pelmenschikov *et al.*[316−318] Details about the geometry, conformation preference of the OH groups, and vibrational features of orthosilicic acid were established by quantum mechanical treatment at the SCF level with basis sets ranging from 4-31G to TZ(O)/DZP. Recently, Pelmenschikov *et al.*[316] have used a scaling procedure for correcting the SCF/3-21G force constant of the OH bond in a series of shell-1 models, namely $Si(OH)_4$, $OP(OH)_3$, $B(OH)_3$, and $H_2OAl(OH)_3$, mimicking various hydroxyls at the surface of the corresponding oxide: the agreement with the experiment was within a few percent. The adoption of a larger model (shell-2 type) is very tempting, but due to high costs of the calculation no

Table 9. Vibrational and Structural Features of Surface Complexes on Geminal Silanol Groups (Vibrational data in cm^{-1}, distances in Å)

model	method	vibrational features[a]		geometrical features		ref
$H_2Si(OH)_2/H_2O$	DZP	$\Delta\nu(OH)_s$	−36	SiOH···OH_2	2.185	321
		$\Delta\nu(OH)_{as}$	−25	HOH···O(H)Si	2.267	
$(HO)_2Si(OH)_2/H_2O$	6-31G*	$\Delta(\nu(OH)_s+\nu(HOH))$	−21	SiOH···OH_2	1.98	318
		$\Delta(\nu(OH)_s+\nu(OH)_{as})$	−30	HOH···O(H)Si	2.12	
$(HO)_3SiOH/CH_3OH$	3-21G	$\nu'(CH_3)_{as}$	2994			317
		$\nu''(CH_3)_{as}$	2949			
		$\nu(CH_3)_s$	2851			
$H_2Si(OH)_2/NH_3$	DZP	$\Delta\delta(NH_3)_a$	−8	SiOH···NH_3	1.997	321
		$\Delta\nu(NH)_s$	−15			
		$\Delta\nu(NH)_a$	−14			

[a] Shifts of the harmonic vibrational frequencies are relative to those computed for the isolated molecules.

data were published so far. In section VI.E some data on the shell-2 model will be discussed. Very recently, Sauer and Hill[319] used much larger, cagelike models of the composition $(Si_8O_{12})(OH)_8$ and $(Si_8O_{12})H_7$-OH to study the dependence of calculated results for isolated silanol groups on the cluster size.

2. Models for Geminal Species

Geminal sites have been the aim of early[320] and more recent studies.[321] Models include silanediol ($H_2Si(OH)_2$), orthosilicic acid, and $(H_3SiO)_2Si(OH)_2$. The energetics involved in the conformational changes due to rotation of the two hydroxyl groups around the corresponding Si−O bond have been studied in detail;[321] the absolute minimum is attained for a gauche−gauche (GG) conformation. This was verified for both shell-0 and shell-2 models. Harmonic OH stretch frequencies were computed at the SCF/DZP level to be 4244 and 4246 cm^{-1}, few wavenumbers lower than the value of 4250 cm^{-1} computed for the H_3SiOH model of the isolated silanol group. This is in fair agreement with the experimental IR spectra, which indicate that IR modes of geminal silanols are indistinguishable from those of the isolated silanol and fall around 3748 cm^{-1}.[322,323] In contrast with what is sometimes stated,[62] there is no H-bonding interaction between the two hydroxyls.

3. Models for Interacting Silanol Groups

Only three computational studies have been reported dealing with self-interacting sites. In the first two[206,302] a pair of freely interacting H_3SiOH molecules has been considered. SCF/3-21G calculations predicted a shift of 224 cm^{-1} of the harmonic OH stretch engaged in the H-bond,[302] while calculations at the SCF/DZP level[206] predict a shift of only 120 cm^{-1}. These values are to be compared with the experimental datum of 230 cm^{-1}, resulting from a broad band centered at 3520 cm^{-1} present in the IR spectra of hydroxylated silica samples.[62] The $\Delta H°$ was −18 kJ/mol at the MP2//SCF/DZP level including corrections for the BSSE.

In a recent work,[324] longer chains of mutually interacting silanols were considered and the cooperative effect to the binding was computed for a string of up to four silanols at the SCF/MINI-1 level. The binding energy (BSSE corrected) for the addition of one silanol to another silanol molecule and to a chain of two and three interacting silanol molecules was 22, 29, and 32 kJ/mol, respectively. Cooperative effects are the reason for such a trend even if a *plateau* is quickly reached. The same effects cause an increase in the acidity of the terminal OH group which is still able to form H-bonds with adsorbed molecules.

C. Interaction with H-Acceptor/H-Donor Molecules

1. Interaction with NH_3

The interaction of ammonia with shell-0 and shell-1 models was studied in the past with the 3-21G basis set and assuming rigid structures.[188,202,325] A binding energy of 56 kJ/mol was computed. Hertl has measured an isosteric heat of adsorption of 37 kJ/mol.[326] By means of microcalorimetry, Fubini *et al.* have measured the heat of adsorption of NH_3 adsorbed on a number of different amorphous and crystalline silicas.[324,327] The range of values of highly dehydrated samples was between 15 to 60 kJ/mol, for high and low coverage, respectively.

From the computational point of view, Ugliengo *et al.*[328] have adopted basis sets ranging from DZ(d,p) to TZ(2d,2p) and electron correlation has been included at the MP2 level. The final computed $\Delta_a H°_{300}$ was −29 kJ/mol, in reasonable agreement with the observed data, even if definitely underestimated. Indeed, the computed $\Delta_a G°_{300}$ value of 7.3 kJ/mol is definitely too large because the corresponding computed $p_{1/2}$ is unreasonably high ($\approx 2 \times 10^6$ Pa) when compared with the few kPa of NH_3 needed to do the experiment. The equilibrium structure in which ammonia acts as hydrogen donor was also calculated, but almost no binding was found, which confirms the limited ability of NH_3 to donate its hydrogens. Vibrational features were computed within the harmonic approximation only. The shift of the SiO−H stretching harmonic frequency caused by hydrogen-bond formation was computed to be −279 cm^{-1}.[328] Numerical calculation of the shift of the fundamental $\Delta\nu_{OH}$ gave −416 cm^{-1} at the SCF/DZ(d,p) level, which became −572 cm^{-1} at the MP2//SCF/DZP level.[328] Experimentally, a value of −950 cm^{-1} obtained at 4 K[68] was recently reported. These results show that anharmonicity and electron correlation are extremely important if strict comparison with experiment is desired. In order to shed some light on this relevant problem, we intend to study the H_3SiOH/NH_3 system

Table 10. *Ab Initio* Results on Surface Complexes of Terminal Silanol Groups:[a] Interaction Energy, ΔE, and Heat of Adsorption, $-\Delta H^c$ in kJ/mol, Shift of the O–H Donor Stretch Mode in cm^{-1}

model	method	$-\Delta E^{a,b}$	$-\Delta H^c(T)^{a,c}$	$\Delta\nu_{OH}{}^d$	ref
H_3SiOH/H_2O	DZP	17^D 26^A		-25^D -134^A	98
	TZ+(2p,2d)	13^D 20^A			
	MP2//SCF/DZP	23^D 32^A	16^D 25^A	-194^A	
	MP2//SCF/TZ+(2p,2d)	19^D 26^A	12^D 19^A		
$Si(OH)_4/H_2O$	4-31G+corr.[e]	27^A	18^A		329, 86
	QPEN (4-31+corr.[e])	28.5 ± 4^A	21 ± 4^A		320
	QPEN(MINI-1)	31	22		308
H_3SiOH/H_2O	6-31G(d on Si)	20^D 36^A			334
H_3SiOH/H_2O	3-21G	56^A		-336	188
$(HO)_3SiOH/H_2O$	6-31G*	26.4^A		-146	318
	6-31G**//6-31G*	25.9^A			
	MP2/6-31G**//6-31G*	30.4^A			
$(HO)_3SiOH/CH_3OH$	3-21G	57^A 35^D			317
	6-31G*	30^A 16^D			
			$T = 0$		
H_3SiOH/CH_3OH	6-31G**	29^A 18^D			206
	DZP[f]	27 [24]^A 17 [15]^D		-159^A -58^D	
	MP2//SCF/6-31G**	38^A 26^D			
	MP2//SCF/DZP[f]	34 [28]^A 23 [18]^D	[22]^A [13]^D		
			$T = 0$		
H_3SiOH/H_3SiOH	6-31G**	24			206
	DZP[f]	22 [19]		-130^A	
	MP2//SCF/6-31G**	32			
	MP2//SCF/DZP[f]	29 [23]	[18]		
H_3SiOH/H_3SiOH	3-21G			-224^A -35^D	302
H_3SiOH/NH_3	3-21G	56^A		-419^A	188
	DZP	33^A 7^D	24^A 3^D	-13^D -279^A	328
	TZ+(2p,2d)	26^A 5^D	17^A 1^D		
	MP2//SCF/DZP	44^A 11^D	35^A 7^D		
	MP2//SCF/TZ+(2p,2d)	37^A 9^D	28^A 5^D		
			$T = 0$		
F_3SiOH/NH_3	DZP	47^A	37^A	-464^A	360
			$T = 170$		
H_3SiOH/H_2CO	DZ(p,d)	22 [20]	17	-129	341
	DZ+(2p,2d)	21 [19]	15		
	MP2//SCF/DZP	29 [23]	23		
	MP3//SCF/DZP	27	22		
H_3SiOH/CO C-bound	3-21G	16^C		-15^C	188
			$T = 77$		
H_3SiOH/CO	6-31G*	8^C 6^O	3^C 2^O		345
	DZ(p,d)	8^C 6^O	3^C 1^O	-29^C $+2^O$	
C-bound; O-bound	MP2//SCF/6-31G*	15^C 9^O	9^C 5^O		
	MP2//SCF/DZP	14^C 9^O	9^C 4^O		
	CASSCF//SCF/DZP	10^C 4^O	5^C -1^O		
H_3SiOH/CO	6-31G*	8^C 7^O		-6^C $+3^O$	346
C-bound, O-bound	MP2//SCF/6-31G*	14^C 9^O			
			$T = 0$		
H_3SiOH/N_2O	DZP	5 [3]^N 11 [10]^O		-2^N -29^O	351
N-bound, O-bound	MP2//SCF/DZP	12^N 12^O	9^N 9^O		
H_3SiOH/H_2	6-31G**	0.8 [0.6]^T 2.2 [0.7]^F		0^T -2^F	355
	DZ++(2p,2d)	1.2 [0.7]^T 2.2 [0.7]^F			
	TZ(2p,2d)	0.9 [0.8]^T 1.2 [1.0]^F			
T-shaped	MP2//SCF/6-31G**	1.2 [0.9]^T 4.0 [1.4]^F			
F-shaped	MP2/SCF/DZ++(2p,2d)	3.5 [1.5]^T 4.7 [1.9]^F			
	MP2//SCF/TZ(2p,2d)	2.0 [1.7]^T 2.4 [1.9]^F			
H_3SiOH/H_2	3-21G	1.1^T 8^F		-5^F	357
T-shaped	6-31G**	0.2^T 2^F		-2^F	356
F-shaped	MP2/6-31G**	1.1^T 4^F			
	CISD/6-31G**	3.2^F			
			$T = 0$		
H_3SiOH/C_2H_2	DZP	8.6 [7.5]	5.7 [4.6]	-39	367
	MP2/DZP	16.5 [9.6]	12.6 [5.7]	-73	

[a] Superscripts A and D identify the adsorbed molecule as H-acceptor or H-donor with respect to the surface OH group. [b] Energies corrected for BSSE in brackets. [c] Heats of adsorption computed at $T = 298$ when not otherwise specified. [d] Shifts of the harmonic vibrational frequencies relative to those computed for the isolated molecules. [e] BSSE + estimate of dispersion energy + multiple correction, ref 329. [f] On the O-atoms a valence triple-ζ basis set was employed.

Table 11. *Ab Initio* Results on Surface Complexes of Geminal Silanol Groups and Siloxane Bridges: Interaction Energy, ΔE, and Heat of Adsorption, $-\Delta H^c$, in kJ/mol, Shift of the O–H Donor Stretch Mode in cm^{-1}

surface site	model	method	$-\Delta E^{a,b}$	$-\Delta H^c(T)^{a,c}$	$\Delta\nu_{OH}{}^d$	ref
geminal hydroxyl	$(OH)_3SiOSi(OH)_3/H_2O$	QPEN(MINI-1)	24	17		308
				$T = 0$		
	$H_2Si(OH)_2/H_2O$	DZP	31 [28]	21 [18]	−93 −18	321
		MP2//SCF/DZP	43 [35]	32 [25]		
	$(HO)_2Si(OH)_2/H_2O$	6-31G*	37.3		−111	318
		6-31G**//6-31G*	36.5			
		MP2/6-31G**//SCF/6-31G*	47.1			
	$(HO)_3SiOH/CH_3OH$	3-21G	77			317
		6-31G*	39			
				$T = 0$		
	$H_2Si(OH)_2/NH_3$	DZP	35 [32]	24 [21]	−287	321
		MP2//SCF/DZP	47 [39]	36 [28]		
siloxane bridge	$(H_3Si)_2O/H_2O$	QPEN (4-31G+corr.[a])	25.5 ± 4	19 ± 4		308

[a] Superscripts A and D identify the adsorbed molecule as H-acceptor or H-donor with respect to the surface OH group. [b] Energies corrected for BSSE in brackets. [c] Heats of adsorption computed at $T = 298$ when not otherwise specified. [d] Shifts of the harmonic vibrational frequencies relative to those computed for the isolated molecules.

Table 12. Observed Data for the Interaction of Molecules with Amorphous Silica Surface Sites:[a] Heat of Adsorption, $-\Delta_a H°$, in kJ/mol, Shift of the Donor OH Stretch Band and Other Vibrational Features in cm^{-1}

adsorbate	method	$-\Delta_a H°(T)^b$	$\Delta\nu_{OH}{}^c$	other vibrational features	ref
H_2O	adsorption techniques (heat of immersion)	25			368
H_2O	adsorption techniques (microcalorimetry)	15–45			324, 327, 331–333
H_2O	adsorption techniques (isosteric heat on silicalite)	25			330
H_2O	IR		−85		53
H_2O	diffuse reflectance		−130	$\Delta(\nu(OH)_s+\delta(HOH))$ −19	335–337
			−200	$\Delta(\nu(OH)_s+\nu(OH)_{as})$ −25	
H_2O	FIR			$\nu(O\cdots O)^w$ 225	39
NH_3	adsorption techniques (isosteric heat)	37			326
NH_3	adsorption techniques (microcalorimetry)	15–60			324, 327
NH_3	FTIR, $T = 298$ K		−650	$\Delta\nu(NH_3)$ + 100^s -27^a	63–67
				$\Delta\delta(NH)$ -17^s -44^a	
NH_3	IR, $T = 4$ K		−950		68
CH_3OH	adsorption techniques (microcalorimetry)	55–65			324
CH_3OH	IR		200	$\nu'(CH_3)_{as}$ 3000 $\nu''(CH_3)_{as}$ 2950	340
				$\nu(CH_3)_s$ 2845	
CO	IR		−78	$\Delta\nu(CO)$ +14 $\Delta\nu(SiOH)$ +25	348
CO	adsorption techniques (isosteric heat)	11			347
N_2O	FTIR		−38 −20	$\Delta\nu_3$ +4 $\Delta\nu_1$ +11, +3	351
CH_2O	FTIR		−210	$\Delta\nu(CH_2)$ +1 $\Delta\nu(CH_2)_a$ +51	342
				$\Delta\nu(CH_2)_s$ +47 $\Delta\nu(CO)$ −21	
H_2	FTIR		−6	$\Delta\nu(HH)$ −24	355
C_2H_2	FTIR		−120	$\Delta\nu(CC)$ −12	367

[a] Reader should refer to the original references for details about the sample preparation and the temperature of treatment. [b] Calorimetric heats of adsorption ($q = -\Delta_a H$) refer to $T = 303$ K. Higher values in a given range are attained in the limit of zero coverage; lower values are for higher coverage. [c] Shifts of the vibrational frequencies relative to those observed for the isolated molecules.

with basis sets of the same quality as those which have been used to compute the GPA of H_3SiOH and which gave, for that quantity, a value in excellent agreement with experiment. MP2 harmonic frequencies and anharmonic calculation of the OH frequency stretch are also planned.

2. Interaction with H_2O

The largest share of the studies addressed the interaction of water with the siloxane bridge, isolated and geminal silanol groups. In the following we use the notation WD and WA to refer to water interacting with silanol as either H-bond donor (WD) or H-bond acceptor (WA). Bifurcated configurations may also be formed. Such complexes were studied in the early 1980's by adopting shell-0 and shell-1 models, but due to limited computer facilities, relatively poor basis sets were used.

SCF/4-31G calculations on the $H_2O/(H_3Si)_2O$ cluster were also performed[329] with the purpose of deriving QPEN potential parameters (Quantum mechanical Potential based on Electron pairs and Nuclei); a

binding energy of 26 ± 4 kJ/mol was obtained which corresponds to a $-\Delta H°_{298}$ of 19 ± 4 kJ/mol. A binding energy of 24 kJ/mol was reported by the same authors at the QPEN-SCF/MINI-1 level on the larger $(HO)_3SiOSi(OH)_3$ model. This is in reasonably good agreement with the isosteric heat of adsorption of 25 kJ/mol of water in silicalite[330] and with the heats of adsorption (from 15 to 45 kJ/mol for high and low coverage, respectively) obtained by a microcalorimetric study of water interacting on a variety of pyrogenic silicas dehydrated at high temperature.[324,327,331-333] Obviously, due to the relevance of both water and the siloxane bridge for adsorption studies on zeolites and silicas, it would be desirable to have at hand results with much better basis sets inclusive of electron correlation. The main conclusion reached was that the siloxane bridge is unable to break the $H_2O\cdots H_2O$ dimer bond, in agreement with the hydrophobicity of the siloxane bond.[299] It was also concluded that isolated silanols were only marginally able to compete with the strength of the H-bond of the water dimer. Dissociation of the water dimer is easier if some assistance is provided either by a nearby strained siloxane bridge or by another silanol.

More recent papers have extended these early findings about the interaction of water molecules with isolated and geminal silanol sites.[98,318,321,334] Gibbs *et al.*[334] adopted a 6-31G(d on Si only) basis set for studying the interaction between H_2O and H_3SiOH. The interaction energies (no BSSE correction) for the H-bond acceptor (WA) and H-bond donor (WD) structures of H_2O were −20 and −36 kJ/mol, respectively. The adsorption of two water molecules per site was also studied. A ring-like structure was considered, but no analysis of the energetics was made. Due to the lack of polarization functions on oxygen and hydrogen atoms, the intermolecular distances are too short and the binding energies overestimated due to dipole moments that are too large. In ref 98 basis sets from DZ(d,p) to TZ++(2d,2p) were adopted and the best estimates of the relative binding energies of WA and WD structures on silanol obtained at MP2/TZ++(2d,2p)//SCF/DZP were 19 and 26 kJ/mol, respectively. Corresponding SCF/TZ++(2d,2p)//SCF/DZP values are 13 and 20 kJ/mol, respectively. The bifurcated structure was found to spontaneously collapse to the WA structure during the optimization process. The BSSE corrections to the binding energies were within 5−8% of the uncorrected values at the SCF level, whereas at the MP2 level they were about 20−30% of the uncorrected value. Of course, the relatively large BSSE indicates that such basis sets still do not properly account for electron correlation. The thermodynamic functions of the relevant equilibria were also obtained and comparison was made with the dimerization of water, following the suggestion of Hobza *et al.*[86] It was found that the equilibrium

$$(H_2O\cdots H_2O)_{gas} + (H_3SiOH)_{surf} \rightleftharpoons (H_3SiOH\cdots OH_2)_{surf} + (H_2O)_{gas}$$

was characterized by a $\Delta G°$ value of 0.65 kJ/mol, which confirms previous findings about the ability of silanol to break the H-bond of the water dimer. The equilibrium between WD and WA structures is such that the share of WD structures is at the most about 4% of the total coverage, ruling out water as proton donor at the silica surface.

In the case of water, IR spectra are difficult to interpret because the OH modes of H_2O and SiOH fall in the same narrow range. It is not possible to determine even the basic feature, i.e. the $\Delta\nu_{OH}$ of silanol engaged in H-bonding. There are some indications from measurements in the overtone region that $\Delta\nu_{OH}$ should be larger than 200 cm^{-1}.[53,335-337]

The vibrational features of the H_3SiOH/H_2O system have been calculated, mainly at the harmonic level.[98] However, the same authors[98] have treated anharmonically the SiO−H stretch, following a similar procedure as already described for the study of the anharmonicity of the O−H bond in the H_3SiOH.[99] The shifts of the harmonic and the fundamental frequencies and of the anharmonicity constant computed at the MP2//SCF/DZP level (TZP on O atoms) were $\Delta\nu°_{OH} = -194$ cm^{-1}, $\Delta\nu_{OH} = -234$ cm^{-1}, and $\Delta(\omega_e x_e) = 22$ cm^{-1}. The corresponding values at the SCF level were −129, −154, and 16 cm^{-1}, respectively, which shows that it is more important to include electron correlation than to make anharmonicity corrections to get reliable estimates of the OH shift.

The equilibrium constant calculated for the formation of WA surface complexes is 5.1×10^{-3} atm^{-1}, which corresponds to a pressure of 2×10^7 Pa for a coverage of half of these surface sites, when Langmuir behavior is assumed (cf. section III.D.4). This value is exceedingly large when compared with the value of the pressure at which extensive interaction with the silica surface is achieved in experiments. Possible reasons are that the H_3SiOH model is much less acidic than the real surface site (low ΔE values) or that the calculation of the entropic corrections by means of the semiclassical rigid-rotor harmonic oscillator method within the RCM approximation (see section III.D.4) is too crude and yields a too high ΔS value.

Another possibility is that a siloxane bridge, belonging to the same silicon atom to which the OH group is bound, will assist the binding of water by means of its nucleophilic oxygen atom. This problem has been recently addressed by Pelmenschikov *et al.*,[318] who adopted the orthosilicic acid (shell-1) model, i.e. the nearby Si−O−Si bridge was replaced by the Si−O−H moiety in their model. The highest computational level was MP2//SCF/6-31G* and the binding of water acting as hydrogen acceptor was 30 kJ/mol, in good agreement with the value of 32 kJ/mol computed at the MP2//SCF/DZ(d,p) level for the simplest shell-0 model[98] (both data are BSSE uncorrected). An extra stabilization of about 18 kJ/mol was then found for water which, at the same time, is acceptor for the H-atom of one hydroxyl group and donor of its H-atom to the nearby hydroxyl of the orthosilicic acid. The calculation was meant to model properties of the *terminal* OH group of silica but, in fact, they have modelled a possible structure relevant for the *geminal* site.

The problem of assessing the adsorption capability of geminal sites with respect to both water and

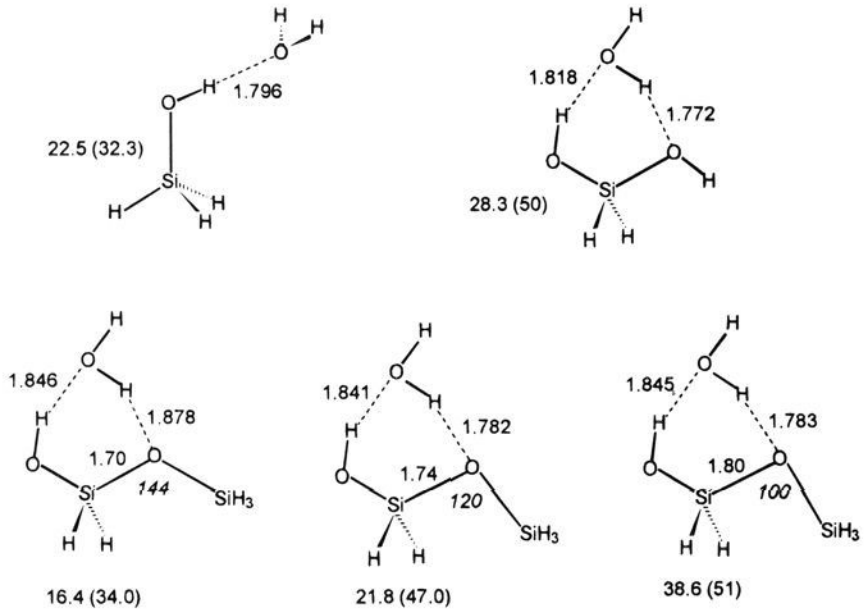

Figure 8. SCF/MINI-1 optimized complexes of water with shell-0 models of isolated and geminal silanol groups; also shown are structures in which a progressively strained nearby siloxane bond interacts with the H-atom of the adsorbed water molecule Bond lengths in angstroms, bond angles in degrees, binding energies in kJ/mol. BSSE-corrected binding energies are shown as bare numbers.

ammonia has recently been tackled,[321] following earlier suggestions.[320] With respect to water adsorption, a new structure has been determined at the SCF/DZP level in which water acts simultaneously as H-acceptor and as H-donor to a model of geminal sites. The shell-0 model silanediol ($(OH)_2SiH_2$), was adopted in a gauche−gauche (GG) conformation. The interesting feature of such a structure is its ability to add another water molecule without the need of a structure rearrangement. The increase of the binding energy with respect to the value of 32 kJ/mol computed for the H_3SiOH/H_2O complex is about 10.5 kJ/mol (MP2//SCF/DZP). BSSE corrections reduce this value to 7.7 kJ/mol and zero point energy corrections further to a mere 4.3 kJ/mol. A similar analysis of the data reported in ref 321 for the structure closest to that proposed by Pelmenschikov shows that the increase in binding with respect to H_3SiOH/H_2O is a mere 3.6 kJ/mol. Furthermore, only the GG conformation is likely to be present at the surface, due to the energetic cost for assuming a different conformation.

To understand how a nearby siloxane bridge may possibly extrastabilize the interaction of water with the terminal OH group, Ferrari[338] has done a series of calculations on the $H_3SiOSi(OH)H_2\cdots H_2O$ model (cf. Figure 8) using the MINI-1 basis set, which has been shown to give binding energies of DZP quality when BSSE corrections are made[101,102] (cf. section III.B). Figure 8 gathers relevant structural and energetic data, both corrected and uncorrected for BSSE for an isolated site, a geminal site, and a series of structures in which a siloxane bond is engaged in hydrogen bonding with the adsorbed water molecule. The angle Si−O−Si was constrained to 144° (average value in silica), 120° (typical of a strained ring), and 100° (typical of a seriously strained defect on the surface). The binding for the almost unstrained siloxane bond is 27% *less* than that resulting from the interaction with H_3SiOH. A comparable value results indeed for the structure with the Si−O−Si angle set to 120°, whereas the most strained structure shows a definite 70% increase in the binding

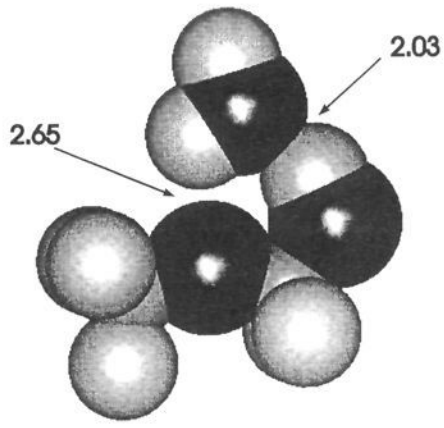

Figure 9. van der Waals representation of the SCF/DZP (*valence TZ on O-atoms*) *optimized structure of* H_2O *bound* to a $H_3SiOSiH_2OH$ model. Reported are intermolecular H···O distances in angstroms.

energy. The BSSE is large, but the same trend is found for uncorrected data. To further check the reliability of the MINI-1 results, we have made a series of calculations using a TZ(O)/DZP basis set. The structures were optimized (C_s symmetry), and very good agreement was found with respect to the MINI-1: the binding energy (BSSE corrected) for the double bonded structure was 17 kJ/mol, whereas a value of 23 kJ/mol was found for the open structure. Single point MP2//SCF/DZP calculations yielded values of the binding energy, corrected for the BSSE, of 24 and 26 kJ/mol, respectively. Comparison with the value of 27 kJ/mol obtained for the H_3SiOH/H_2O complex at the MP2//SCF/DZP level[339] shows that there is no extrastabilization due to a siloxane bridge. Figure 9 shows the van der Waals representation of the structure: the water molecule experiences a nonspecific interaction with the siloxane bridge as penetration of the van der Waals spheres of the H and O atoms does not occur. Such results show that a nearby *unstrained* siloxane bridge is not playing a significant role in stabilizing surface complexes of water on terminal OH groups on silica surfaces.

3. Interaction with CH_3OH

The interaction of methanol with isolated silanol groups has been addressed in two studies.[206,317] Pelmenschikov *et al.*[317] performed geometry optimizations at the SCF/3-21G level, because they were mainly concerned with the absolute prediction of the frequency shifts of the C−H modes; a shell-1 model was considered and the scaling procedure proposed by the same authors[316] was adapted to the harmonic frequencies. They considered a cyclic structure in which CH_3OH acted as both proton donor and acceptor with respect to terminal hydroxyls of orthosilicic acid. For the same reasons discussed above for water adsorption, this conformation seems to be more relevant for *geminal* species rather than for a true *isolated* silanol. The binding energy for methanol acting as hydrogen donor was 35 kJ/mol, in comparison with the value of 57 kJ/mol when acting as hydrogen acceptor. For the cyclic structure, a binding energy of 77 kJ/mol was computed. Neither BSSE corrections nor shifts of the SiO−H frequency were reported. The preference of silanol to behave as hydrogen donor in H-bonds with methanol has been carefully analyzed by Ugliengo *et al.*[206] Geometry optimizations on all possible dimers between silanol (S) and methanol (M) were done at the SCF

level using 6-31G** and DZP (valence TZP on O atoms) basis sets. Single point calculations at the MP2 level and BSSE correction yielded the following estimate of the order of stability for the different dimers: SM > SS ≥ MM > MS, with final $-\Delta H^\circ_0$ values of 22, 18, 16, and 13 kJ/mol, respectively. Values of 29 and 18 kJ/mol were reported by Pelmenschikov *et al.*[318] for the SM and MS dimers, respectively, at the SCF/6-31G** level. Comparison of these numbers with the 3-21G results of Pelmenschikov *et al.* show that the latter are affected by a huge BSSE as pointed out in section III.B.

Ugliengo *et al.*[206] have also shown that the binding is mainly due to electrostatic interactions. The classical Coulombic energies between potential-derived off-center charges on the molecules and *ab-initio* computed binding energies correlate indeed fairly well. The harmonic SCF/DZP (TZP on O atoms) shift computed when silanol is acting as proton donor with respect to methanol was 150 cm^{-1}, while a value of 250 cm^{-1} was measured by Borello *et al.*[340] Calorimetric measurements of the heat of adsorption of CH_3OH on a highly dehydrated pyrogenic silica yielded values in the range 55–65 kJ/mol.[324]

D. Interaction with H-Acceptor Molecules

1. Molecules with Free Lone Pairs

The adsorption of formaldehyde is of interest because it mimics the keto group of the amido moiety in proteins. A computational study concerning the H_3SiOH/CH_2O structure was carried out;[341] IR data at 170 K of the interaction of CH_2O on amorphous silica were also reported.[342] The computed harmonic vibrational frequencies were in fair agreement with those measured. For the most relevant one, the SiO–H stretch, a red shift of 129 cm^{-1} was predicted, while the observed shift was 210 cm^{-1}. Experimental data on the heat of adsorption are not available, but comparison with related systems, in particular the complexes of FH, HCl, and H_2O with H_2CO, allowed us to place H_3SiOH inbetween FH and HCl, as far as its ability to form H-bonds is concerned. The conformation of the adduct follows the Legon–Millen rules:[343,344] the axis of the lone pair protruding outside the oxygen of H_2CO is aligned to the O–H axis of the acidic H_3SiOH. This structure ensures the best match of the negative and positive regions of the molecular electrostatic potential (MEPs) of each subunit. However, large amplitude motions were shown to occur, even at a very low temperature. For instance, H_2CO can rotate in the SiOH plane (perpendicular to its main axis) by as much as 50° around its minimum position, increasing the total energy by no more than 1.5 kJ/mol, an energy which is readily available already at 170 K. Hence, anharmonicity corrections to the intermolecular frequencies are expected to play a significant role in the calculation of the entropy corrections to the binding, a topic which has not received enough consideration so far.

Adsorption of the weakly polar CO and N_2O molecules was also studied. Both molecules may be protonated at both ends, and HCO^+, COH^+, $HNNO^+$, and $NNOH^+$ species do indeed exist. When engaged in hydrogen-bond interactions or adsorbed on cations at the surface of ionic crystals, both molecular ends will be able to interact (see section IV). The experimental evidence for the CO molecule is, however, that it will adsorb exclusively via the C end on both silica and ionic surfaces. Instead, data for N_2O show that both molecular ends can interact with the surface, depending on the very nature of the actual site.

From the computational point of view, previous studies about CO/silica interaction by Geerlings *et al.* used small basis sets and were far from being conclusive.[188] Ugliengo *et al.*[345] studied the H_3SiOH–CO complex of CO with the SCF, CASSCF, and MP2 methods. A range of basis sets from 3-21G to TZP was employed. Bates *et al.*[346] studied complexes not only with H_3SiOH but also with zeolitic Brønsted acidic sites ($H_3SiO(H)AlH_3$) as well as with Lewis Al$(OH)_3$ sites. The calculations were carried out at the SCF and MP2 levels with the 6-31G* basis set. Good levels of theory (electron correlation is mandatory) and large basis sets are needed to discriminate between the O-down and the C-down adsorption structures of CO. Heats of adsorption computed at the MP2//SCF/DZP level were about 9 and 4 kJ/mol for the C-down and O-down structures, respectively. Larger values, 14 and 8 kJ/mol, respectively, were obtained at the MP2//SCF/6-31G* level.[346] The experimental heat of adsorption was estimated by Beebe *et al.*[347] to be about 11 kJ/mol by spectroscopic means. Experimental IR results are $\Delta\nu$(SiO–H) = -78 cm^{-1} and $\Delta\nu$(CO) = 14 cm^{-1}.[348] The corresponding SCF/DZP values are -29 and 25 cm^{-1} for the C-down structure. At the SCF/6-31G* level, a much smaller shift of -6 cm^{-1} was computed for the SiO–H mode whereas a shift of 22 cm^{-1} was predicted for the CO stretch.[346] Preliminary calculations at full MP2/DZP performed by some of us[349] showed that the $\Delta\nu$(SiO–H) and the $\Delta\nu$(CO) shifts become -52 and 20 cm^{-1} for the C-down structure; corresponding values for the O-down structure were 7 and 4 cm^{-1}, respectively. The comparison of calculated and experimental vibrational features leaves no doubt that only the C-down configuration occurs, though the corresponding binding energies are not so clear-cut. As in the case of ionic solids, for CO the level of treatment must necessarily go beyond SCF, otherwise the correct polarity of the CO dipole is not reproduced (cf. Table 4). This is clearly seen from the MEP published by Luque *et al.*:[350] two minima are found, one at the C end and the other at the O end, the corresponding MEP values differ by a factor larger than 2.

Similar considerations apply to the study of the N_2O/silica interaction.[351] The experiment carried out simultaneously with the calculations suggests that the interaction is weak and that adsorption takes place at both molecular ends. Indeed, the heat of adsorption obtained by spectroscopic means is around 8 kJ/mol, *i.e.* of the order of the heat of condensation of N_2O itself. The calculation showed that electron correlation is essential for establishing the relative propensity to bind *via* the oxygen or nitrogen end. Møller–Plesset perturbative treatment is, however, not completely satisfactory because the Hartree–Fock solution is not a good starting point for describ-

ing the electronic state of N_2O. The best $\Delta H°_0$ values computed at MP2//SCF/DZP were about the same (−9 kJ/mol) for O-bound and N-bound complexes, respectively. Clearly, both ends were predicted to bind to the surface, a fact which is also suggested by the experimental shifts of the ν_3 and ν_1 frequencies of N_2O. Poor agreement was found when SCF/DZP shifts were compared with experiment. This was expected, because of the rough description of the binding by the SCF approximation, which strongly favored the O-bound complex. The relevance of electron correlation was shown by computing the SCF and MP2 molecular electrostatic potential for N_2O with the DZP basis set in the van der Waals region around the molecule. Minima in the MEP were located at both ends, their values being −33 (−69) kJ/mol around the N-atom and −83 (−41) kJ/mol around the O-atom at SCF (MP2) levels, respectively. Clearly, electron correlation is reversing the relative order of the minima.

2. Molecules with σ and π Bonds

Molecular hydrogen is the simplest probe molecule for assessing the physicochemical properties of various surface sites in zeolites and silicas.[352] Its interaction with silica is also of technological relevance, because H_2 trapped in SiO_2-based optical fibers is known to decrease the optical performance of such materials.[353,354] Three recent studies appeared in the literature, modeling the interaction of H_2 with the isolated silanols.[355−357] The charge distribution of H_2 has a quadrupole moment which becomes obvious when looking at the MEP map. Consequently, two structure types of the surface complex are expected, a T-shaped one in which H_2 *accepts* a proton from silanol and an F-shaped one in which H_2 *donates* one of its protons to the basic hydroxyl oxygen (see Figure 7). The stability of the two structures is an extremely delicate case. The best estimate of the binding energies[355] is given by MP2//SCF/TZ(2d,2p) calculations, in which diffuse functions were also added to the basic oxygen atom of silanol. The ΔE values were −2.0 and −2.4 kJ/mol for the T-shaped and F-shaped structures, respectively. The BSSE was sizeable, and CP correction reduced those values to −1.7 and −1.9 kJ/mol, respectively. De Almeida *et al.*[356] reports calculations on the F-complex only. The structure was optimized at both the SCF/6-31G** and CISD/6-31G** levels. Electron correlation caused the H···O distance to decrease by 0.18 Å with respect to the SCF value. ΔE values of −2.2 and −3.2 kJ/mol were obtained at the SCF and CISD levels, respectively. Harmonic frequencies and IR intensities were computed at the SCF level only. The calculated shifts of the H−H and the SiO−H modes were −14 and −2 cm^{-1}, respectively (6-31G** basis set[356]). With the TZ(2d,2p) basis set, values of −10 and −2 cm^{-1}, respectively, were obtained,[355] in good agreement with the former. The shifts for the T-complex and the F-complex were −12 and 0 cm^{-1}, respectively. De Almeida *et al.*[357] carried out an MP2/6-31G** geometry optimization. The binding energies of the F-complex at the SCF and MP2 levels were 2.2 and 4.4 kJ/mol, respectively. Harmonic SCF shifts of the H−H and the SiO−H stretching frequencies were −14 and −2 cm^{-1}, respectively. From these data, no clear discrimination between the T- and the F-type structures is possible. The F-complex seems, however, to have a better chance to be the one formed on the surface.

Very recently, an experimental IR study of the interaction of acetylene (C_2H_2) with zeolite H-ZSM-5 and amorphous silica has been reported by Zecchina *et al.*[33] A series of calculations involving full geometry optimization and subsequent characterization of the stationary points at the SCF/DZP and MP2/DZP levels has been carried out for the H_3SiOH/C_2H_2 model.[358] Two stable structures were found; a T-shaped one in which the triple bond of the C_2H_2 molecule behaves as a proton acceptor with respect to the OH group and a second one in which acetylene acts as hydrogen donor toward the relatively basic oxygen of the OH group. A situation similar to the adsorption of H_2 was found here: the two conformers were almost isoenergetically bound at both the SCF and MP2 levels. The harmonic frequency shifts of the OH, CC, and CH modes were computed. As previously reported for water adsorption, the OH shift is largely underestimated at the SCF level, even after inclusion of electron correlation. The MP2/DZP value computed for the OH shift was 73 cm^{-1} for the T-conformer, compared with the observed shift of 120 cm^{-1} for acetylene adsorbed on amorphous silica. The experimental shift of the C≡C stretch is −12 cm^{-1}, still three times larger than the best MP2/DZP result of −4 cm^{-1}. Due to the abundance of experimental data, C_2H_2 is a good test molecule for assessing the performance of models alternative to the H_3SiOH molecule. Preliminary calculations[301] on the F_3SiOH/C_2H_2 model show that the SCF/DZP shift of the C≡C stretching frequency is now −6 cm^{-1}, whereas a shift of −77 cm^{-1} is computed for the OH frequency. SCF/DZP values for H_3SiOH/C_2H_2 system are[358] −4 and −40 cm^{-1}, respectively.

E. Validation of Cluster Models

1. General Comments

In preceding sections it has been mentioned that adsorption energies, in particular those of H_2O and NH_3, calculated so far for cluster models of surface silanol groups appear to be too small when compared with the observed values. There may be three reasons connected with the cluster approach: (i) The acidity of the silanol group is underestimated by the molecular model adopted, possible reasons being the shell-type and/or the nature of the saturator atoms. (ii) The dispersive contribution to the binding is underestimated as compared with that of the real surface because of the limited extension of the model, particularly for the shell-0 models. (iii) Long-range electrostatic effects are missing due to the finite nature of the molecular cluster.

It is clear from the discussion in section VI.B that there is a number of different ways to assess how well a given cluster represents the real surface site before studying any interactions with adsorbed molecules at all.

The first way is to calculate the vibrational features of the cluster itself at the highest possible level of theory and compare the results with experimental

data available for silica: electron correlation, large basis sets (TZP), and anharmonicity correction to the harmonic value of the OH stretching mode are all relevant in bringing the computed data closer to the experimental value. A second possibility is to study the gas-phase acidity (GPA) of a given cluster, defined as the difference in total energies of the cluster and that of its conjugate base. GPA is relevant in assessing the absolute acidity of the model, which in turn may be related to its ability to form H-bonds with a given adsorbate. Well-balanced basis sets which include one set of diffuse functions to properly account for the negative excess charge on the anion should be used and electron correlation should be included in any calculation of GPA if reliable data are desired. A third way is based on the fact that weak H-bond interactions are mainly dictated by electrostatic interactions between the electron densities of the subunits. That means that the comparison between values of the molecular electrostatic potential (MEP) of different isolated clusters in the spatial region where adsorption takes place is of great relevance in characterizing the propensity of a given cluster to form H-bonds. SCF calculations with medium sized basis sets are sufficient to give good estimates of the MEP. Attention will be paid to these three aspects when clusters of different sites are compared in the next section.

The most direct procedure for assessing the quality of a given cluster model is to study its interaction with various molecules and compare selected data with those available from experiments on the real silica surface. Good candidates for comparison are the value of the computed shift in the OH stretch and the binding energy corrected for both zero point energy and thermal contributions. Section 3 below provides an example.

2. Comparison of Different Cluster Models

It is of vital relevance to study the dependence of the reported results (energetic and vibrational) on the size and the structure of the adopted cluster. It should be noted that the dependence on the cluster size can be quite different for different properties.[319]

As an example of size dependence, a comparison of the most relevant data for the interaction of NH_3 with shell-0, shell-1, and shell-2 clusters is made below.

A sequence of calculations have been performed[338] at the SCF/MINI-1 level, in which the effect of the shell type chosen was monitored with respect to both the binding energy and the OH harmonic shift caused by adsorbed ammonia. Figure 10 shows that the binding energy is quite insensitive to the termination shell chosen. However, the red shift of the OH group varies markedly as does the dipole moment of the bare cluster. These data indicate that caution has to be exerted when dealing with *predictions* of frequency shifts, particularly when the model adopted is of the shell-0 type. The present calculations cast indeed some doubts on the extension of scaling procedures, which compare frequencies calculated for *models* with frequencies observed for the *real surface*.[316] The scale factors so defined do not seem to be transferable to slightly different molecular models.

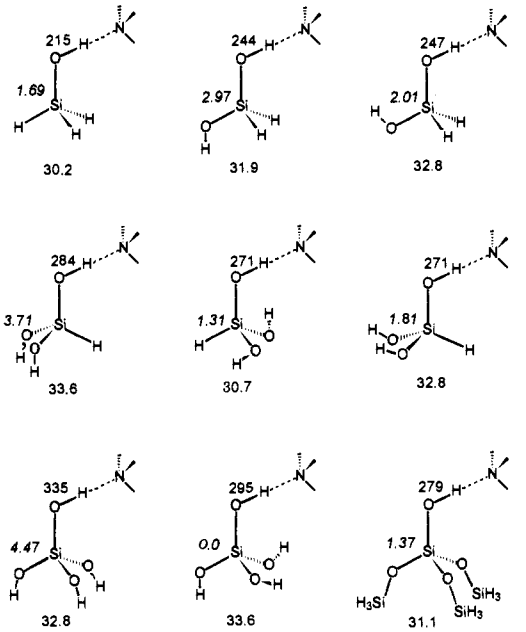

Figure 10. Results of SCF/MINI-1 calculations on complexes of NH_3 with the shell-0, shell-1, and shell-2 models on surface silanol groups. BSSE-corrected binding energies (kJ/mol), OH harmonic frequency shifts (cm^{-1}), and dipole moments (D) of the bare clusters.

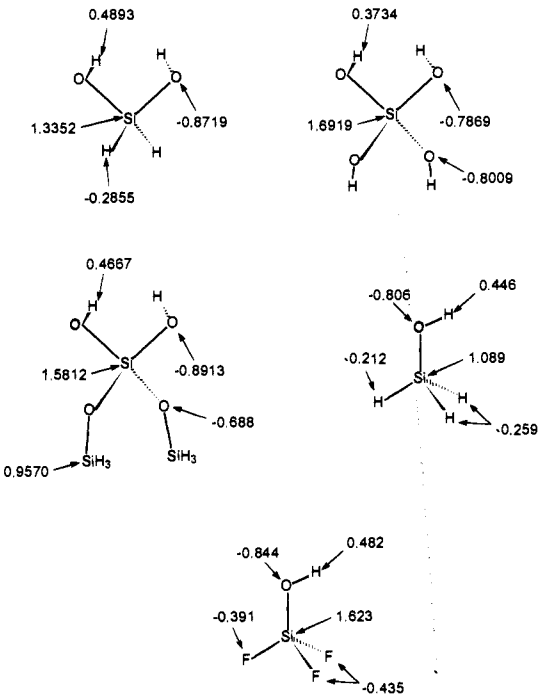

Figure 11. SCF/DZP molecular electrostatic potential derived net charges[359] computed for shell-0, shell-1, and shell-2 models of the geminal site as well as for the H_3SiOH and F_3SiOH models of the isolated site.

Fortunately, the hydrogen-bond ability of the OH group does not seem to be affected to a significant extent by the way the cluster is terminated. This finding supports the adoption of shell-0 clusters in more expensive calculations. Further evidence that shell-2 clusters show physicochemical properties similar to those of shell-0 models is given in Figure 11, for models of geminal sites. The *ab-initio* molecular electrostatic potential (MEP) computed on a series of shells in the van der Waals region around the nuclei has been fitted by means of a classical

expression based on charge monopoles centered at the nuclei, as coded in GAUSSIAN-92.[359] Indeed, net charges on the acidic OH groups are closer for shell-0 and shell-2 models than those computed for shell-1 models, in agreement with the similar conformational behavior shown by these two models.[321] It is worth mentioning that the relatively small net charge computed for the oxygen belonging to the siloxane bridge of the shell-2 model confirms that the oxygen is less nucleophilic when it is in a siloxane bridge than when it is in a OH group. Physicochemical properties computed for a given cluster are expected to oscillate as a function of the cluster size. Therefore, careful checking has to be made to ensure that the oscillations in the quantity of interest (frequency shift, binding energy, GPA, net charges, etc.) will not bias the data.

The effect of enhanced electronegativity of the terminator atoms is addressed here by showing so far unpublished[360] data on F_3SiOH, both alone and when interacting with ammonia, and comparison is made with the shell-0 SiOH cluster.

The structure of F_3SiOH was optimized at the SCF/DZP level, and the same procedure for calculating the potential-derived charges has been used here. A much higher electronegativity of fluorine with respect to silicon (and also with respect to oxygen) is found; the silicon charges increase by about 0.6 electron with respect to the value computed for silanol (see Figure 11). The increase of the absolute magnitude of the net charges for the O and H atoms is also noticeable. To gain some insight into the true hydrogen-bond capability of F_3SiOH, we compare the binding and vibrational features of the F_3SiOH/NH_3 complex obtained at the SCF/DZP level with those reported in the literature for H_3SiOH/NH_3 (see Figure 12). A binding energy (uncorrected for BSSE) of 47 kJ/mol is obtained, which corresponds to an increase of 44% with respect to the value of 33 kJ/mol for H_3SiOH/NH_3. These findings are in line with the relative values of the GPA of H_3SiOH and F_3SiOH. The SCF/TZ(O)DZ(d,p) results are 1576 and 1468 kJ/mol for H_3SiOH and F_3SiOH, respectively. The decrease in GPA is quite large. The computed value for F_3SiOH is close to the value of 1470 kJ/mol computed at the same level for the much larger $(HO)_8Si_8O_{12}$ model.[319] The data on the effect of terminator atoms on both the binding energy and frequencies are gathered in Figure 12 for the F_3SiOH/NH_3 adduct. The enthalpy of adsorption, $-\Delta H°_0$, becomes 37 kJ/mol and the harmonic $\Delta\nu$(SiO–H) is now as large as -464 cm^{-1} at the SCF/DZP level. If credit is given to the scaling factor which brings the $\Delta\nu°_{OH}$(SCF) to $\Delta\nu_{OH}$(SCF) for the H_3SiOH/NH_3 adduct, a shift of -696 cm^{-1} is obtained for H_3SiOH/NH_3; the $\Delta\nu_{OH}$(MP2) then becomes as large as -951 cm^{-1}, not far from the experimental datum.[68] Other modes are in accord with the experiment, even if the NH stretch shifts are still underestimated. Clearly, much work is needed to assess the performance of F_3SiOH as a model, even if these preliminary data seem to suggest that as a hydrogen donor it is too strong. Such findings make F_3SiOH the most acidic model available for mimicking the isolated silanol, and a more systematic series of tests to check its performance as a model is in progress.[360]

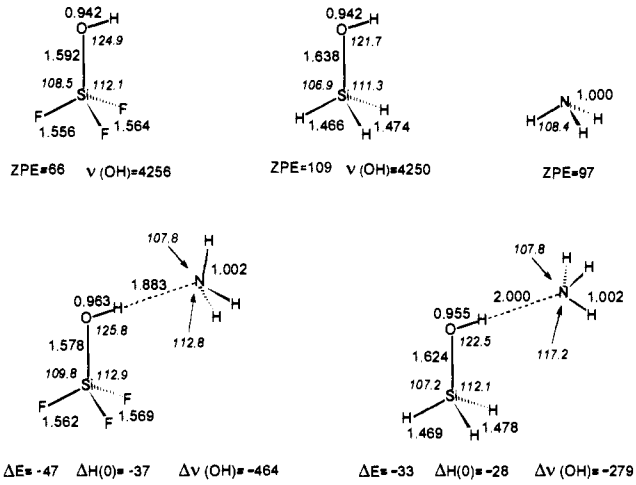

Figure 12. SCF/DZP optimized structures for isolated H_3SiOH, F_3SiOH, and NH_3 molecules and for H_3SiOH/NH_3 and F_3SiOH/NH_3 complexes. Also reported are harmonic zero point energies, ZPE, binding energies, ΔE, heats of formation at 0 K, $\Delta H(0)$, OH harmonic frequencies, ν_{OH}, and the corresponding shift upon complexation, $\Delta\nu_{OH}$. Bond distances in angstroms, bond angles in degree, energies in kJ/mol, and vibrational data in cm^{-1}.

It may also be useful to explore the drawbacks of the H_3SiOH model from a different viewpoint. It is known from both Raman and NMR experiments[62] that structural strain may be present at the surface of highly dehydrated silica. This is mainly due to the presence of six-membered rings (ring made of 3 oxygens and 3 silicon atoms). This fact arises the following question: will an isolated silanol group belonging to a strained ring be so perturbed as to significantly increase its acidity? This is a relevant issue, because in case of a positive answer, all open tree-like models used so far should be reconsidered with more criticism. Indeed, preliminary results show that for a single hydroxyl group belonging to an adamantane-like cage structure (three interconnected six-membered rings), a significant increase in both the binding energy and the OH shift is computed for the interaction with the NH_3 molecule.[360] The increment of the shift and the binding energy are close to those computed with the most acidic shell-0 model available, namely F_3SiOH.

3. Comparison between Data Calculated for Models and Observed for Real Surfaces: H-Bond Formation and Acidity

Two papers appeared in which the main focus was to establish a general conclusion about the performance of the shell-0 model, H_3SiOH, to represent the real silanol present at the silica surface.[361,362] A number of correlations were reported between quantities relevant to H-bond formation. A strict comparison was made between the binding energies computed using H_3SiOH and FH as donors of the acidic proton. A good correlation was obtained showing that H_3SiOH is a weaker proton donor in H-bonds than HF. One can go a step further and make an attempt to use such spectroscopic data as a measure of acidity of surface Brønsted groups. Given any base molecule B, the ratio of the shifts in the stretching

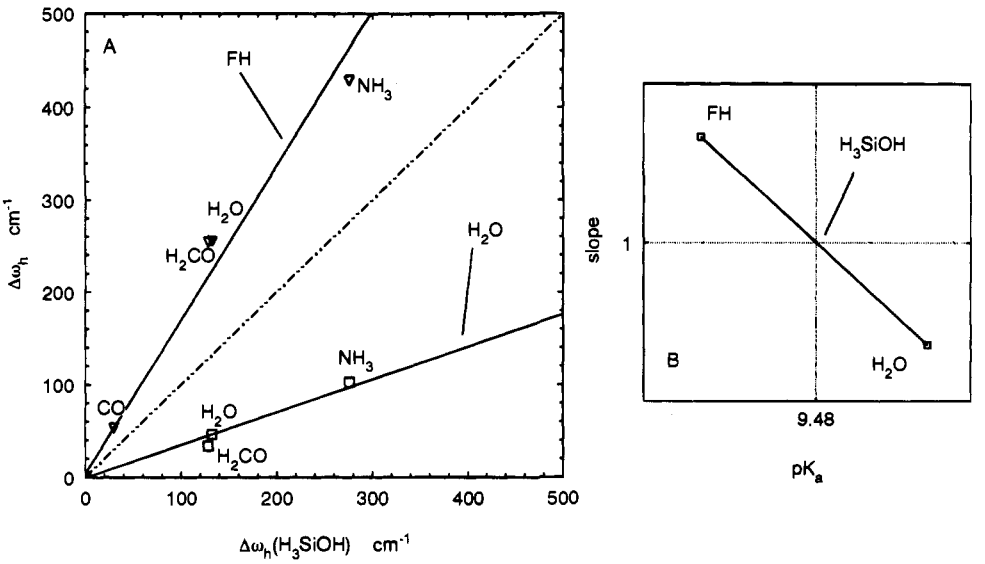

Figure 13. (A) Correlation between computed shifts of the harmonic OH frequency, $\Delta\omega_h$, of H_3SiOH, FH, and H_2O due to the interaction with a number of base molecules. (B) Correlation between slopes of the lines obtained in (A) with the pK_a of H_2O and FH molecules.

modes which the two acidic groups A_1–H and A_2–H show upon coordination of B is independent of B. This means that the plot of $\Delta\nu(A_1\text{–}H)$ *vs* $\Delta\nu(A_2\text{–}H)$ yields a straight line, the slope of which is considered to be a measure of the relative acidity of A_1–H and A_2–H.[74,326,363] The slopes are then traditionally related to the pK_a values of the A_1–H and A_2–H groups (cf. section II). By this procedure, it is found[326,363] that $(\equiv SiOH)_S$ has a pK_a value around 7.0, whereas that for $(CH_3)_3SiOH$ is 11, *i.e.* trimethylsilanol is less acidic than $(\equiv SiOH)_S$. An entirely computational version of the spectroscopic method described above to measure acidity can be set up. We have considered three sets of $\Delta\nu°_{OH}$ concerning the interaction of a set of base molecules (CO, H_2CO, H_2O, and NH_3) with H_3SiOH, HF, and H_2O as H-donors. The relevant data partly come from the literature and partly have been computed by some of us.[362] In Figure 13, two sets of $\Delta\nu°_{OH}$ data are plotted against the third set relative to H_3SiOH. These points line up reasonably well, and the two slopes (FH *vs* H_3SiOH; H_2O *vs* H_3SiOH) may be measured: the slope of H_3SiOH *vs* itself is, of course, one. Figure 13B shows the plot of the slopes m relative to water and fluoridic acid against their pK_a measured in solution. Analogously to what is done experimentally (with much richer data sets), we can draw a straight line through the two points and estimate the pK_a value which corresponds to silanol (m = 1). Notwithstanding the poor data set, the result is encouraging, as a pK_a value of about 9.5 is obtained, intermediate between that of $(CH_3)_3SiOH$ (pK_a = 11) and that of $(\equiv SiOH)_S$ (pK_a = 7), in agreement with the guess made above.

A similar procedure was used by Paushktis *et al.*[48] to derive gas-phase acidity (GPA) data from relative values of gas-phase frequency shifts. They obtained 1390 ± 25 kJ/mol for surface silanol groups. Note that the GPA is defined as the heat of deprotonation and that low (positive) values mean high acidity. The GPA of the gas-phase H_3SiOH molecule has been recently measured as 1502 ± 21 kJ/mol,[303] which confirms the above conclusion that the H_3SiOH molecule is less acidic than the surface silanol groups. A GPA value of 1520 kJ/mol for H_3SiOH was predicted earlier by Sauer and Ahlrichs,[204] who performed high-quality *ab-initio* calculations. In a recent paper Sauer and Hill[319] show that the GPA increases when the model of the surface silanol group is significantly extended. For a cage-like model as large as $(HO)_8Si_8O_{12}$, the computed[319] GPA is 1400 ± 25 kJ/mol, in close agreement with the spectroscopically derived value.

In spite of such successes, one should be aware that the propensities for H-bond formation and gas-phase acidities or basicities are not identical. For example, previous work indicates that H_3SiOH forms weaker H-bonds than HF, in contrast with the GPA values of the HF and H_3SiOH molecules, which are 1554[364] and 1502 ± 21 kJ/mol,[303] respectively. Similarly, the gas-phase basicity of H_2O is smaller than that of formaldehyde, while the binding in its complexes with H_3SiOH, HF, etc., is stronger. We have also recently shown[206] that the gas-phase basicities of H_3SiOH and CH_3OH are about the same, though the latter forms by far stronger H-bonded complexes as a proton acceptor.

The GPA scale corresponds to the concept of an OH species isolated from the rest of the solid and, thus, corresponds somehow to the cluster approach. As far as the adsorbate is concerned, the GPA refers to the low-coverage (Henry) region, while the pK_a characterizes high coverages at which the adsorbate is in a liquid-like environment. If, however, the dielectric nature of the solid is taken into account, the use of pK_a gets some justification also for low coverages. Evidence for the role of the solid as a "solvent" comes from the study of the reverse process, *i.e.* the adsorption of acidic molecules on basic substances such as MgO.[365,366] The propensity to dissociate follows the pK_a scale and not the GPA scale of the molecules investigated. (Note that metal surfaces behave in the opposite way.[365])

Another aspect of this debate (GPA or pK_a) is that pK_a values of surface hydroxyls can be directly measured, and in some cases have been, while there is no way to measure the GPAs for surface species.

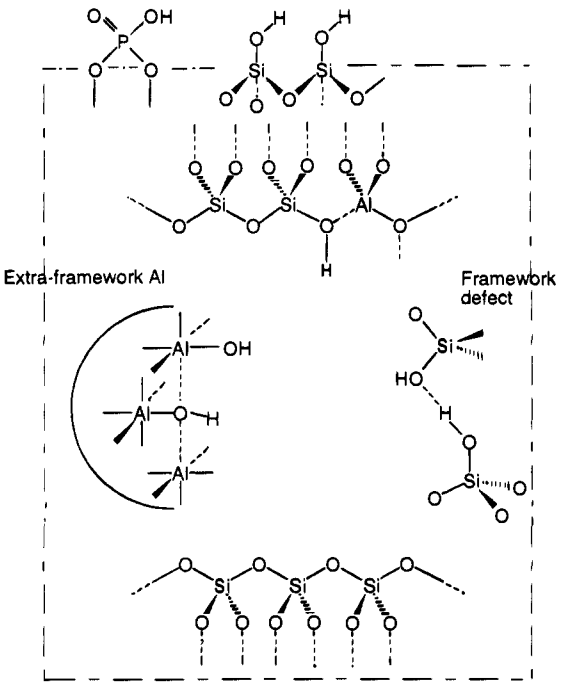

Figure 14. Schematic view of a microcrystallite of a zeolite catalyst. Besides the bridging hydroxyls, SiO(H)Al, there are terminal SiOH groups and, for modified catalysts, POH groups on the external surface. Moreover SiOH groups and AlOH groups may be present at internal defects and extra-framework material, respectively.

The opposite is true for cluster models of acidic sites, for which GPA values are readily calculated but not the pK_a values.

VII. Interaction of Molecules with Surface Hydroxyls in Zeolites, SiO(H)Al

A. Introduction

All zeolitic systems in protonic form possess one OH species, bridged between Si and Al, which is usually referred to as SiO(H)Al and which is the structural origin of acidic catalytic activity. Other hydroxyls occur in zeolites, related to (i) termination of microcrystals, (ii) imperfections within the lattice, (iii) segregation of extra-framework aluminum, and (iv) chemical modification, *e.g.* by phosphoric acid (cf. Figure 14). The former two causes yield SiOH groups similar to those found at the silica surface,[369] dealt with in preceding sections of this review. Extra-framework species contribute to the acidity of zeolite catalysts. Among them are species which absorb around 3670 cm^{-1} and have been ascribed to structures such as Si−O−Al(OH)−O−Si.[370] ^1H NMR signals at about 2.5−3.6 ppm are also ascribed to extra-framework Al species.[371,372] On the basis of *ab-initio* calculations they have been assigned to bridging AlO(H)Al hydroxyl groups.[373] Among the different types of hydroxyls which may be present in a zeolitic catalyst, only the bridging SiO(H)Al hydroxyl sites have been considered in theoretical studies of the interaction with external molecules which will be reviewed below.

The main tools for identification and characterization of zeolitic hydroxyls are vibrational spectroscopy (both IR and INS, cf. section II.C.3) and high-resolution solid-state ^1H NMR spectroscopy. The characteristic OH stretching mode of the SiO(H)Al species shows some variation both with the framework structure and with the composition of the particular zeolite considered. Also the acidity of the SiO(H)Al species is known to be different in different zeolitic structures, as is the ν_{OH} value. It is not straightforward, however, to relate the two: instead, the shift of ν_{OH} caused by H-bond formation with the same molecule is suggested as a measure of the OH acidity[226,370,374] (cf. sections II.C.3 and VI.E).

On adsorption of CO and benzene on proton-containing zeolites, H-bond formation is readily observed by IR spectroscopy.[76,370,374] While $\Delta\nu_{OH}$ is the same in both cases (about 300 cm^{-1}), there are indications that the strength of interaction is different. While with benzene H-bond formation takes place at room temperature, with CO it is observed at 77 K only. Similarly, molecular nitrogen has recently been used to form H-bonded complexes with acidic hydroxyls in zeolites.[375,376] Other molecules for which H-bonding with the Si(OH)Al species have been observed are CO_2, N_2O, and *n*-pentane.[20] The $\Delta\nu_{OH}$ values (about −106, −160, −160, and −90 cm^{-1} for N_2, CO_2, N_2O, and *n*-pentane, respectively) are about three times that observed with the SiOH species on silica. For H-ZSM5, Makarova *et al.* recently reported OH frequency shifts (in parentheses, cm^{-1}) for the interaction of SiO(H)Al groups with Ar (−50), H_2 (−50), O_2 (−60), CH_4 (−115), N_2 (−120), C_2H_6 (−140), C_3H_8 (−140), CO (−310), and C_2H_4 (−445).[377]

Because of their marked acidity, the SiO(H)Al species are able to form very strong H-bonded complexes which, depending on subtle details of the composition and the pore structure of the particular zeolite, may convert by proton transfer in ion pairs; *i.e.*, acidic zeolites are able to protonate adsorbed molecules. Ammonia is a prominent example. In fact, protonic forms of zeolites are prepared from the respective ammonium forms by heating. When ammonia is adsorbed on the SiO(H)Al sites, the ammonium form is reproduced:

$$ZO^-NH_4^+ \rightleftharpoons ZOH + NH_3$$

Whether or not the less basic H_2O and CH_3OH molecules form protonated species on zeolitic SiO(H)Al hydroxyls is currently debated. We will review the experimental evidence and the results of calculations in detail below.

In many instances, neutral complexes stabilized by H-bonds may be the precursors to ion-pair structures generated by proton transfer. As reported in section II, this is the case for unsaturated hydrocarbons. For complexes of ethylene, propene, acetylene, and methylacetylene, the lifetime of these complexes is in the time scale of modern FTIR instruments.[33]

B. Surface Hydroxyls without Adsorbate

We limit this section to models adopted for bridging hydroxyl sites and to results obtained by *ab-initio* techniques. Our interest is directed to the structure, the vibrational properties, and the ^1H-NMR chemical shift. The smallest reasonable model,[202] $H_3SiO(H)$-

AlH_3, is the analogue of the H_3SiOH model for terminal silanols. As the prototype of a series of models, it is denoted {SiO(H)Al}shell-0. The next members of this series are the $(HO)_3SiO(H)Al(OH)_3$, {SiO(H)Al}shell-1, and $(H_3SiO)_3SiO(H)Al(OSiH_3)_3$ models, {SiO(H)Al}shell-2. Another type of models is based on the AlO_4 tetrahedron as the basic unit with the acidic proton attached to one of the four oxygen atoms. The starting member of this series is the $HO(H)Al(OH)_3$ model, which will be denoted {H-(AlO_4)}shell-1. The {H(AlO_4)}shell-2 model, H_3SiO-$(H)Al(OSiH_3)_3$, has a complete Si coordination shell, and the {H(AlO_4)}shell-3 model, $(HO)_3SiO(H)Al[OSi$-$(OH)_3]_3$, three complete coordination shells around the central Al atom (O−Si−O). For surface complexes of the hydronium and the methoxonium ion, it proved meaningful to consider the $H_3SiO(H)Al$-$(OH)_2OSiH_3$ model[378] which has two O sites with shell-2 saturation and two O sites with shell-1 saturation and, therefore, will be denoted {H(AlO_4)}-shell-1.5. Hence, shell-0 and shell-2 refer to Si/Al-H-terminated models while shell-1 and shell-3 refer to OH-terminated models.

At the first glance, the OH-terminated models seem to be more realistic as there is only one saturating H atom per boundary O atom, while the Si−H-terminated models need three H atoms per boundary Si atom for saturation. However, the OH groups are strong dipoles which may affect interaction energies in a nonrealistic way. Moreover, there is the issue of geometry optimization. Using fully relaxed structures as reference geometries proved extremely important when aiming at binding energies, energies of deprotonation, and, particularly, proton-transfer energies. Unfortunately, the dihedral angles that determine the orientation of the terminal OH groups converge very slowly in optimization runs. Moreover, a completely unconstrained optimization of structural parameters may result in structures with intramolecular H-bonds which are not realistic. The hydrogen atoms forming these bonds are introduced as saturating atoms. They replace in the models silicon atoms of the lattice. For example, the geometry optimization of the 2-aluminatrisilicic acid within the C_s point group yields a structure with two intramolecular hydrogen bonds unless the values of some of the dihedral angles are constrained (Figure 15).[379] Fixing values of dihedral angles has also been used as a means of introducing some degree of lattice specificity.[380] When the models get larger, rings and cages (double rings) of TO_4 tetrahedra (T = Si, Al) are more realistic and more appropriate models. They have relatively fewer saturating hydrogen atoms than the tree-like models of the {SiO(H)Al}-shell-x and {H(AlO_4)}shell-x series and an increasing number of dihedral angles are constrained by the connectivity of the atoms in these models.

Structural data on bridging hydroxyl sites are difficult to get from experiments because of the low concentration of these sites in zeolite catalysts and the fact that they are not ordered into unit cells. Hence, quantum chemical calculations on models can add significantly to our knowledge of the local structure of these sites. Table 13 shows the structural parameters predicted for a variety of models

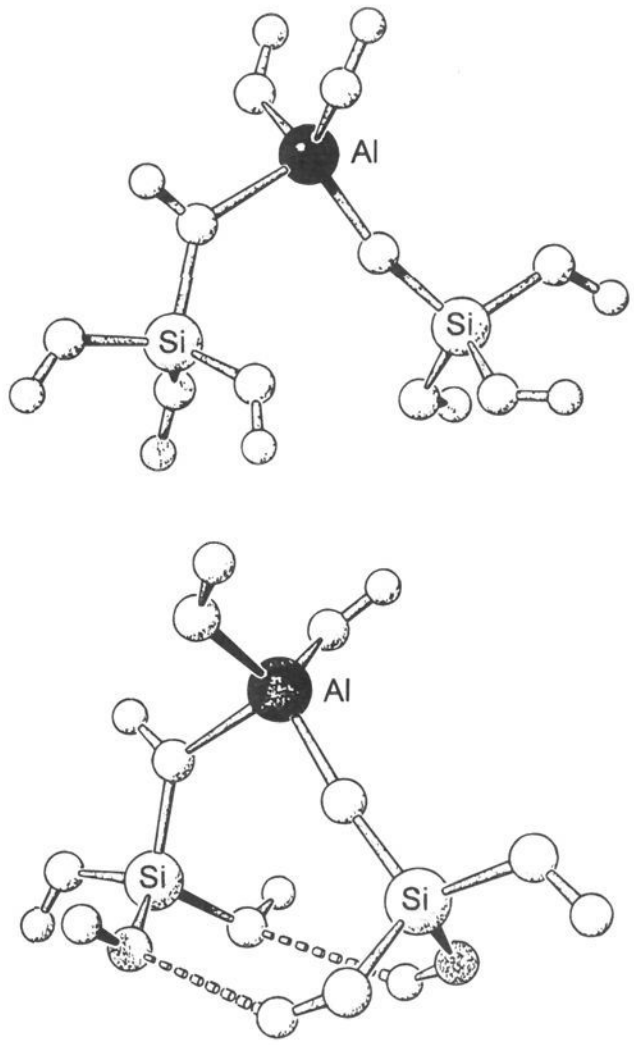

Figure 15. Two conformations of 2-aluminatrisilicic acid (C_s point group). Top: dihedral angles have been constrained to avoid intramolecular hydrogen bonds. Bottom: result of the unconstrained optimization with two intramolecular hydrogen bonds.

mostly obtained within the SCF approximation using a basis set of double-ζ plus polarization (DZP) quality on all the atoms except on the O atoms which are described by a triple-ζ plus polarization basis set (TZ-(O)/DZ(d,p)). The results reported in Table 13 show some scatter even when excluding the smallest models. Systematic deviations of the OH bond distance of −1.2 ppm are connected with this approximation.[378] Taking both of these factors into account, the following ranges of structural parameters are predicted:

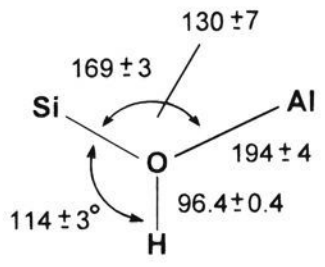

Note that contrary to early assumptions connected with scanty experimental data and computational limitations, the proton is not in the Si−O−Al plane. The out-of-plane angle is between 5 and 15 degrees.[379,381] These predictions apply to an "average" and unconstrained bridging hydroxyl group. Specific framework structures will put some strain on the active sites. *Ab-initio* calculations on models which are large enough to include constraining features such as double-six-membered rings[380,382] or the fused rings of the faujasite model (Figure 17) show that deviations from the average ranges specified above are small. This is confirmed by lattice energy minimizations of periodic zeolite structures using *ab-initio*-derived potentials.[382]

Table 13. Predictions for Models of Bridging Hydroxyl Sites:[a-e] Bond Lengths and Angles (pm, degree), Energies of Deprotonation (kJ/mol)

model	method	ΔE_{DP}[f]	r_{OH}	∠SiOH	r_{SiO}	r_{AlO}	∠SiOAl
$H_3SiO(H)AlH_3$	DFT-BH/DNP+ [a,g]	1268 +49	97.1	120.3	171	199	125
$H_3SiO(H)AlH_3$	MP2/DZ+2P[b]	1306	96.4	117.9	171	202	130
$H_3SiO(H)AlH_3$	SCF/6-31G* [c]	1329 −32	95.1	117.4	171	203	131
$H_3SiO(H)Al(OH)_3$	SCF/6-31G* [c]	1353 −32	95.6	121.4	169	195	134
$(HO)_3SiO(H)Al(OH)_3$	SCF/DZP[d,h]	1362 −46	95.3	114.8	166	198	134
$(HO)_3SiO(H)Al(OH)_2OSiH_3$	SCF/DZP[d,h]	1277 −46	95.3	120.5	167	198	137
$(HO)_3SiO(H)Al(OH)_2OSi(OH)_3$	SCF/DZP[d,h]	1320 −46	95.3	115.0	167	194	133
H-[4-ring(Al)]	SCF/DZP[d,h]		95.5	118.3	168	195	135
$HO(H)Al(OH)_3$	SCF/6-31G* [c]	1391 −32	95.2			196	
	SCF/DZP[e,h]	1411 −46	95.4			197	
	MP2/DZP[e,h]	1405 −28	97.4			198	
$H_3SiO(H)Al(OH)_2OSiH_3$	SCF/DZP[e,h]	1320 −46	95.0	117.4	172	193	123
	MP2/DZP[e,h]	1318 −28	96.8	116.8	174	193	117
$H_3SiO(H)Al(OSiH_3)_3$	SCF/DZP[e,h]	1273 −46	95.1	117.6	171	194	126
H_2[8-ring(2Al)]	SCF/DZP[h,i]	1338 −46	95.3	117.2	170	198	132
faujasite model[j]	SCF/SVP[c]	1206 −29	96.0	114.8	171	193	135

[a] Reference 205. [b] Reference 414. [c] Reference 373. [d] Reference 379. [e] Reference 381. [f] The second entry is the correction for the systematic error connected with each approximation. It has been estimated on the basis of the accurate results available for H_3SiOH and CH_3OH,[204] cf. Table 5 and ref 308. [g] Local density approximation with numerical basis set (Dmol code). [h] DZP basis set on all atoms except oxygen for which a valence triple-ζ set has been used. [i] J. Sauer, unpublished results. [j] Cf. Figure 17.

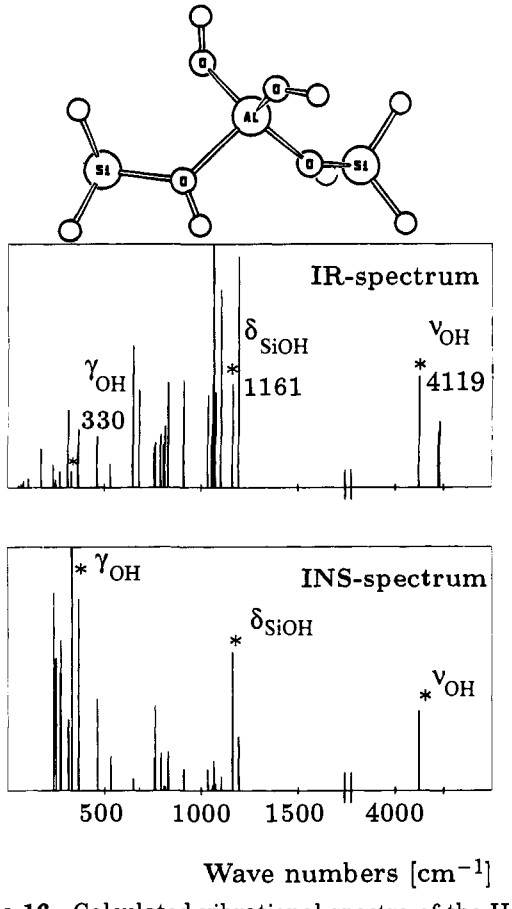

Figure 16. Calculated vibrational spectra of the $H_3SiO(H)AlOSiH_3$ model: while the in-plane and out-of-plane SiOH deformation modes δ_{SiOH} and γ_{SiOH} are hidden under framework vibrations in the IR spectrum, they are clearly visible in the INS spectrum (refs 441 and 442).

The importance of three vibrational modes of the SiO(H)Al proton for identifying and characterizing surface hydroxyl groups has already been outlined in section II.C.3. As mentioned there, the in-plane and out-of-plane deformations at about 1100 and 400 cm^{-1}, respectively, are hidden by framework vibrations and can only be observed either as combination modes with the OH stretching mode[55-57] or using inelastic neutron scattering (INS).[57-59] Figure 16 compares calculated IR and INS spectra and clearly shows the advantage of the latter in the region below 1500 cm^{-1}. Calculations on molecular models played a crucial role in the correct assignment of the γ_{SiOH} band[383] in the first INS spectrum.[58] Table 14 summarizes the computed harmonic vibrational frequencies for a variety of models.

Table 14. Calculations on Models of Bridging Hydroxyls: Harmonic Wavenumbers of Vibrational Modes Involving the Acidic Proton

model	method	ν_{OH}	δ_{SiOH}	γ_{SiOH}
$H_3SiO(H)AlH_3$, C_s	MP2/TZ2P[a]	3800	1105	222
$H_3SiO(H)AlH_3$, C_s	SCF/6-31G* [b]	4090	1200	420
$H_3SiO(H)Al(OH)_3$, C_s	SCF/6-31G* [b]	4000	1180	435
$(HO)_3SiO(H)Al(OH)_3$	SCF/DZP[c,d]	4070	1185	460
$(HO)_3SiO(H)Al(OH)_2$-$OSi(OH)_3$	SCF/DZP[c,d]	4080	1190	265
$HO(H)Al(OH)_3$	SCF/DZP[c,d]	4120/4030	1735	722
$H_3SiO(H)Al(OH)_2$-$OSiH_3$	SCF/DZP[c,d]	4120	1160	330; 360[e]
$H_3SiO(H)Al(OSiH_3)_3$	SCF/DZP[c,d]	4100	1210	320; 330[e]
H_2[4-ring(2Al)]	SCF/DZP[c,d]	4075	1280	395
			1240	500

[a] Reference 415. [b] Reference 373. [c] Reference 379. [d] DZP basis set on all atoms except on oxygen for which a valence triple-ζ basis set is used. [e] There are two normal modes with strong γ_{SiOH} components.

Calculations within the SCF approximation using DZP basis sets are known to yield systematically wavenumbers that are too large. Hence, the scaled force field approach described in section III has become a standard. Using the common factor of 0.9, the calculations predict that the ν_{OH}, δ_{SiOH}, and γ_{SiOH} modes should be observed around 3665−3710, 1035−1070, and 240−415 cm^{-1}, respectively (Table 15). These predictions are valid for an "abstract" or "average" active site and do not reflect variations due to the framework structure or the composition. It is well-known that the observed wavenumber of the OH stretching mode depends on the width of the pore hosting the OH species.[384] It is in the range of 3630−3610 cm^{-1} when the SiO(H)Al species is located in large rings (about 12-membered) and in the 3530−3520 cm^{-1} region when in small, *e.g.*, 6-membered

Table 15. Vibrational Modes of the SiO(H)Al Proton: Comparison of Observed and Calculated[a] Wavenumbers (cm^{-1})

		observed		
mode	calculated[a]			
ν_{OH}	3665–3710		3520–3630 (3645)[e]	
δ_{SiOH}	1035–1070	1060[b]	1060[c]	1090[d]
γ_{SiOH}	240–415	360[b]	420[c]	420[d]

[a] Harmonic wavenumbers taken from Table 14 and scaled using $f = 0.9$. [b] Reference 58. [c] Reference 59. [d] Reference 57. [e] Extrapolated value, see text.

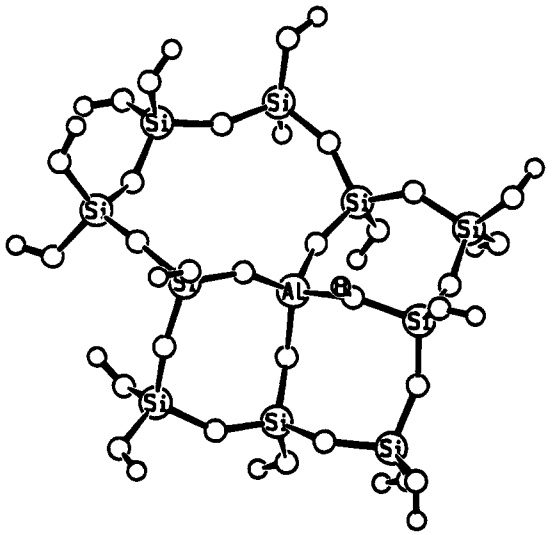

Figure 17. Model of the bridging hydroxyl site in faujasite involving closed rings: $H[Si_{10}AlO_{14}(OH)_{16}]$.[443]

rings. This is clearly seen for instance in HY zeolites, which possess both types of rings. For the same zeolite structure, some dependence of ν_{OH} on the Al content is also observed. Use has been made of Sanderson electronegativity to rationalize this dependence.[384] From these experimental correlations[384] it is possible to extrapolate a wavenumber of 3625 cm^{-1} for an "infinite" ring size and a very low concentration of bridging hydroxyl sites. When the composition of the relevant models in Table 14 is considered, the extrapolated value is 3645 cm^{-1}.

Table 13 shows also the energies of deprotonation calculated for the various models. An estimate of the heats of deprotonation of surface silanols based on these energies should take into account both the systematic error of the computational technique and nuclear motion corrections. From previous studies[308,373] we know how large the systematic deviations due to neglect of electron correlation and basis set truncation are. These corrections are also given in Table 13. The loss of three vibrational degrees of freedom on deprotonation yields a zero point energy correction of about −30 kJ/mol and thermal corrections of about −5 kJ/mol. For the faujasite model of Table 13, which is by far the largest one (see Figure 17), this yields an estimate of about 1206 − 29 − 35 ≈ 1142 kJ/mol.[381] For the {H(AlO_4)}shell-2 model this estimate is 1192, and for the $(HO)_3SiO(H)Al(OH)_2OSi(OH)_3$ model 1240 kJ/mol. The estimate for the uncertainty is about ±25 kJ/mol. From comparisons of the shifts of the OH-stretching frequencies of bridging SiO(H)Al hydroxyls in various surface complexes with those of other molecules with acidic OH groups, the following values for the heat of deprotonation were inferred (cf. section VI.E.3): 1140 (H-mordenite), 1170 (H-ZSM5), and 1190 (HY) (all values taken from Figure 2 of ref 385); 1200 kJ/mol (HNaY);[225] 1180–1333 kJ/mol (HNaZSM5).[386,387] The ranges of computed and spectroscopically derived values overlap substantially and we conclude that the models used are large enough to properly account for the acidity of bridging hydroxyl groups in zeolites.

When the bridging hydroxyl groups in zeolites are compared with the terminal ones on silica surfaces, the following observations are made: (i) the OH bond is longer, (ii) the OH-stretching frequency is lower, and (iii) the heat of deprotonation is lower, *i.e.* the acidity is higher. All of them are consequences of the fact that the oxygen atom extends a third bond to the aluminum atom of the lattice. Another reasoning is based on the view that the SiO(H)Al site is a SiOH Brønsted site activated by a neighboring trivalent Al Lewis site[388] so that the stabilization of the SiO^- site formed on deprotonation is much larger than the stabilization of the SiOH group in the initial state.

C. Interaction with H-Acceptor/H-Donor Molecules

1. Interaction with NH_3

There is no doubt that the interaction of NH_3 with hydroxyl sites is so strong that NH_4^+ ions are formed. Zeolites containing NH_4^+ ions are in fact the precursors of acidic zeolite catalysts. They are obtained by ion-exchange. For the NH_4^+-exchanged natrolite, $(NH_4)_2Al_2Si_3O_{10}$, an X-ray structure refinement has been reported.[389] It was possible to localize the NH_4^+ ions in difference Fourier maps. On average, three of the four NH_4^+ protons are found to be involved in H-bonds of different lengths with framework O atoms. The majority are nearly linear single H-bonds with H···O distances between 186 and 208 pm, while the H···O distances of the few bifurcated bonds are between 220 and 242 pm. The computed structures (Figure 18) are in accord with these observations. The predicted distances of the single and bifurcated bonds are in the ranges of 164–191 and 220–260 pm, respectively. ^1H NMR chemical shifts of the NH_4^+ protons have also been calculated.[83] They show the expected close correlation with the length of the H-bonds: 13.6–8.2 and 6.3–5.0 for protons involved in single and bifurcated H-bonds, respectively. Shifts between 2.4 to 3.0 ppm are calculated for "free" NH_4^+ protons. Unfortunately, only values averaged over all four protons can be measured. These averages for the three complexes shown in Figure 18 are very close to each other (7.3, 6.8, and 7.1 ppm, cf. Table 16). This shows that there is some "conservation of bond strength" among the different types of coordination of NH_4^+ to the framework: The average shift is nearly the same for a structure with a single strong H-bond and two weaker bifurcated ones (8-ring model, 7.1 ppm) and for a structure with three nearly equally strong single H-bonds (shell-1 model, 7.3 ppm). From the calculated shifts one also reaches the conclusion that the NH_4^+ ion attached to a negatively charged aluminosilicate surface site (the ion pair structure) is the preferred structure formed

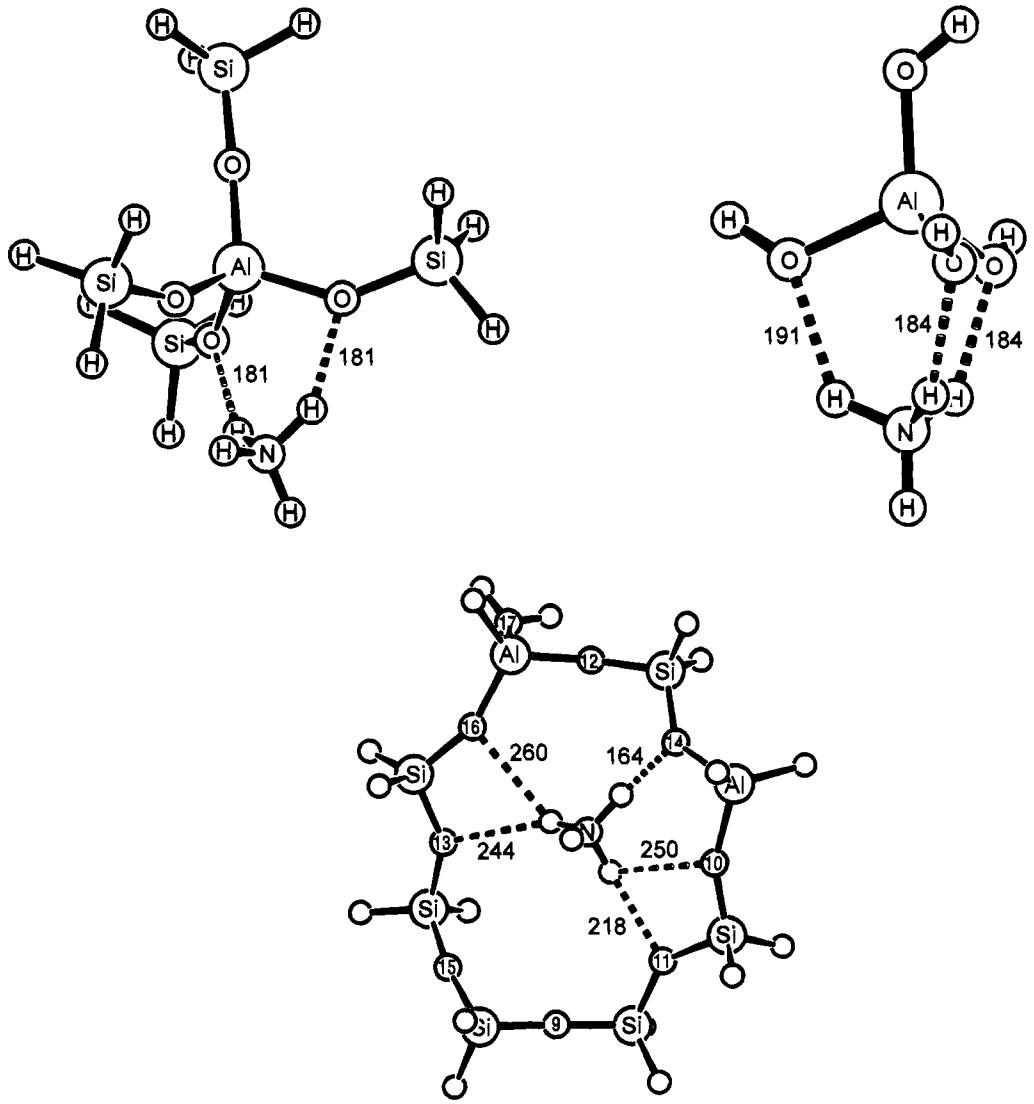

Figure 18. Structures of different complexes of NH_4^+ with models of negatively charged zeolite surface sites.[83,416]

Table 16. Observed ^1H NMR Chemical Shifts of NH_3 on Bridging Hydroxyls and Values Predicted for the Two Possible Adsorption Structures (ppm)

	calculated[a]			
SiO(H)Al Model	NC[b]	IP[b]	zeolite	observed
shell-1	4.4	7.3	NH_4-rho	6.0[c]
shell-1.5	3.4	7.0	NH_4-Y	7.0[d]
shell-2	3.7	6.8	NH_4-Y	6.5; 7.0[e]
8-ring, H-saturated		7.1		

[a] Calculated results from refs 83 and 416. [b] NC, neutral complex; IP, ion pair. [c] Reference 417. [d] Reference 418. [e] References 419 and 420.

on adsorption of NH_3 on acidic bridging hydroxyl groups, even if both species show roughly the same binding energies (cf. Figure 17). While the average shifts calculated for this structure type nicely agree with observed data (Table 16), the results for the neutral adsorption complex (NH_3 H-bonded to the proton of the bridging hydroxyl group) show a significantly larger deviation from them. There were many indications that both structures may be local minima on the potential energy surface. Calculations on shell-2-type models (a full shell of SiH_3 groups around the central $(H)AlO_4$ tetrahedron) involving the diagonalization of the force constant matrix have shown that this is indeed the case. Smaller models have occasionally failed to reproduce this feature.[390,391] Table 17 shows calculated binding energies for both types of structures and various models of the SiO(H)Al site. Comparison with observed heats of adsorption are made below (section VII.C.4, Table 26). There are a few calculations which made the nonrealistic assumption of a linear H-bond for the surface complex of NH_3 with the bridging hydroxyl group. These are presented separately in Table 18.

Table 19 compares the observed vibrational transition energies in the N–H stretch and deformation region with predictions made within the harmonic approximation. Two types of N–H stretch bands can be distinguished. Those belonging to "free" N–H protons (not involved in H-bonds) at about 3320–3400 cm^{-1} (3420–3500 cm^{-1} in the calculations of Teunissen *et al.*[392]) and those belonging to protons which are engaged in H-bonds between 2975 and 3110 cm^{-1}. According to these predictions, the highest energy (3360–3400 cm^{-1}) band in the N–H stretch region can be clearly assigned to free N–H protons. The band second highest in energy at 3260–3320 cm^{-1} is separated by 80–124 cm^{-1} from the highest energy band. It could be assigned to the second member of a pair of free N–H stretch bands

Table 17. Adsorption of NH_3 on Bridging Hydroxyls and the Formation of NH_4^+ Cations on the Surface: Calculated Binding Energies, $-\Delta E$, for Both Structures with Respect to NH_3 Separated from the Zeolite Surface (kJ/mol, Results Corrected for the BSSE in Parentheses)

		NH_3		NH_4^+			
model	method	SCF	MP2	SCF	MP2	ΔE_{DP}	ref
$H_3SiO(H)AlH_3$	6-31G*	65		31			391
	MP2/D95**//SCF/6-31G*		76		53		
$H_3SiO(H)Al(H_2)OSiH_3$	6-31G*	64		57			391
	MP2//SCF/6-31G*		88		105		
	MP2/6-31G*		101		112		
$HO(H)Al(H_2)OH$	6-311+G** [a]			110 (98)		1379	392
	MP2//SCF/6-311+G** [a,b]				141 (114)	1377	
$HO(H)Al(OH)_2OH$	SCF/TZ(O)DZP	60		37		1398	421
	MP2//SCF/TZ(O)DZP						
	MP2/TZ(O)DZP		102		99		
$H_3SiO(H)Al(OH)_2OSiH_3$	SCF/TZ(O)DZP	57		67		1319	421
	MP2//SCF/TZ(O)DZP		80		101		
$H_3SiO(H)Al(OH)(OSiH_3)_2$	SCF/TZ(O)DZP	60		46		1300	421
$H_3SiO(H)Al(OSiH_3)_2OSiH_3$	SCF/TZ(O)DZP	63		56		1274	421
8-ring, H-saturated	SCF/TZ(O)DZP	57		58		1338	422

[a] On bordering H atoms STO-3G only. [b] O···N distance optimized for MP2 and/or BSSE corrected energies.

Table 18. Calculations on Complexes of H_2O and NH_3 with Bridging Hydroxyl Sites, SiO(H)T, T = Al, B, Ga, Making the (Unrealistic) Assumption of a Linear Structure: H···O Bond Distance, R_{H-O} (pm), Binding Energy, $-\Delta E$ (kJ/mol), OH Frequency Shift, $\Delta\nu_{OH}$ (cm^{-1}) and, for Comparison, Energy of Deprotonation, ΔE_{DP} (kJ/mol)

				ΔE			
adsorbate	SiO(H)T model	basis set	R_{H-O}	SCF	MP2//SCF	$\Delta\nu_{OH}$	ΔE_{DP}
H_2O	$(HO)_3SiO(H)Al(OH)_3$	STO-3G	145[a]	70[a]			1740[b]
		MINI-1	163[c,d]	58[c,d]			
	$H_3SiO(H)AlH_3$	3-21G	175[c,e]	91[c,e]		771[e]	1430[f]
		6-31G*	180	47			1325
		DZP	~174[g]	56 (45)[g]	73[g]	290[g]	1335[h]
	$H_3SiO(H)BH_3$	DZP	~176[g]	49 (39)[g]	70[g]	252[g]	1400[h]
	$H_3SiO(H)GaH_3$	DZP	~178[g]	49 (39)[g]	65[g]	222[g]	
NH_3	$H_3SiO(H)AlH_3$	6-1G* [i]	179[i]	57 [49][i]	78 [60][i]	619	1395[i]
		6-31G*	180[j]	62[j]			1325[j]
		3-21G	169[k]	101[k]		1150[k]	1430[f]
	$H_3SiO(H)BH_3$	3-21G	169[k]	86[k]		548[k]	1460[l]

[a] Reference 423. [b] Reference 424. [c] Structure of the model not optimized. [d] Reference 425. [e] Reference 188. [f] Reference 202. [g] Reference 426, TZP results in parentheses. [h] Reference 414. [i] Reference 390, STO-3G basis set on dangling bond H-atoms. [j] Reference 187. [k] Reference 427. [l] Reference 428.

since the calculations predict a splitting of 78 cm^{-1}. Unfortunately, an explanation for the two bands around 2950–3068 and 2790–2840 cm^{-1} is missing. These bands, which are separated from each other by 160 to 240 cm^{-1}, cannot be ascribed to the two N–H protons involved in H-bonds, at least not within the harmonic approximation, since the calculations predict only a small splitting of 13 cm^{-1} between such bands. Hence, it seems that an adsorption structure of NH_4^+ with two short H-bonds to the zeolite framework (shell-2 model) explains the IR spectra in the NH bending region. This lead Paukshtis *et al.*[393] to the conclusion that such a structure is the preferred one in faujasite, while Teunissen *et al.*[392] suggest that both this structure and the structure in which NH_4^+ forms three strong H-bonds with the surface may appear at the same time. We feel, however, that experimental and computational evidence is not yet sufficient to draw a conclusion on this subtle structure problem.

The bending modes of the free NH_4^+ cation give rise to two bands, 2- and 3-fold degenerated. On interaction with the zeolite surface these bands are predicted to split, while the mean value of the respective multiplet of bands remains roughly the same as in the free cation. The bands predicted for the {$HAlO_4$}shell-2 model, in particular the strong ones at about 1420 and 1520 as well as that at about 1650 cm^{-1}, corresponds to the bands observed for faujasite at about 1430, 1490, and 1670–1690 cm^{-1} (Table 19) and confirm the assignment of the latter to NH-bendings.

Since for the adsorption of NH_3 there is no doubt that the ion-pair (IP) complex of the NH_4^+ cation on the negatively charged aluminosilicate surface is stable (a minimum on the potential surface), this is an interesting test case for calculations. Table 20 summarizes some results which illustrate the important influence that the structure of the models and the choice of the basis set have. Besides the interaction energy for the neutral complex, ΔE_{NC}, it shows the energy difference between the ion-pair structure and the neutral complex which is defined as the proton-transfer energy, ΔE_{PT}:

$$\Delta E_{PT} = \Delta E_{IP} - \Delta E_{NC}$$

The most reliable calculations (Table 17) predict

Table 19. Wavenumbers of Observed Infrared and INS Spectra of Ammonium Forms of Zeolites and Results of *ab Initio* Calculations[a]

zeolite	ref	NH-stretch				NH-bend				
ERI	429	3384	3260	3068	2840					
MOR	392	3360	3270	3040	2800					
FAU	419					1720			1475[b]	
FAU	430	3400[c]	3180	2950	2790	1670			1430	
FAU	393					1690	1620	1490[d]	1433[d]	1370

model	ref	NH-stretch				NH-bend				
$HOAlO_3$-shell2	416	3396	3318	2987	2974	1658	1642	1518[d]	1421[d]	1324
$HOAlO_3$-shell1	416	3402	3108	3040	3027	1653	1642	1534	1368	1352
8-ring, H-saturated	416									
free	416	3310	3310	3310	3194	1646 (2)[e]			1418 (3)[e]	
$HO(H)Al(H)(OH)_2$, 3H	392	3478	3141	3103						
$HO(H)Al(H_2)OH$, 2H	392	3495	3418	2740	2623					

[a] Harmonic approximation, scaled, $f = 0.92$ and 0.90 for refs 392 and 416, respectively. [b] In zeolite Rho, this band appears at 1450 cm^{-1}, ref 431. [c] Shoulder at 3320 cm^{-1}. [d] Strong bands. [e] Degeneracy.

Table 20. Energy of Adsorption of NH_3 on SiO(H)Al Sites, ΔE_{NC}, and Proton-Transfer Energy, $\Delta E_{PT} = \Delta E_{IP} - \Delta E_{NC}$. Influence of the Structure of the Model and the Basis Set Used. The Energy of Deprotonation, ΔE_{DP}, is Given for Comparison. All Energies in kJ/mol

model	basis set	structure	$R_{N\cdots O}$	ΔE_{NC}	ΔE_{PT}	ΔE_{DP}	ref
$H_3SiO(H)AlH_3$	6-31G*	opt	280	−62	89	1325	187
	6-31G		278	−63	112	1365	
$(HO)_3SiO(H)Al(OH)_3$	6-31G		276		111	1405	
		FAU			−13		
$H_3SiO(H)AlH_3$	3-21G	opt.	264	−100		1430	
	3-21G	opt.	opt[a]	−109	(38)[b]	1430	391
$H_3SiO(H)AlH_3$	3-21G	ZSM5, O_{13}	(250)[c]	−154	−62	1140	432
$(HO)_3SiO(H)Al(OH)_3$				−157	−92	1205	
{SiO(H)Al}sh-2				−170	−105	1060	
$H_3SiO(H)AlH_3$	3-21G	ZSM5, O_{24}	(250)[c]	−136	−3	1280	432
$(HO)_3SiO(H)Al(OH)_3$				−133	−16	1340	
{SiO(H)Al}sh-2				−152	−38	1200	
{SiO(H)Al}sh-3				−146	−28	1300	
$H_3SiO(H)AlH_3$	STO-3G	CHA-SH[d]	259	−83	168	1822	394
$Si_6Al_2O_{10}H_{16}$, MC			265	−53	186	2114	
$Si_{10}Al_2O_{15}H_{22}$, LC			263	−82	168	1945	
$Si_{10}Al_2O_{26}H_{22}$, GC			265	−61	207	1927	
Periodic HF			272	−72	194		
$Si_6Al_2O_{10}H_{16}$	STO-3G	CHA-SH[d]	267	−56	196		144
$Si_6Al_2O_{10}H_{16}$ emb.			266	−69	189		
$H_3SiO(H)AlH_3$	STO-3G	CHA-WY[e]	(255)[c]	−87	149	1780	433
8-ring(2Al), H-sat.			255	−96	135	1825	
8-ring(2Al), OH-sat.			251	−99	128	1751	
periodic HF	STO-3G	CHA-WY[e]	251	−101	86		394

[a] Full optimization (all six intermolecular degrees of freedom). [b] No local minimum, energy for assumed N···O distance. [c] Assumed distance, no optimization. [d] Chabasite, structure obtained by shell model optimization, ref 394. [e] Chabasite, observed structure, locally adapted for SiO(H)Al sites, ref 394.

about the same energy for both structures, *i.e.* $\Delta E_{PT} \approx 0$. Positive ΔE_{PT} values indicate that the ion-pair structure is unfavorable compared with the neutral complex. The following comments can be made on the data in Table 20: (i) The 3-21G basis set largely overestimates the binding energy of the H-bonded neutral complex NC and fails to yield the IP structure at a reasonable energy (provided that optimized geometries are used). The reason is that the energy of deprotonation of the model of the bridging hydroxyl group is about 100 kJ/mol larger than that obtained for, for example, the 6-31G basis set. (ii) When models are adopted which use the observed structure of a particular zeolite such as ZSM-5, the binding energies are even larger and it is predicted that the IP complex is more stable than the NC complex. The reason is again the deprotonation energy. It is particularly low for "observed" structures which assume the same average T−O bond distance for the Si−O and the Al−O bond of the Si−O(H)−Al bridge. There are also significant differences between the O_{13} and O_{24} sites of ZSM-5, which can also be explained by different energies of deprotonation. (iii) STO-3G basis sets for the NC yield binding energies of the right order of magnitude, but the IP structure is unstable with respect to desorbed NH_3. Again, exceedingly large deprotonation energies explain the instability of the IP structure. (iv) For two different chabasite structures, one observed (CHA-WY) and one optimized using a force field (CHA-SH), periodic SCF calculations have been made using the CRYSTAL code.[394] The following conclusions can be only preliminary as rigid structures were adopted and a minimal basis set was used. (iv.a) The 8-membered ring model used also in much better calculations (cf. Table 17) yields a binding energy for the NC which

Table 21. Observed Vibrational Transitions of Water Surface Complexes and Results of *ab Initio* SCF Calculations on {H-AlO$_4$}shell-*x* Type Models[a]

		OH-stretch region			OH-bend region		
		(H)OH-a	(H)OH-s	(Si)OH(Al)	δ_{HOH}	δ_{SiOH}	γ_{SiOH}
separated systems	obsd	3756	3657	3610[d]	1595	1090[c]	420[c]
						1060[b]	320[b]
	shell-1.5	3784	3694	3707	1575	1045	300–330
	shell-2			3690		1090	300
neutral complex	shell-1.5	3755	3605	3353	1571	1194	747
	shell-2	3748	3612	3278	1574	1217	761
		HO	HOH-a	HOH-s	HOH-bend	HOH-twist	HOH-wag
free H_3O^+	calcd	3523	3523	3431	877 (?)	1589	1589
ion-pair complex	shell-1.5	3694	2198	1809	1585	1385	1385
	shell-2	3682	2284	1902	1614	1432	1383
complex	obsd	3695[d]	2885[d]	2457[d]	1635[d]		
		3700[e]	2900[e]	2470[e]	1620[e]		
		3678[f]	2890[f]	2475[f]	1610[f]		
					1670[b]	1385[b]	

[a] shell-1.5, $H_3SiO(H)Al(OH)_2OSiH_3$; shell-2, $H_3SiO(H)Al(OSiH_3)_3$; harmonic approximation, scaled, $f = 0.90$, ref 398. [b] INS spectra H-mordenite, ref 434. [c] INS spectra, ref 57. [d] IR spectra H-ZSM5, ref 395. [e] IR spectra H-ZSM5, ref 435. [f] IR spectra SAPO-34, ref 396.

Table 22. Observed Vibrational Transitions of Methanol Surface Complexes and Results of *ab Initio* SCF and Density Functional Calculations for {H-AlO$_4$}shell-*x* Models[a]

		OH-stretch region			OH-bend region		
systems studied[f]	method	(C)OH		(Si)OH(Al)	δ_{COH}	δ_{SiOH}	γ_{SiOH}
separated systems	obsd	3667[b]–3682[e]		3610[d]	1334[b]–1346[e]	1090[c]	420[c]
separated; shell-1.5	SCF/DZP[g]	3731		3707	1328	1045	300–330
	DFT-BP/DZVP	3685			1357		
NC, shell-1.5	SCF/DZP[g]	3636		3298	1350	1213	706
NC, shell-1.5	MP2/DZP[g]	3276		2548	1421	1353	1015
NC, shell-1.5	DFT-BP/DZVP		2963	2378	1392		
			s-HOH-stre	as-HOH-stre	HOH-bend	HOH-wag	HOH-twist
free $CH_3OH_2^+$	SCF/DZP[g]		3522	3596	1624	599	288
IP, shell-1.5	SCF/DZP[g]		2457	2161	1665	1339	1294
IP, shell-1.5	MP2/DZP[g]		2131	(i)[h]	1634	1386	1306
complex, obsd		3545[d]	2900[d]	2440[d]	1690[d]		
		3576[e]	2800–2900[e]	2400–2550[e]	1610–1720[e]		

[a] Harmonic approximation, SCF and MP2 results scaled, $f = 0.90$ and 0.954, respectively, from ref 402; DFT results from ref 397. [b] Infrared spectra, ref 436. [c] INS spectra, ref 57. [d] IR spectra, ref 401. [e] IR spectra, ref 400. [f] NC, neutral complex; IP, ion-pair complex; shell-1.5, $H_3SiO(H)Al(OH)_2OSiH_3$. [g] Double-ζ plus polarization basis set on all atoms except on oxygen for which a valence triple-ζ basis set is used. [h] To this mode belongs an imaginary frequency.

deviates by only 5% from the periodic result. Note, however, that larger deviations occur for less favorable choices of the cluster model. (iv.b) The extra stabilization of the IP structure in the periodic calculation with respect to the cluster calculation is strongly affected by the structure chosen (CHA-SH or CHA-WY) or by the cluster model adopted. For the 8-ring model it is 44 kJ/mol.

2. Vibrational Spectra and Potential Surfaces of Adsorbed H_2O and CH_3OH

The cases of H_2O and CH_3OH are intriguing, because the triplet of bands which appears at 2900–2800, 2550–2400, and 1700–1600 cm^{-1} upon adsorption on H-forms of zeolites (Tables 21 and 22) has been subjected to conflicting interpretations. While there is agreement on the main features of the observed spectra, two interpretations of the data have been offered. The most recent one interprets the three bands in terms of the so-called A–B–C pattern known for strong H-bonded complexes.[70,72] The basic idea is the following: the zeolitic OH band engaged in H-bonding is shifted to lower wavenumbers and broadened by superposition with the intermolecular stretch mode. The in-plane and out-of-plane SiOH deformations are shifted to higher wavenumbers so that their overtones fall into the region of the broad strongly perturbed OH band. Fermi resonances then create "Evans windows" at about the position of these overtones and the result is three bands. The other interpretation assumes the formation of protonated species, H_3O^+ and $CH_3OH_2^+$, as part of an ion-pair complex at the surface and assigns the bands at 2900–2800 and 2550–2400 cm^{-1} to the symmetric and antisymmetric HOH-stretch of the H-bonded H_3O^+ and $CH_3OH_2^+$ ions, respectively, and the band at 1700–1600 cm^{-1} to the corresponding HOH-bend.[395,396]

So far, for neither interpretation is presently sufficient support available from quantum chemical calculations. Figure 19 shows the structures of the neutral (left) and ion-pair complexes (right) as ob-

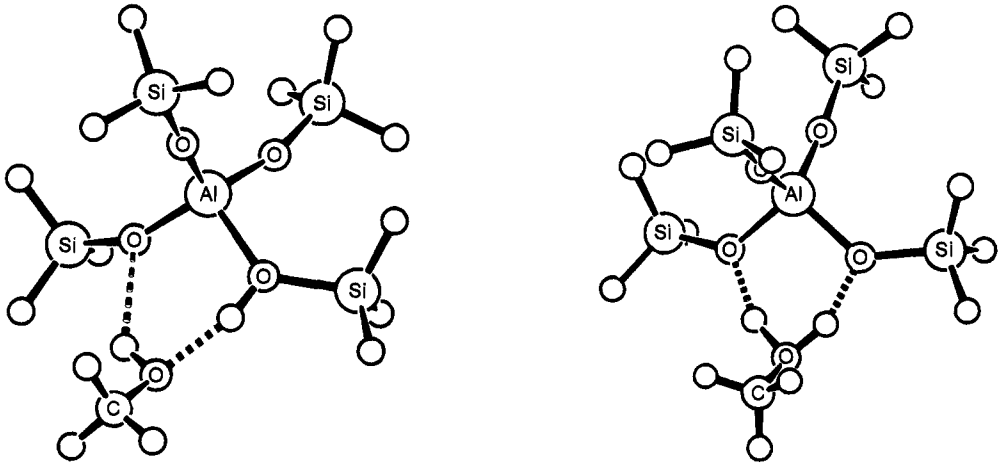

Figure 19. Surface complexes of CH_3OH with the {H-AlO_4}shell-2 model of the bridging hydroxyl group. Left: neutral complex (NC). Right: ion-pair complex (IP).

tained in SCF/DZP (valence triple-ζ on O atoms) optimizations.[83] We first discuss the results predicted for the ion-pair complex (Tables 21 and 22) and note that it proved to be a saddle point, with no local minimum in the calculations reported.[83,381,397,398] The following comments can be made for the SCF and MP2 results: (i) The lowest-wavenumber member of the band triplet at about 1700−1600 can be ascribed to the HOH deformation involving the two H-bonded protons of the XOH_2^+ species (X = H, CH_3). (ii) SCF calculations predict frequencies that are too low for the pair of symmetric and antisymmetric stretches of these two protons. Moreover the predicted splitting is too small. The agreement is even poorer for the MP2 results which are the most reliable ones: Only one of the two possible OH stretches (symmetric and asymmetric ones) gives rise to an IR band. The other describes the reaction coordinate for the motion of the system over the saddle point which is represented by the IP structure, and the corresponding frequency has an imaginary value. (iii) The bands observed at 3694/3682 and 3576/3545 cm^{-1} for adsorbed H_2O and CH_3OH, respectively, can not be explained, neither by SCF nor by MP2 calculations.

The interpretation in terms of an A−B−C triplet assumes a neutral H-bonded surface complex. We first discuss the results obtained within the SCF/DZP approximation for the neutral surface complex of CH_3OH (Table 22): (i.a) To create Evans windows, the overtones of the in-plane and out-of-plane deformations should assume values of about 2675 and 2050 cm^{-1}, i.e. the respective fundamentals should be at about 1340 and 1030 cm^{-1}. The predicted values are 1250 and 784 cm^{-1}, too low by 130 and 250 cm^{-1}. (i.b) The A−B−C interpretation also requires that on adsorption of H_2O or CH_3OH the zeolitic OH band shifts to wavenumbers as low as about 2600−2400 cm^{-1}, i.e. by 1000−1200 cm^{-1}. The predicted shift by 500 cm^{-1} down to 3200 cm^{-1} is too small. (ii) The extra band observed at 3576−3545 cm^{-1} can be assigned to the OH stretch of CH_3OH which weakly interacts with a lattice O-atom bridged by the Al-atom with the zeolitic OH group. The same comments apply to the SCF/DZP calculations for H_2O adsorption (Table 21). The MP2 results, however, are in closer agreement with the assumptions of the A−B−C interpretation. Generally, larger shifts are predicted since on inclusion of electron correlation the interaction becomes stronger. (i.a) The in-plane and out-of-plane deformation bands are now predicted at 1353 and 1015 cm^{-1}, respectively, very close to the above experimental estimated 1340 and 1030 cm^{-1}. (i.b) The zeolitic OH stretch band is shifted down to 2548 cm^{-1} and falls into the region required for the A−B−C interpretation. (ii) The prediction for the methanol OH stretch frequency is too low compared with the observed band at 1376/3545 cm^{-1}. This leaves some doubt on this assignment.

The neutral sorption complex of CH_3OH with the shell-1.5 model has recently been studied within the DFT-BP/DZP approximation.[397] Very large shifts are predicted for the OH stretch of both CH_3OH and the zeolite, which appear at 2963 and 2378 cm^{-1} and are assigned to the 2900−2800 and 2550−2400 cm^{-1} bands of the A−B−C pattern, respectively. The third band of the triplet at 1700−1600 cm^{-1} and the extra band at 3575−3545 cm^{-1} are ascribed to a second surface species. Also this interpretation should be taken with caution as the DFT-BP method was employed which may not properly describe the OH bonds. In section III.B.3 we showed that it predicts exceptionally long bonds and exceptionally low frequencies and, in particular, frequency shifts on H-bond formation that are too large.

In conclusion, no final decision about the existence of a neutral or an ion-pair complex can be made on the basis of vibrational spectra, however, the formation of a neutral complex seems to be more likely. A closer look at the potential energy surface (Figure 20) reveals that there is a broad potential well which comprises both the neutral and the ion-pair complex. The predicted relative energies of these two forms (Tables 23 and 24) depend on the model adopted and the method used, but the better calculations leave no doubt that both forms have very close energies. In all calculations reported, the ion-pair structure proved to be a saddle point. As illustrated in Figure 20 this saddle point is the transition structure for the proton exchange between neighbored basic O-sites of the zeolite framework *via* an adsorbed H_2O or CH_3OH molecule. It is, of course, also the transition structure for the H/D exchange between H-

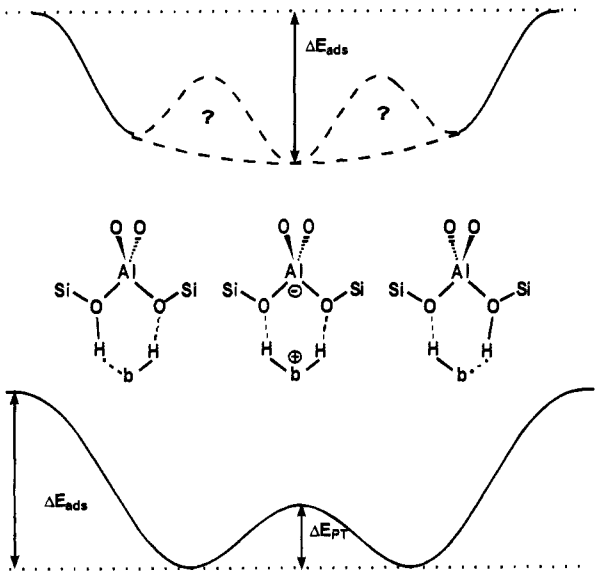

Figure 20. Sketch of the shape of the potential energy surface (PES) for the proton transfer from a SiO(H)Al site onto an adsorbed H_2O or CH_3OH molecule. This PES is also relevant for H/D exchange between the adsorbed molecule and the zeolitic OH group.

Table 23. Binding Energy of H_2O Molecules onto Different Models of SiO(H)Al Sites, ΔE_a, and Energy Difference between the Ion-Pair Structure and the Neutral Adsorption Structure, ΔE_{PT}, in kJ/mol[a]

		$-\Delta E_a$		$-\Delta E_{PT}$	
$\{AlO_4\}$ model	method	SCF	MP2	SCF	MP2
$HO(H)AlH_2OH$	SVP[d]	77		52	
shell-1	DZP[e]	62	83	56	22
shell-1.5, C_s constr	DZP[e]	47	67[c]	45	2[c]
shell-1.5	DZP[e]	48	67[c]	60	17[c]
shell-2	DZP[e]	55		53	
	ΔE(DZP)+ZPE[b]	45	57[c]	40	4[c]

[a] Results from ref 398. [b] Zero point energy calculated for shell-1.5 model. [c] MP2 single point energy calculated at the SCF equilibrium geometry. [d] Split valence polarization basis set. [e] Double-ζ plus polarization basis set on all atoms except on oxygen for which a valence triple-ζ basis set is used.

Table 24. Binding Energy of CH_3OH Molecules onto Different Models of SiO(H)Al Sites, ΔE_a, and Energy Difference Between the Ion-Pair Structure and the Neutral Adsorption Structure, ΔE_{PT}, in kJ/mol[a]

	$-\Delta E_a$	$-\Delta E_a$		$-\Delta E_{PT}$	
$\{AlO_4\}$ model	DFT-BP[b]	SCF[d]	MP2[d]	SCF[d]	MP2[d]
shell-1	84	63	88	49	15
shell-1.5, C_s constr		49	71[c]	31	−7[c]
shell-1.5	69	49	80	49	12
shell-2		55	76[c]	43	6[c]
ΔE+ZPE	64	47	69[c]	39	−7[c]

[a] SCF and MP2 results from ref 402. DFT results from ref 397. [b] Density functional theory with nonlocal corrections according to Becke–Perdew Double-ζ Gaussian basis set with polarization functions on non-hydrogen atoms (DZVP). MP2 single point energy calculated at the SCF equilibrium geometry. [c] DZP basis set on all atoms except on oxygen for which a valence triple-ζ basis set is used.

zeolites and D_2O or CH_3OD, which readily occurs at room temperature—in agreement with the small barrier. It seems that there is a broad and shallow potential well which accommodates both symmetry equivalent neutral surface complexes and the ion-pair transition structure connecting them. (Actually there will be even more of such equivalent structures as the proton could be exchanged between all four O-atoms belonging to the AlO_4 tetrahedron.) Hence all these structures will be accessible when the protons move. We conclude that a nonconventional treatment of the dynamics of the system will be necessary to understand the observed transitions between the eigenstates of the moving nuclei. Specifically we recommend the solution of the Schrödinger equation for the proton in a four-dimensional potential. From an experimental point of view, no convincing evidence has been presented so far for the presence of more than one surface species. Temperature variations down to low values and the study of deuterated samples will be very interesting.

A different type of model has been used in early SCF/STO-3G and SCF/3-21G calculations of the interaction of methanol with acidic hydroxyls. It consists of a cluster of three TO_4 tetrahedra cut-out of an observed ZSM-5 structure, $[O_3SiO(H)Al(O_2)OSiO_3]^{8-}$, and a set of 69 point charges (+2 and −1) on positions of neighboring ions of the ZSM-5 lattice.[127] Optimization of an initial H-bonded structure of methanol with this model yielded a structure in which—contrary to expectation and all other findings—a proton is transferred *from* the methanol *onto* the framework. This result is an artifact of the model adopted for the active site. Due to its large net charge (−8) its energy of deprotonation is as high 2650 kJ mol^{-1} (SCF/3-21G)[399]—more than 1000 kJ mol^{-1} higher than typical values for zeolitic hydroxyls. This means that the model is not an acid, but a base and, hence, it is understandable that it readily accepts protons. Obviously, the embedding in an array of point charges can not fully compensate for the high total charge of the part of the system that is treated quantum-mechanically.

3. CH Stretch Bands of Adsorbed Methanol

Kubelkova *et al.*[400] consider the possible shift of the triplet of CH stretch bands of the CH_3 group and make a tentative assignment of observed shifts to different types of sites. For CH_3OH on bridging hydroxyl sites, however, both Kubelkova *et al.*[400] and Mirth *et al.*[401] report only small shifts of about 10 cm^{-1}, which are not very specific. In fact, the values actually observed may have even different signs (Table 25). Shifts have been calculated for different models of the H-bonded complex and for the ion-pair type complex. For the latter case, shifts between 30 and 80 cm^{-1} are predicted (MP2 results). Hence their formation should be detectable in the IR spectra. The absence of any significant shift in the spectra reported in refs 400 and 401 seems to indicate that the ion-pair structure does not play a role, *i.e.* that $CH_3OH_2^+$ is not formed on the zeolite surface under the conditions of these studies. A similar conclusion is reached for a possible species resulting from the methylation of the bridging hydroxyl group, for which

Table 25. Predicted[a] and Observed Shifts of CH_3 Stretching Frequencies (cm^{-1}) on Binding of CH_3OH on Bridging Hydroxyls (Relative to Free CH_3OH)

system studied[b]	method	CH_3 stretch as(A′)	as(A″)	s(A′)	ref
free (gas phase)	obsd	3005	2961	2847	436
	SCF/3-21G[c]	2996	2926	2890	
	SCF/TZ(O)DZP[d]	2998	2933	2882	402
	MP2/TZ(O)DZP[f]	3008	2939	2865	
	DFT-BP/DZVP[g]	3062	2970	2913	397
H-ZSM5	obsd	−7	−3	9	401
HY, H-ZSM5	obsd	3	0	11	400
NC {H-AlO_4}shell-1	SCF/3-21G[c,e]	−14	15	31	317
NC {H-AlO_4}shell-1	SCF/TZ(O)DZP[d]	3	27	16	402
NC {H-AlO_4}shell-2		16	46	27	
NC {H-AlO_4}shell-1	MP2/TZ(O)DZP[f]	−5	35	16	402
NC {H-AlO_4}shell-1.5		14	42	24	
NC {H-AlO_4}shell-1	DFT-BP/DZVP	22	98	166	397
IP {H-AlO_4}shell-1	SCF/TZ(O)DZP[d]	43	96	59	402
IP {H-AlO_4}shell-2		61	119	74	
IP {H-AlO_4}shell-1.5	MP2/TZ(O)DZP	33	80	47	402
free $CH_3OH_2^+$	SCF/TZ(O)DZP[d]	118	177	95	402
	MP2/TZ(O)DZP[f]	100	161	90	402
	DFT-BP/DZVP	114	190	115	397
$HO(CH_3)Al(OH)_3$	SCF/3-21G[c,e]	69	97	62	317

[a] Scaled harmonic wavenumbers, scale factor determined to give the best average match of observed and calculated CH_3 stretching frequencies. [b] NC, neutral surface complex; IP, ion-pair complex; {H-AlO_4}shell-1, $HO(H)Al(OH)_3$; {H-AlO_4}shell-1.5, $H_3SiO(H)Al(OH)_2OSiH_3$ {H-AlO_4}shell-2, $H_3SiO(H)Al(OSiH_3)_3$. [c] Scale factor $f = 0.9096$. [d] Scale factor $f = 0.9136$. [e] Results of ref 317 have been rescaled using a uniform scale factor for all 3 modes. [f] Scale factor $f = 0.9346$. [g] Density functional method, unscaled frequencies.

shifts between 60 and 100 cm^{-1} are predicted (Table 25):

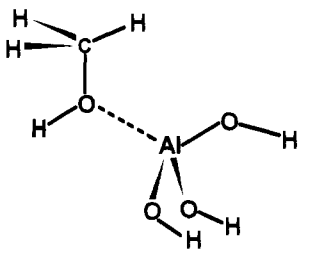

The DFT method with inclusion of Becke–Perdew gradient corrections already predicts unrealistically large shifts for the neutral adsorption structure.[397] Comparison with MP2 results[402] in Table 25 shows that this is not a problem of the model, but another weakness of the DFT-BP method.

4. Heats of Adsorption for H_2O, CH_3OH, and NH_3

Table 26 shows that the experimental data available are limited and show a large scatter. It is interesting to compare the results for CH_3OH on H-ZSM5 with those for silicalite which has the same structure as H-ZSM5 but does not contain bridging hydroxyl groups. Thamm[403] reports heats of adsorption of 43 kJ/mol. However, for very small loadings below 0.25 mmol/g, the heat of adsorption increases to 80–90 kJ/mol with the slight indication of a plateau at about 75 kJ/mol. The nature of the sites which are responsible for such values of the heat of adsorption is presently not clear (active H-ZSM5 catalysts have an active site concentration of 0.2 to 1 mmol/g). The most consistent set of data for NH_3, H_2O, and CH_3OH are probably those of Gorte *et al.*[404,405] on H-ZSM5. For comparison with the experimental data, nuclear motion corrections to the calculated binding energies are necessary. While thermal corrections are negligible, zero point vibrational energy corrections amount to about 8–16 kJ/mol (Table 26). If we use the binding energy calculated at the MP2 level for the equilibrium geometry of the $H_3SiO(H)Al(OSiH_3)_3$ model, we obtain an estimate of −78 kJ/mol for $\Delta_a H$ of NH_3. The corresponding values for CH_3OH and H_2O are smaller (Table 26), as expected from their lower basicity. There is an estimate of ±20 kJ/mol for the uncertainty limit which reflects both the incompleteness of the model (cf. the results for the shell-1- and shell-2-type and of the 8-ring models in Table 17) and the approximations connected with the computational technique chosen. A possible explanation for the fact that weaker interactions are predicted by the calculations than observed is that long-range effects may contribute to the stabilization of the ion-pair structures. Unfortunately, the periodic calculations performed by the CRYSTAL code for NH_3 on SiO(H)Al sites in chabasite,[394] though an important step in the proper direction, do not provide a conclusive answer yet because the unrealistic assumption of rigid framework structures had to be made to make the calculations feasible.

Table 26. Observed Heats of Adsorption (H-ZSM5) and Values Predicted by Calculations[e] (kJ/mol)

adsorbate	calculated[e] $-\Delta E_a$	ZPE	$-(\Delta E_a + ZPE)$	$-\Delta H^0$ H-ZSM5	H-ZSM5	HY
H_2O	73	11	62	~85[a]	51[c]	
CH_3OH	76	8	69	110–120[a]	63[d]	
NH_3	94	16	78	~150[b]	100–120[f]	120–140[g]

[a] Reference 404. [b] Reference 405. [c] Reference 437. [d] Reference 438. [e] {$HAlO_4$}shell-2 model; MP2 single point energy at SCF equilibrium geometry, ZPE calculated from SCF frequencies. [f] Reference 439. [g] Reference 440.

D. Interaction with Hydrocarbons and CO

H-Forms of zeolites catalyze the conversion of hydrocarbons. Hence, there is much interest in their interaction with the bridging hydroxyl sites, not only from the experimental but also from the computational point of view (cf. ref 406 for a recent example and ref 407 for a recent view on the problem). Senchenya and Kazansky have shown by calculations that in the case of ethylene the most stable product is a surface alkoxide, at least at low temperatures.[408] However, they also found an additional stationary point which corresponds to the vdW surface complex of ethylene and is higher in energy by 17 kJ/mol (Figure 21). The stabilization with respect to the hydrocarbon molecule separated from the surface is 29 kJ/mol. The vdW complex is separated by a barrier of 64 kJ/mol from the alkoxide structure. Very recently Viruela-Martin *et al.*[100] extended this study in several respects. They considered the reaction of propylene and isobutene and used the larger H_3SiO-

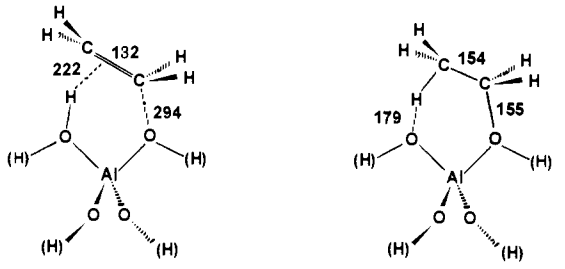

Figure 21. Structures and relative energies of the vdW- and alkoxid-type surface complexes of ethylene on SiO(H)-Al sites (data from ref 408).

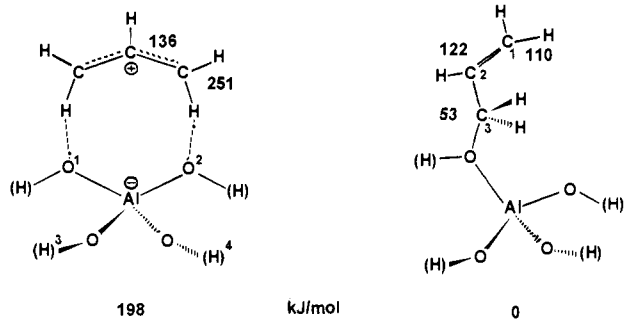

Figure 22. Structures, relative energies, and ^{13}C-NMR chemical shifts (ppm) of the ion pair- and alkoxid-type surface complexes of the allylcation on the SiO(H)Al sites (data from ref 409).

(H)Al(OH)$_2$OSiH$_3$ model. The same stationary points were found: a vdW complex, stabilized by 25 and 34 kJ/mol for the propylene and isobutene, respectively, an alkoxide structure (stabilization of 73 and 65 kJ/mol, respectively), and a transition structure which corresponds to the barrier between the two minima. Models in which the Al atom was replaced by B or Ga atoms were also studied. The energies reported in both studies are of qualitative value only, as SCF calculations have been performed with the 3-21G basis set without correction for the BSSE and the small models were used. Note that MP2 energies calculated with the 3-21G basis set as done in ref 100 are meaningless and should not be reported. A general finding of both studies is that the interaction of a hydrocarbon molecule with the zeolite catalyst does not only involve the acidic hydroxyl group but also a neighbored basic oxygen site.

A similar picture emerges for the interaction of the allyl cation with the zeolite framework: The vdW surface complex (Figure 22, left) is a minimum on the potential energy surface, but the surface alkoxide (Figure 22, right) is by almost 200 kJ/mol more stable.[409] These calculations adopted the same small model but used a much better TZ(O)DZP basis set. Nothing is known from calculations about the barrier separating the two surface species, but it seems to be high enough to allow detection of the vdW surface complex in NMR experiments. Haw et al.[410] observed an extreme downfield peak at ~250 ppm in their *in situ* ^{13}C NMR study of the reactions of propene on the zeolite HY catalyst and ascribed it to alkyl-substituted allyl cations. The shifts of 236 and 251 ppm calculated by the IGLO method[411] for the CH_2 carbon atoms of the free allyl cation and its vdW surface complex (Figure 22, left), respectively, support this assignment and make it very likely that allyl cations form vdW complexes with zeolite surfaces. It should be noted that the substituted allyl cations studied in the experiments are more stable than the prototype species considered in the calculations.

Ugliengo et al.[358] studied the vdW complex of acetylene with the bridging hydroxyl group. In FTIR experiments this complex had been identified as the precursor species for the formation of polyacetylene[33] (see Figure 23). The observed frequency shifts are in qualitative agreement with the values computed for the complex of acetylene with the small H_3SiO-(H)AlH_3 model, in particular after including correlation (Figure 23). The binding energies corrected for the BSSE are 17 and 19 kJ/mol and the $-\Delta H°_0$ values are 13 and 14 kJ/mol at the SCF and MP2 levels, respectively. In subsequent studies, models should be considered which allow for a two-site contact. Moreover, it is not obvious that an alkoxid-type structure can be ruled out as alternative of the ion-pair structure of Figure 23.

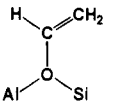

Early studies of the interaction of molecules with bridging hydroxyls relied on SCF calculations using the 3-21G basis set. For computational reasons this level of approximation is still adopted from time to time and a few comments on their reliability are pertinent. One of the first studies was that of Geerlings *et al.* on the binding of CO, H_2O, and NH_3[188] which made the significant point that it is characteristic for bridging hydroxyls that they undergo a substantially larger OH-frequency shift than terminal hydroxyls (cf. Table 27). On the basis of such calculations Pelmenschikov *et al.* argued[316] that

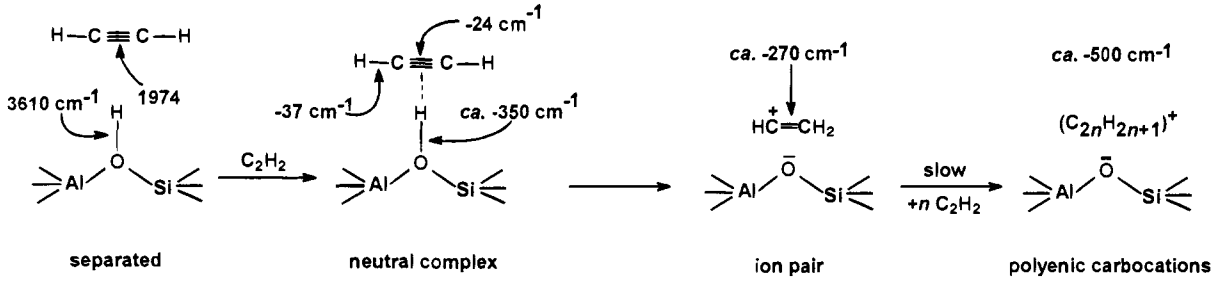

Figure 23. Shift of the CC stretch frequency accompanying protonation and polymerization of acetylene on SiO(H)Al sites (data from ref 358).

Table 27. Calculated[a] and Experimental Shifts of Vibrational Frequencies (cm^{-1}) on Binding of CO on Surface Hydroxyls

		ν_{OH}		ν_{CO}	
site	method/basis set	OH−CO[b]	OH−OC[b]	OH−CO[b]	OH−OC[b]
terminal SiOH on silica	obsd	−78[e]		14[e]	
	SCF/3-21G	−14[g]			
	SCF/DZP	−29[c]	2[c]	25[c]	−7[c]
	SCF/DZP	−25[h]	−1[h]	23[h]	−8[h]
	MP2/DZP	−52[h]	7[h]	20[h]	4[h]
bridging SiO(H)Al on zeolites	obsd	−310; −298[f]		32; 36[f]	
	SCF/3-21G	−183[g]			
	SCF/DZP	−74[d]	−21[d]	35[d]	−23[d]
	SCF/DZP	−84[h]	−30[h]	38[h]	3[h]
	MP2/DZP	−174[h]	−31[h]	31[h]	−5[h]

[a] Harmonic approximation. [b] Two adsorption structures. [c] Reference 345. [d] Reference 346. [e] See ref 345 for the original references of the observed data. [f] See ref 346 for the original references of the observed data. [g] Reference 188. [h] Reference 412.

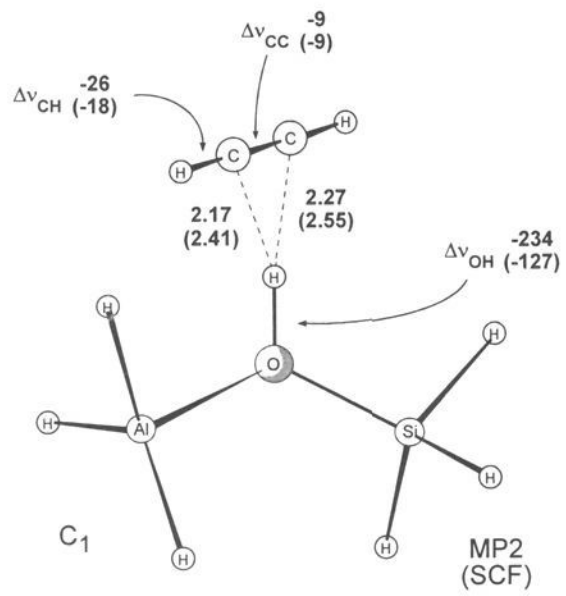

Figure 24. Calculated structure and frequency shifts of the complex of acetylene with the $H_3SiO(H)AlH_3$ model.[358]

in amorphous aluminosilicates a special type of bridging hydroxyl sites, possibly generated according to

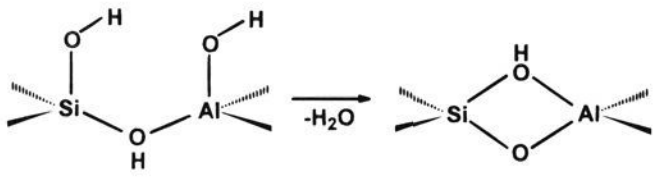

may be responsible for an infrared band at about 3750 cm^{-1} which shifts to 3200 cm^{-1} on adsorption of CH_3CN. This shift of 550 cm^{-1} was in apparent agreement with the prediction by the calculation for the $(HO)_2SiO_2(H)Al(OH)_2$ model when a specific scale factor was applied which was based on the assumption that the shift for the SiO(H)Al bridging hydroxyl site is about 740 cm^{-1}. In a more recent paper, however, Pelmenschikov *et al.* interpret the bands at about 2770 and 2400 cm^{-1} which are characteristic for the surface complex of acetonitrile on the SiO(H)Al site in a different way:[70,71] These are two parts of the shifted ν_{OH} band which is split due to Fermi resonance with the $\delta_{2,SiOH}$ overtone. Hence, a shift of about 1100 cm^{-1} would be the proper reference point. This shows that the assumption of a special scale factor for force constants of OH bonds engaged in H-bonds is a very dangerous procedure, at least when based on questionable assignments. Consequently, the assignment of the IR band at 3750 cm^{-1} observed in aluminosilicates to structures such as

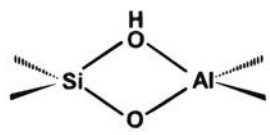

made by Pelmenschikov *et al.*[316] is no longer supported by their calculations. One of the later papers[70] compares the frequency shift calculated (scaled) for the CN stretching mode of CH_3CN on adsorption on SiO(H)Al sites (23−26 cm^{-1}) with those calculated for adsorption on terminal hydroxyls (11 cm^{-1}) and possible Al-Lewis sites (50−58 cm^{-1}).

CO forms vdW surface complexes with the SiO(H)Al sites. The precise value of $\Delta\nu_{OH}$ may be used as a measure of the hydroxyl acidity, as may in principle the *positive* $\Delta\nu_{CO}$, which is, however, 1 order of magnitude smaller.[370] An SCF study of the interaction of CO with bridging hydroxyls[346] adopted the small $H_3SiO(H)AlH_3$ model and used the 6-31G* basis set. From a previous study[345] of the interaction of CO with surface silanol groups (section VI), we know that within the SCF approximation the stabilization energy is much too low (provided that sufficiently extended basis sets are used and corrections are made for the BSSE) and that it is not possible to discriminate between the binding of the CO molecule *via* its O and C ends. However, from the same study we know that the calculated vibrational frequencies allow a clear-cut distinction between the two adsorption structures possible. Table 27 compares the calculated frequency shifts with the observed ones. The observed blue shift of the CO stretch on adsorption excludes the OH−OC approach. For the OH−CO structure the predictions are in qualitative agreement with the observations, although the magnitude of the shift predicted for the O−H stretch is too small, in particular for the bridging hydroxyl group. Recently, some of us performed calculations on the interaction of the CO molecule with the $H_3SiO(H)AlH_3$ model at the MP2/DZP level.[412] The results for the OH−CO structure (Table 27) are closer to the observed data, but the predicted OH-frequency shift is still too small.

E. Effects of Including an External Crystal Potential in Cluster Calculations on Silica and Zeolites

In the following we will review results which can possibly shed some light on the effect that long-range

potentials may have on the computed properties of cluster models. We first look at atomic charges calculated for H-saturated cluster models and compare them with results for these clusters embedded in point charge arrays. In a few cases periodic calculations are available as a reference. The reader should keep in mind that atomic charges are model-dependent quantities. Hence, we do not discuss here what the most meaningful definition of an atomic charge would be. For the observed structure of all-silica sodalite, both a periodic calculation (CRYSTAL code) and a cluster calculation were completed.[308] The cluster model included a complete sodalite cage. The atomic charges (Mulliken population analysis) on the O atom were −1.11 e and −1.13 e for the periodic calculation and the finite model, respectively. Also for crystals with a larger Al content such as the H-chabasite studied by Teunissen et al. (Si/Al = 3),[144] the charges calculated for the periodic structure and the cluster models are virtually identical. The charges on the Si, O, Al, and H atoms of the bridging hydroxyl group, SiO(H)Al, calculated for the periodic structure (CRYSTAL code) and for a cluster model consisting of two fused four-membered rings (composition $Si_6Al_2O_{16}H_{16}$) are +1.443, −0.534, +1.212, and +0.213 and +1.449, −0.532, +1.224, and +0.215, respectively (in units of e, STO-3G basis set). We conclude that obtaining the proper charge distribution does not require the inclusion of an external potential which corrects for neglected long-range effects.

Table 20 shows energies for the binding of NH_3 on the bridging hydroxyl group in chabasite.[394] The periodic calculation yields 72 kJ/mol while the results for different cluster models are between 53 and 82 kJ/mol. These deviations are not large, in particular if one considers that these calculations are still affected by errors connected with frozen geometries and the basis set chosen (SCF/STO-3G). The binding energies quoted refer to the neutral H-bonded complexes. Frequently, the opinion is expressed that the influence of the crystal potential may be much larger for the more polar ion-pair structures of these complexes. Table 20 reports the energy difference between the (polar) ion-pair structure and the (nonpolar) neutral adsorption complex, ΔE_{PT}. Calculations made with proper basis sets on relaxed structures show that the stability of both types of structures is about the same (cf. Table 17), i.e. ΔE_{PT} is about zero. Due to the use of the STO-3G basis set which is not appropriate for describing anions and, hence, yields deprotonation energies that are by far too large, and due to the assumption of rigid geometries, the ΔE_{PT} values calculated for the chabasite models are much too large (100−200 kJ/mol). Nevertheless, a comparison of the ΔE_{PT} result of the periodic calculation (194 kJ/mol) and the results obtained for different cluster models (between 168 and 207 kJ/mol) may still be regarded as a useful source of information for the influence of the crystal potential. Contrary to what many expect, the influence is not significantly larger than that for the neutral adsorption structure.

One may expect even larger effects of the crystal potential on the results when a proton is completely removed from the bridging hydroxyl site, as we do when calculating deprotonation energies. Again contrary to such expectations, Bleiber and Sauer (cf. ref 308) found that the deprotonation energy of the small $H_3SiO(H)AlH_3$ model (3-21G basis set, 1205 kJ/mol) changed by 15 kJ/mol only when they embedded the cluster in the silicalite Madelung field (composition SiO_2, charges of +2 e and −1 e assigned to the Si and O atoms, observed ZSM-5 structure). The effect of passing from the observed structure to the optimized structure was much larger, 150 kJ/mol. Table 20 confirms this large dependence on the structure assumed.

The small dependence of the deprotonation energy on the crystal potential is a beneficial feature of neutral clusters obtained by saturating the dangling bonds with H-atoms. This is clearly seen from deprotonation energies calculated for a series of differently embedded models of the bridging hydroxyl site in quartz.[413] For the H-saturated H-{Al[OSi-$(OH)_3]_4$} model ("shell-3" in the nomenclature of section VII.B), a deprotonation energy of 1350 kJ/mol is obtained.[308] This is a realistic value. After corrections for the systematic error of the 3-21G basis set (−115 kJ/mol) and further corrections for nuclear motion effects, it yields an estimate of the enthalpy of deprotonation of 1200 kJ/mol, which falls into the range of spectroscopically derived values for acidic zeolites (cf. section VII.B). For the highly charged H-{Al[$OSiO_3^{3-}]_4$} model, obtained by a heterolytic cut from the periodic structure, Sim et al.[413] calculate a deprotonation energy as large as 5280 kJ/mol. Embedding in a cluster of point ions chosen to mimick the Madelung potential of α-quartz for assumed Si/O charges of +2 e/−1 e reduces the deprotonation energy to 3020 kJ/mol—a value still too large by far.[413] (cf. Table 8.7 of ref 308, note some misprints: the references given in that table should be incremented by 1). A similar value of the deprotonation energy (2650 kJ/mol) is obtained for the $[O_3SiO(H)AlO_3]^{6-}$ model embedded in a ZSM-5 lattice of point ions with +2 e/−1 e charges.[399] Only when a fully ionic model with Si/O charges of +4 e/−2 e is adopted does the energy of deprotonation of the H-{Al[$OSiO_3^{3-}]_4$} model drop to 770 kJ/mol.[413] This shows that small changes in the embedding potential have a large effect when the cluster is charged.

From all that we gather: The errors due to neglected long-range effects are minor and do not significantly change the calculated properties of silica and zeolites. Errors connected with assuming fixed or only partially relaxed structure or errors connected with the choice of the computational method/basis set are as relevant as the former. Evidence on the effect of the crystal potential is still limited, and more investigations are needed. They should use periodic codes since adding an external electrostatic potential to a cluster is a severe approximation and adopt good basis sets which describe anions properly and yield reliable energies of deprotonation.

VIII. Summary and Conclusions

Experimental Results. vdW systems involving solid surfaces are not as thoroughly characterized as vdW molecules in the gas phase. To get conclusive results, working with well-prepared and well-characterized surfaces is very important. Moreover, in adsorption

studies the combined use of different techniques on the same sample is highly recommended. IR and NMR spectroscopic investigations should be complemented by microcalorimetric studies and/or measurements of adsorption isotherms. Heats of adsorption measured at very low coverage ($\theta = 0$) are suitable for a direct comparison with those computed using cluster models. Lateral interactions can be estimated by the heat measured at high coverage, and comparison can be made with periodic calculations. Extreme care should also be taken to use samples free of structural defects and/or chemical impurities. This is particularly important for silica materials dehydrated around 1000 K (for structural defects) and for zeolites in which defects and extra-framework materials in the channels may alter the properties of the zeolite.

The largest body of data on vdW interactions between molecules and oxidic surfaces comes from classical IR spectroscopy. Changes on adsorption of characteristic modes of both the surface site and the adsorbed molecule can be monitored. Prominent examples are the shift of the OH-stretch frequency of surface hydroxyl groups and the shift of the stretch frequency of the adsorbed CO molecule. Sometimes, however, only hints on adsorption structures are obtained and the assignment of observed spectral features to microscopic structures is debatable. Examples are the conflicting interpretations offered for the IR spectra observed on adsorption of H_2O and CH_3OH on zeolitic SiO(H)Al groups.

Computational Methods and Strategies. For surface complexes the need for a combination of observed data and quantum chemical results may be even larger than for vdW molecules, but, unfortunately, the computational problems are more severe. A successful computational study of *vdW interactions* between molecules and surface sites has to find a *good balance* between the level of the quantum chemical treatment and the type and the size of the *surface model.*

The limits and merits of the methods described depend on the details of the systems studied, so that their discussion is inevitably spread over different sections of this review. To make easy access to that material we provide a list of recommendations. They should be taken as a personal view of the authors, necessarily limited by their own experience in subfields of the whole area of molecule−surface interactions. In this respect, they may be a useful guide for a novice and a matter of critical consideration for the experienced researcher.

The *quantum chemical approximation* should meet the following requirements: (i) Reliable structures and force constants of the surface site and the adsorption complex. (ii) Good description of the electric moments and the polarizability of the subsystems. A specific case is the CO molecule, for which large corrections in the electric properties are due to the electron correlation. (iii) Reasonably small and balanced BSSE between the components of the model (e.g. the cations and anions of an ionic crystal).

These result in the following recommendations: (1) the SCF/DZP or SCF/SVP approximations as the minimum theoretical level; (2) the MP2/DZP approximation as the cheapest method for checking the influence of dynamic electron correlation; (3) the MP2/DZP approximation with a basis set augmented with diffuse functions and special exponents for polarization functions (lower than usually used) for really weak interactions dominated by dispersion forces; (4) a multireference treatment, e.g. CASSCF, if the one-determinant description is not adequate for a subsystem.

In the case of very large models, or when computational resources are too limited, the following alternatives may be considered, depending on the need of treating electron correlation: (1) DFT methods to handle electron correlation. Gradient corrected functionals are the only sensible choice, because all local functionals overestimate the binding energies for weakly bound systems. Comparison with good experimental data on well-defined systems or accurate *ab-initio* results for related small molecules, when available, is certainly worthwhile. It should also be kept in mind that at the moment no systematic study has yet been published on the performance of various DFT approaches for hydrogen-bonded systems. Frequency shifts predicted by DFT methods, even when gradient-corrected functionals are used, should be considered with some caution (OH mode in H-bonds, CH mode in adsorbed methanol). (2) Employing 3-21G basis sets (as any other nonpolarized basis sets) is meaningless in studies which take electron correlation into account. (3) The SCF/3-21G approximation may be a reasonable choice in studies of the structure and vibrational spectra of a *single isolated* molecule. It is, however, of *very limited use* in studies of *weakly bounded systems* due to the large BSSE, exaggerated intramolecular charge separation, and a polarizability of each moiety that is too low. (4) The SCF/MINI-1 approximation may be successfully used to study intermolecular interactions. The computed binding energies, when BSSE corrected, are close to those computed with the more demanding 6-31G** basis set.

The reliability of the chosen method may be checked by applying better approximations for the smallest meaningful model. The limitations of the adopted cluster model may be removed by enlarging it in calculations using the least expensive method which still describes the dominating interactions qualitatively correctly.

With respect to the choice of a *model*, the following strategies may be useful:

(1) *Periodic approaches* are the theoretically most satisfactory methods, in that no *a priori* subdivision or cut of the surface is made. Presently, even the most advanced code (CRYSTAL) is limited to the SCF approximation and to single point calculations. Analytic gradients with respect to the displacements of the nuclei are not available. Electron correlation can be taken into account in an *a posteriori* scheme only, using DFT methods.

(2) *Cluster models* are attractive because molecular codes are applicable so that, in a straighforward way, geometry optimization can be performed and electron correlation can be included. When chosing a given cluster as a model, a number of suggestions should be considered: (i) the chosen cutting procedure

should give clusters the interaction of which with the surroundings is small; (ii) the electric properties of the model should be as similar as possible to those of the surface site; (iii) the composition of the model (stoichiometry) should be as close as possible to that of the real surface; (iv) the acid–base properties of the model should be similar to those of the surface site. To this purpose, calculation of both the deprotonation energy and the proton affinity for clusters of different size and topology will ensure that a peculiarity of the chosen model will not significantly alter the results. For ionic or partially ionic crystals this means that models with a net charge are not suitable if the surface site is not charged. When the surface is neutral, the model can then be built from neutral layers of ions. Specifically, in studies of adsorption on ionic surfaces, stoichiometric models are a much better choice than highly charged models built from shells of ions around the binding site such as $(MgO_5)^{8-}$. For solids with electron pairs in covalent bonds this means that the homolytic cut of the bonds between the cluster and its surroundings is the more reliable procedure. The number of dangling bonds should be kept at minimum, by designing models with rings and cages. This is true even for partially ionic solids (SiO_2, zeolites). The corresponding dangling bonds can then be saturated with hydrogen atoms.

Two types of *embedding techniques* have been discussed in this paper: (i) Starting form a periodic description, a solution for a localized perturbation is attempted (perturbed cluster approach). (ii) Attempts to correct the cluster calculations for neglected long-range effects by adding an external potential. All techniques assume rigid geometries. This is in conflict with the need of optimized structures for predicting frequency shifts and reliable interaction energies for all but the weakest interactions. The ICECAP code is the only one which offers a strategy for solving this conflict, but its applicability in the field of intermolecular interactions still has to be proven. It is important to stress at this point that embedding techniques can not compensate for an improperly chosen cluster model. In particular, embedding by point charges or point multipoles can not compensate for errors connected with an exceedingly large total charge of the models. Moreover, the unrealistic polarization of the cluster by the embedding charges can cause errors, unless special measures are taken to minimize such effects. Among the suggested methods are an "isolating shell" of ions described by full ion pseudo or model potentials and the application of the external correction potential which is limited to an inner zone of the cluster. Any attempts to optimize structures in the presence of embedding charges should be avoided. In conclusion, errors made on designing a model can not be compensated by an external potential and embedding in an external long-range potential does not necessarily improve the cluster results. The need to use optimized structures (except for really weak interactions) is frequently in conflict with the intention to use embedding techniques because of the absence of the Pauli repulsion between the cluster and the embedding ions.

In the following paragraphs, we recapitulate the most relevant results for ionic and covalent systems (amorphous silica and zeolites).

CO Adsorption on MgO(001) Surface. A large number of computational studies have been reported on this system, which mainly adopt clusters embedded in a set of unscreened point charges of assumed values of ±2 e. A better procedure is to use the CRYSTAL code to make proper corrections to the values of the charges, so that a best fit is obtained between the electrostatic potential of the crystal and that of the embedded cluster in the binding region.[155] No definite value for the computed binding energy can be quoted, but it is clear that the adsorption is dominated by electrostatic and dispersive forces. The best values obtained for neutral clusters as large as $(MgO)_{21}$ are around 10 kJ/mol (BSSE corrected). The corresponding computed blue shift of the CO stretching frequency of about 4 cm^{-1} is underestimated compared with the measured value of 14 cm^{-1}.[229] The use of repulsive full ion model potentials which isolate the quantum cluster from the exterior set of bare charges further decreases the above estimate.[232] Results obtained by means of CRYSTAL with the P91 correlation correction on a three-layer slab give a value of 23 kJ/mol without BSSE correction.[155] Experimental data based on various adsorption techniques (isosteric heat, microcalorimetry) span the range of 13–42 kJ/mol, with some preference for the lower side. Measurement of the heat of adsorption of CO on clean MgO(001) is virtually impossible at room temperature because chemisorption occurs at steps, kinks, and corners. Measurements at low temperature are more difficult to perform. Before a meaningful comparison with the experiment can be made, a better internal consistency of the computed values is needed. This requires improved periodic calculations, inclusive of BSSE corrections and adopting much larger basis sets (TZ2P on the CO molecule). Supercell calculations with large unit cells are also desirable. Within the cluster approach the adsorption on large, neutral, and stoichiometrically correct MgO clusters should be studied. Due to the steady increase of the available computer power, such calculations are within reach now.

NO Adsorbed on NiO(001) Surface. Much less computational work has been done on the NO/NiO than on the CO/MgO system. Experimental data are, however, more definitive. Both TDS on the UHV (001) clean surface and microcalorimetry at zero coverage on well-defined NiO crystal tablets show that the binding energy is between 50 and 83 kJ/mol. FTIR and HREELS measurements of the shift of the NO-stretching frequency yield −71 and −76 cm^{-1}, respectively. From NEXAFS measurements it is inferred that the structure of the complex on the surface is bent with the axis of NO forming an angle of about 45°. Calculations show that a bent structure is indeed preferred with respect to the linear one but the actual value of the binding has been found to be strongly dependent on the Madelung field in which the clusters are embedded. The best estimate is 56 kJ/mol, inclusive of electron correlation and BSSE correction.[253] A blue shift of the NO-stretching frequency is computed for the adsorption on the Ni^{2+}

site, a result opposite to the observations. A red shift is predicted only for adsorption on an oxygen site with a reduced charge. It is clear that new investigations are needed, in particular to assess where the NO molecule will be adsorbed (Ni^{2+} or O^{2-} ions) and to explain the origin of the vibrational red shift.

Adsorption on Silica. To model isolated surface silanol groups, H-saturated models have been used almost exclusively. Both tree-like models, $HO\text{-}SiX_3$ obtained by adding an increasing number of coordination shells (X = H, OH, $OSiH_3$, ...), and cage-like models have been used with success. Vicinal and geminal silanol groups have been represented by similar models. The interaction of H_2O and NH_3 has been studied at the MP2 level with good basis sets for H_3SiOH and $H_2Si(OH)_2$ modeling isolated and geminal silanol groups. The effect of extending these models was investigated. Comparison with the experimental heats of adsorption has also been carried out. The interactions of other molecules have been studied both computationally (mainly SCF/DZP) and experimentally (mainly FTIR and microcalorimetry): CH_3OH, CH_2O, CO, N_2O, H_2, C_2H_2, and C_2H_4. The simplest H_3SiOH model gives results which are qualitatively consistent with the formation of hydrogen-bonded species at the silica surface. The available calorimetric data for molecules interacting with the silica surface are, unfortunately, not abundant. Furthermore, the measurements of the heats of adsorption of H_2O, CH_3OH, and NH_3 are particularly delicate on highly dehydrated silicas. These molecules can also react with the surface, opening strained siloxane bridges and giving rise to interacting silanol groups. As a consequence, the measured heats of interaction of NH_3, H_2O, and CH_3OH with such a modified surface, may be higher than those expected on the pristine surface, where isolated silanol groups were predominant. At the opposite, heats of adsorption for much less reactive molecules such as H_2, CO, C_2H_2, and C_2H_4 are so weak as to require specific equipment suitable for low-temperature work (liquid nitrogen), which obviously hinders the application of standard and reliable techniques. Infrared data are however much more abundant, and experiments even at low temperatures are feasible and fairly reproducible. Even considering the above difficulties, the general conclusion is that the best estimate of the binding energy and the shift of the OH-stretching frequency due to the H-bond formation are both underestimated when compared with the experimental evidence. From the theoretical point of view, more sophisticated calculations are needed to assess the systematic errors which affect both the computed binding energy and the OH frequency shift of the H_3SiOH model (vide infra).

Adsorption on Zeolites. The observed data on the adsorption of molecules on *cation sites* in zeolites can be rationalized in first approximation by *ab-initio* calculations on free cation–molecule complexes. Great care is necessary to improve the treatment beyond this level. Semiempirical quantum chemical studies on larger cluster models do not yield reliable results. Embedding of the quantum mechanically treated cluster in an array of point ions does not allow for optimization of structures as outlined above. Spectroscopic evidence is rich, and there are many opportunities for quantum chemical studies provided that the proper techniques will be used.

Among the many types of surface hydroxyl groups which may occur in zeolite catalysts, only the bridging SiO(H)Al sites have been studied in interactions with external molecules by quantum chemical *ab-initio* techniques. Calculations on models of different types and of increasing size have led to a fully computational characterization of the structure, the vibrational properties, and the acidity (energy of deprotonation) of the bridging hydroxyl site. The predicted results are consistent with the known experimental data. As free space models are used, the influence of specific zeolite lattices can only be studied when the models are large enough to include whole secondary building units typical of specific frameworks. Due to recent advances in computer technology (parallel architecture) and quantum chemical methodology, this is now possible. For example, the model shown in Figure 17 is typical of the faujasite lattice.

The zeolites with bridging hydroxyl groups catalyze the conversion of hydrocarbons. Computational studies for acetylene, ethene, propene, and isobutene show that a vdW complex is always formed which is separated by a barrier from the more stable intermediates such as surface alkoxides. In spite of the numerous experimental studies of catalytic hydrocarbon conversions, experimental data on the formation of vdW complexes are scarce. *Ab-initio* calculations have been used to support the assignments of the FTIR spectra of adsorbed acetylene to a vdW complex and the assignment of ^{13}C NMR data to a vdW complex between the allyl cation and the deprotonated hydroxyl group, $Si{-}O{-}Al(O{-})_2{-}O{-}Si$.

The CO molecule has also been used as a probe molecule for the interaction with bridging hydroxyl groups. Comparison of the calculated and observed OH- and CO-frequency shifts predicts an OH–CO structure as the most stable form of the surface complex.

The adsorption of proton donor/proton acceptor molecules such as NH_3, CH_3OH, and H_2O can lead to a neutral adsorption complex (NC) or, when the zeolitic proton is transferred to the adsorbed molecule, to an ion-pair complex (IP). In the case of NH_3 the existence of stable ion-pair complexes is obvious because NH_4^+ forms of zeolites are easily prepared. The experimental infrared spectra also show, in a definite way, features which are peculiar of the NH_4^+ species. The calculations predict about the same stability for both the NC and IP structures and a multisite coordination of NH_4^+ to the aluminosilicate framework. In accord with the results of the few X-ray structure refinements, the NH bonds form both single and bifurcated H-bonds with the framework oxygen atoms. The calculated average ^1H NMR chemical shifts are in agreement with observed values for NH_4^+. The harmonic vibrational frequencies calculated for the NH stretch and HNH deformation modes are in general agreement with observed spectra. However, not every detail of the multiplets of bands can be assigned. There is not sufficient evidence to make inferences about the

preference of adsorption structures involving two or three H-bonds with the surface.

On adsorption of H_2O and CH_3OH molecules a characteristic triplet of bands appears in the OH-stretch region. This is interpretated either as due to the neutral complex structure (the triplet is created from the broadened and shifted OH band by Fermi resonance with the overtones of the in-plane and out-of-plane SiOH deformations) or as due to the formation of a protonated surface species (IP structure). The *ab-initio* calculations performed so far do not permit a discrimination between the two suggested structures. Interestingly, the calculations of the infrared spectra for the IP structure predict that marked blue shifts (about 30−80 cm^{-1}) of the C−H stretch modes of the surface $CH_3OH_2^+$ should occur. If such large shifts are not observed—and this is the case in the studies reported so far—this shows that the IP structure does not play any role on the surface.

The potential energy surfaces for the conversion of the NC and IP complexes calculated at various approximation levels and for various models have minima for the NC structures only, while the IP structures prove always to be saddle points. The barrier is small, however, when electron correlation is included. This is in accord with the observation that the H/D exchange with the acidic proton of zeolites is rapid when H_2O or CH_3OH molecules are present.

General Remarks. The predicted heats of adsorption of the NH_3, CH_3OH, and H_2O molecules on the bridging hydroxyl site of zeolites are significantly smaller than the calorimetric data. A similar discrepancy has been found for the interaction of NH_3 with isolated silanol groups on silica surfaces. In accord with extremely low interaction energies, very low OH stretch frequency shifts are calculated. In section VII.E we produce evidence that neglected long-range effects can not account for the whole difference between calculated and experimental values. We have also already mentioned that the smaller models underestimate the energy of the H-bond because they are too small to reproduce the electronic properties at the surface OH group. Indeed, by comparison with a much larger cage-type model ($Si_8O_{12}H_7OH$), the shell-0 model for the isolated hydroxyl group, H_3SiOH, is found to be not acidic enough. Other possible reasons are (i) the estimate of the entropy according to the rigid cluster model needs improvement (many calculations have shown that large amplitude motions of the adsorbed molecule are possible for which the harmonic approximation may be not appropriate); (ii) the model adopted neglects dispersion contributions from an extended part of the solid; (iii) our idea of the binding site, its local structure, and/or composition on the surface is incomplete. This may be particularly relevant for the presumed local structure of the active site on silica. The isolate silanol, instead of being protruded outside the surface, may stay at the bottom of a structure depression. This will presumably increase the dispersive and electrostatic interactions of the probe molecule with the neighbor atoms belonging to the wall of the basin. To test this hypothesis, much better structural models of the surface of amorphous materials are needed. Useful contributions can be expected from modern modeling techniques based, for instance, on the newly derived force field for siliceous materials.[444] A further possibility worth exploring is that structural strain will increase the acidity of the OH group in a significant way.

These are challenges for future studies, both experimental and computational. Due to the fast development of computer technology and *ab-initio* computational techniques, we expect that the body of computational data will grow faster than that of the experimental data. There is reasonable hope for solving some of the yet-unsolved problems encountered in the field of vdW interactions between molecules and surfaces.

IX. Acknowledgments

We thank Drs. Mauro Causà, Erik Teunissen, and Ivan Senchenya and many other colleagues for sharing with us unpublished data. Special thanks go to Anna Maria Ferrari, Mariann Krossner, and Drs. Andreas Bleiber, Frank Haase, and Jörg-R. Hill who did a lot of calculations, many of them still unpublished, which have been partially included in sections VI and VII. This work has greatly benefitted from the use of the semidirect SCF and MP2 codes TURBOMOLE developed by Prof. Reinhart Ahlrichs and his co-workers at the University of Karlsruhe. P.U. and E.G. are also grateful to many colleagues of the Dipartimento di Chimica Inorganica, Chimica Fisica e Chimica dei Materiali, for helpful discussions and suggestions. We are greatful to Monika Urban and Birgit Kruschwitz for their technical assistance which has been crucial for completing this manuscript and to Audries deMan for his careful proofreading. J.S. also thanks the Fonds der Chemischen Industrie for financial support. P.U. and E.G. are grateful to CSI Piemonte for allowance of computer resources and to both the Italian Consiglio Nazionale delle Ricerche and Ministero della Universitá e Ricerca Scientifica e Tecnologica (MURST, fondi 40%) for financial support. SERC and CCP5 are also gratefully acknowledged for generous allowance of computer resources.

X. Abbreviations

AEOW	all electrons on the water oxygen atom
AES	Auger electron spectroscopy
AIMP	*ab-initio* full ion model potential
ARUPS	angle-resolved ultraviolet photoelectron spectroscopy
ATR	attenuated total reflection
BHW	Bellamy−Hallam−William method
BSSE	basis set superposition error
CADPAC	molecular *ab-initio* computer code
CASSCF	complete active space self-consistent field
CEPA	coupled electron pair approximation
CHA-SH	chabasite, force field optimized structure (shell model)
CHA-WY	chabasite, X-ray structure (Wyckoff)
CI	configuration interaction

CISD	configuration interaction including single and double substitutions
CNDO/2	complete neglect of diatomic overlap parametrization variant 2
CP	counterpoise method
CP/MAS NMR	cross-polarization/magic angle spinning NMR
CPC	counterpoise correction
CRYSTAL	periodic *ab-initio* SCF computer code
CS	Colle–Salvetti correlation functional
CSOV	constrained space orbital variation procedure
DFT	density functional theory
DFT-B-LYP	Becke–Lee–Yang–Parr density functional
DFT-BH	Barth–Hedin density functional
DFT-BP	Becke–Perdew density functional
DFT-VWN	Vosko–Wilk–Nusair density functional
ECP	effective core potential
EELS	electron energy loss spectroscopy
EMBED	embedded cluster method computer code
ESR	electron spin resonance spectroscopy
FIR	far infrared spectroscopy
FT	Fourier transform
FTIR	Fourier transform infrared spectroscopy
GAMESS	molecular *ab-initio* computer code
GAUSSIAN92	molecular *ab-initio* computer code
GG	gauche–gauche conformation
GPA	gas-phase acidity
GTO	Gaussian-type orbital
H-ZSM-5	hydrogen-exchanged zeolite ZSM-5
HOMO	highest occupied molecular orbital
HONDO	molecular *ab-initio* computer code
HREELS	high-resolution electron-energy-loss spectroscopy
HRTEM	high-resolution transmission electron microscopy
IC-ACPF	internally contracted approximate coupled pair functional
ICECAP	embedded cluster method computer code
IGLO	individual gauge localized orbitals
INS	inelastic neutron scattering
IP	ion-pair complex
IR	infrared spectroscopy
IRAS	infrared reflection absorption spectroscopy
LDF-Xα	local density functional X-α method
LEED	low-energy electron diffraction
LUMO	lowest unoccupied molecular orbital
M	methanol
MAS NMR	magic angle spinning nuclear magnetic resonance spectroscopy
MCPF	modified coupled pair functional
MEP	molecular electrostatic potential
MM	methanol/methanol dimer
MP2	Møller–Plesset second-order perturbation theory
MP4(SDTQ)	Møller–Plesset fourth-order perturbation theory with single, double, triple and quadruple substitutions
MR-CCI	multireference contracted configuration interaction
MS	methanol/silanol dimer
Na-ZSM-5	sodium-exchanged zeolite ZSM-5
NC	neutral complex
NEXAFS	near-edge X-ray-adsorption fine structure
NMR	nuclear magnetic resonance spectroscopy
P86, P91	Perdew 1986 and 1991 correlation functionals
PES	potential energy surface
PHF	periodic Hartree–Fock
PSOW	pseudo potential on the water oxygen
QPEN	quantum mechanical potential based on electron pairs and nuclei
RCM	rigid cluster model
RMP4	restricted MP4
S	silanol
SCF	self-consistent field
SERS	surface-enhanced raman spectroscopy
SEXAFS	surface-extended X-ray-adsorption fine structure
SM	silanol/methanol dimer
SS	silanol/silanol dimer
TDS	thermal desorption method
TEM	transmission electron microscopy
TURBOMOLE	molecular *ab-initio* computer code
UHV	ultrahigh vacuum
UPS	ultraviolet photoelectron spectroscopy
UV–vis	ultraviolet–visible spectroscopy
vdW	van der Waals
WA	water as hydrogen-bond acceptor
WD	water as hydrogen-bond donor
XPS	X-ray photoelectron spectroscopy
ZPE	zero point vibrational energy
ZSM-5	Mobil zeolite structure 5 (silicalite)

XI. Basis Sets Description

3-21+G	Pople split valence plus diffuse sp set
3-21G and 4-31G	Pople split valence
6-311G**	Pople valence triple ζ plus a set of p functions on H and a set of d functions on non-hydrogen atoms
6-31G	Pople valence double ζ
6-31G**; 6-31G(d,p)	Pople valence double ζ plus d functions on non-hydrogen atoms and p functions on H
6-31G*; 6-31G(d)	Pople valence double ζ plus d functions on non-hydrogen atoms
DNP	numerical double-zeta basis set plus polarization functions
DZ	double ζ
DZ(d,p); DZP; D95**	double ζ plus d functions on non-hydrogen and p functions on H
DZVP	valence double zeta plus d and p functions
MINI-1	Huzinaga minimal
STO-3G	Pople minimal
SVP	split valence plus polarization functions
SZ	single ζ
TZ(2p,2d); TZ(d2,2p); TZ2P	triple ζ plus double set of p functions on H and d functions on non-hydrogen atoms
TZ(O)DZ(d,p); TZ(O)DZP	triple ζ on oxygen atoms and double ζ on the remaining atoms plus d functions on non-hydrogen and p functions on hydrogen atoms

TZ+(2df,2p)	triple ζ plus a set of diffuse p on non-hydrogen atoms. Double set of d functions and one f set on non-hydrogen atoms and a double set of p functions on H
TZ++(2d,2p)	TZ(2d,2p) plus a diffuse p set on non-hydrogen atoms and a diffuse s set on H
TZ+2d	triple ζ plus a diffuse p set and double set of d functions on non-hydrogen atoms
VTZ	valence triple ζ

Note Added in Proof

Since the completion of this manuscript a number of articles have appeared or have been discovered. They will be mentioned in the order in which they would appear in the review:

Section II.D. Jameson *et al.* use grand canonical Monte Carlo simulations to relate the ^{129}Xe chemical shifts measured for different loadings of Xe in zeolite NaA at different temperatures to the distribution of the Xe atoms in this adsorbent[445] and to the structure of the adsorbed fluid.[446] This work makes use of pairwise additive *ab-initio* intermolecular shielding functions. Vigné-Maeder analyzes the quantitative dependence of the ^{129}Xe chemical shift on the cavity size of various all-silica zeolites in terms of collisions between xenon and the walls using molecular dynamics simulations.[447]

Section IV.A. Pacchioni *et al.* performed *ab-initio* calculations on the physisorption of SO_2 on the MgO(100) surface.[448] A structure was considered in which SO_2 is bridge bonded to two adjacent Mg^{2+} cations. The predicted vibrational and photoemission features are consistent with the experiment.

Section VII.B. Periodic *ab-initio* calculations have been performed on a zeolite which includes a Brønsted acidic site, SiO(H)Al.[449] The sodalite framework was adopted and a partial struture optimization was performed at the SCF/STO-3G level. Comparison was made with results for finite models on which the same structure constraints were imposed. The {SiO(H)Al}-shell0 and -shell1 models and a model including a four-membered silicate ring were considered. The atomic charges differ by 0.02 e (Al) or less between the periodic structure and the largest finite model. The structure parameters determined by the periodic calculations also deviate by less than 1 pm from the results for the largest cluster. The only notable deviation is that the periodic calculations predict an out-of-plane angle of 25° for the acidic proton with respect to the Si−O−Al plane, while the cluster models have the acidic proton within this plane. These findings confirm the statements in section VII.E.

Section VII.C. An integrated NMR and *ab-initio* study has been made of acetonitrile in zeolites.[450] Convincing arguments are produced for the fact that observed shifts can be assigned to unusual surface species only with confidence if *ab-initio* calculations of chemical shifts are available. The energy minimum structure obtained by *ab-initio* calculations for the complex of acetonitrile with a cluster consisting of three tetrahedra ($2SiO_4$, $1AlO_4$) is typical of a neutral complex stabilized by a H-bond between the zeolitic OH group and the nitrogen atom of acetonitrile. It is similar to the structures of the gas phase complexes between acetonitrile and HF, HCl, and HCN as proton donors. The formation of IP-type structures with the proton transfered from the zeolite to the base within the complex could only be achieved when structure constaints were imposed which enforced a close contact between the bridging oxygen of the zeolite and the carbon atom of the CN group in acetonitrile. The ^{13}C NMR chemical shifts calculated for bent and protonated acetonitrile in such constrained structures agree with values observed at higher temperatures, while the results obtained for the weakly perturbed acetonitrile molecule in the neutral complex agree with the room temperature measurements.

References

(1) Hobza, P.; Zahradník, R. *Chem. Rev.* **1988**, *88*, 871.
(2) Hobza, P.; Zahradník, R. *Intermolecular Complexes. The Role of van der Waals Systems in Physical Chemistry and in the Biodisciplines*; ACADEMIA PRAHA: Prague, 1988.
(3) Steele, W. *Chem. Rev.* **1993**, *93*, 2355.
(4) Brosseau, R.; Brustein, M. R.; Ellis, T. H. *Surf. Sci.* **1993**, *294*, 243.
(5) Klemperer, W. *Nature* **1993**, *362*, 698.
(6) Pople, J. A. *Faraday Discuss. Chem. Soc.* **1982**, *73*, 7.
(7) Au, C.; Breza, J.; Roberts, M. W. *Chem. Phys. Lett.* **1979**, *66*, 340.
(8) Sauer, J.; Haberlandt, H.; Pacchioni, G. *J. Phys. Chem.* **1986**, *90*, 3051.
(9) Bauschlicher, C. W., Jr. *Chem. Phys. Lett.* **1987**, *142*, 71.
(10) Klopper, W.; Lüthi, H. P.; Brupbacher, T.; Bauder, A. *J. Chem. Phys.*, in press.
(11) Perdew, J. P. In *Proceedings of the 21st Annual International Symposium on the Electronic Structure of Solids* **1991**; Ziesche, P., Ed.; Nova Science: 1991.
(12) Giamello, E.; Ugliengo, P.; Garrone, E. *J. Chem. Soc., Faraday Trans. I* **1989**, *85*, 1373.
(13) Legon, A. C.; Millen, D. *J. Chem. Soc. Rev.* **1987**, *16*, 467.
(14) Duke, C. B., Ed. *Surface Science: The First Thirty Years*; North-Holland: Amsterdam, 1994.
(15) Klekamp, A.; Reissner, R.; Umbach, E. In *Adsorption on Ordered Surfaces of Ionic Solids and Thin Films*, Springer Series in Surface Sciences, Vol. 33; Umbach, E., Freund, H.-J., Eds.; Springer Verlag: Berlin Heidelberg, 1993; p 35.
(16) Henzler, M.; Stock, A.; Böl, M. In *Adsorption on Ordered Surfaces of Ionic Solids and Thin Films*, Springer Series in Surface Sciences, Vol. 33; Umbach, E., Freund, H.-J., Eds.; Springer Verlag: Berlin Heidelberg, 1993; p 15.
(17) Freund, H.-J.; Kuhlenbeck, H.; Neumann, M. In *Adsorption on Ordered Surfaces of Ionic Solids and Thin Films*, Springer Series in Surface Sciences, Vol. 33; Umbach, E., Freund, H.-J., Eds.; Springer-Verlag: Berlin Heidelberg, 1993; p 136.
(18) Pangher, N.; Schmalz, A.; Haase, J. *Chem. Phys. Lett.* **1994**, *221*, 189.
(19) Jacobi, K. In *Adsorption on Ordered Surfaces of Ionic Solids and Thin Films*, Springer Series in Surface Sciences, Vol. 33; Umbach, E., Freund, H.-J., Eds.; Springer Verlag: Berlin Heidelberg, 1993; p 103.
(20) Garrone, E.; Bartalini, D.; Coluccia, S.; Martra, G.; Tichit, D.; Figueras, F. In *International Symposium on Acid-Base Catalysis* 2, Sapporo, Japan, 1993, unpublished.
(21) Lunsford, J. H. *J. Phys. Chem.* **1967**, *46*, 4347.
(22) Binnig, G.; Quate, C. F.; Gerber, C. *Phys. Rev. Lett.* **1986**, *56*, 930.
(23) Zecchina, A.; Scarano, D.; Reller, A. *J. Chem. Soc., Faraday Trans. I* **1988**, *84*, 2327.
(24) Morterra, C.; Garrone, E.; Bolis, V.; Fubini, B. *Spectrochim. Acta* **1987**, *43A*, 1577.
(25) Garrone, E.; Ghiotti, G.; Giamello, E.; Fubini, B. *J. Chem. Soc., Faraday Trans. I* **1981**, *77*, 2613.
(26) Della Gatta, A.; Fubini, B.; Ghiotti, G.; Morterra, C. *J. Catal.* **1976**, *43*, 90.
(27) Bolis, V.; Fubini, B.; Garrone, E.; Morterra, C. *J. Chem. Soc., Faraday Trans. I* **1989**, *85*, 1383.
(28) Fubini, B. *Thermochim. Acta* **1988**, *135*, 19.
(29) Cardona-Martinez, N.; Dumesic, J. A. *Adv. Catal.* **1992**, *38*, 149.
(30) Roquèrol, J. *Pure Appl. Chem.* **1976**, *47*, 315.
(31) Garrone, E.; Ugliengo, P., unpublished.
(32) Al-Sarraf, N.; Stuckless, J. T.; King, D. A. *Nature (London)* **1992**, *360*, 243.
(33) Bordiga, S.; Ricchiardi, G.; Spoto, G.; Scarano, D.; Carnelli, L.; Zecchina, A.; Areàn, C. O. *J. Chem. Soc., Faraday Trans.* **1993**, *89*, 1843.

(34) Spoto, G.; Bordiga, S.; Ricchiardi, G.; Scarano, D.; Zecchina, A.; Borello, E. *J. Chem. Soc., Faraday Trans.*, to be published.
(35) Cant, N. W.; Hall, K. J. *J. Catal.* **1972**, *25*, 161.
(36) Smirnov, K. S.; Tsiganenko, A. A. *Opt. Spectrosc.* **1986**, *60*, 667.
(37) Heidberg, J.; Cabigon, L.; Kampshoff, E.; Kandel, M.; Kühnemuth, R.; Meine, D.; Redlich, B.; Schönekäs, O.; Suhren, M.; Weiss, H.; Wetter, D. In *Adsorption on Ordered Surfaces of Ionic Solids and Thin Films*, Springer Series in Surface Sciences, Vol. 33; Umbach, E., Freund, H.-J., Eds.; Springer-Verlag: Berlin Heidelberg, 1993; p 46.
(38) Ewing, G. E. In *Adsorption on Ordered Surfaces of Ionic Solids and Thin Films*, Springer Series in Surface Science, Vol. 33; Umbach, E., Freund, H.-J., Eds.; Springer Verlag: Berlin Heidelberg, 1993; p 57.
(39) Bertoluzza, A.; Bonino, G. B.; Fabbri, G.; Lorenzelli, V. *J. Chim. Phys. Phys. Chim. Biol.* **1966**, *63*, 395.
(40) Tobin, R. G.; Richards, P. L. *Surf. Sci.* **1987**, *179*, 387.
(41) Young, Y. S.; Howe, R. F. *J. Chem. Soc., Faraday Trans. I* **1986**, *82*, 2887.
(42) Melendres, C. A.; Beden, B.; Bowmaker, G.; Liu, C.; Maroni, V. A. *Langmuir* **1993**, *9*, 1980.
(43) Khondanov, A. Y.; Kustov, L. M.; Kazansky, V. B.; Williams, C. *J. Chem. Soc., Faraday Trans.* **1993**, *89*, 4123.
(44) Zecchina, A.; Scarano, D. In *Adsorption and Catalysis on Oxide Surfaces;* Che, M., Bond, G. C., Eds.; Elsevier: Amsterdam, 1985; p 71.
(45) Scarano. D.; Zecchina, A.; Bordiga, S.; Geobaldo, F.; Spoto, G.; Petrini, G.; Leofanti, G.; Padovan, M.; Tozzola, G. *J. Chem. Soc., Faraday Trans.* **1993**, *89*, 4123.
(46) Bolis, V.; Fubini, B.; Garrone, E.; Giamello, E.; Morterra, C. In *Proceedings of a European Conference on Structure and Reactivity of Surfaces*, Trieste/Italy 1988, Studies in Surface Science and Catalysis, Vol. 48; Morterra, C., Zecchina, A., Costa, G., Eds.; Elsevier: Amsterdam, 1989; p 159.
(47) Coluccia, S.; Baricco, M.; Marchese, L.; Martra, G.; Zecchina, A. *Spectrochim. Acta* **1993**, *49A*, 1289.
(48) Paukshtis, E. A.; Soltanov, R. I.; Yurchenko, E. N. *React. Kinet. Catal. Lett.* **1981**, *16*, 93.
(49) Zaki, M. I.; Knözinger, H. *Spectrochim. Acta* **1987**, *43A*, 1455.
(50) Richardson, H. H.; Chang, H. C.; Noda, L.; Ewing, C. E. *Surf. Sci.* **1989**, *90*, 93.
(51) Angell, C. L.; Schaeffer, P. C. *J. Phys. Chem.* **1966**, *70*, 1413.
(52) Schindler, P.; Kamber, H. R. *Helv. Chim. Acta* **1968**, *51*, 1781.
(53) Kazansky, V. B.; Gritscov, A. M.; Andreev, V. M.; Zhidomirov, G. M. *J. Mol. Catal.* **1978**, *4*, 135.
(54) Boccuzzi, F.; Coluccia, S.; Ghiotti, G.; Morterra, C.; Zecchina, A. *J. Phys. Chem.* **1978**, *82*, 1298.
(55) Kustov, L. M.; Borovkov, Y. V.; Kazansky, V. B. *J. Catal.* **1981**, *72*, 149.
(56) Kazansky, V. B.; Kustov, L. M.; Borovkov, V. Y. *ZEOLITES* **1983**, *3*, 77.
(57) Jacobs, W. P. J. H.; Jobic, H.; van Wolput, J. H. M. C.; van Santen, R. A. *ZEOLITES* **1992**, *12*, 315.
(58) Wax, M. J.; Cavanagh, R. R.; Rush, J.; Stucky, G. D.; Abrams, L.; Corbin, D. R. *J. Phys. Chem.* **1986**, *90*, 532.
(59) Jobic, H. *J. Catal.* **1991**, *131*, 289.
(60) Tsiganenko, A. A. *Russ. J. Phys. Chem.* **1982**, *56*, 1428.
(61) Pimentel, G. C.; McClellan, A. L. *The Hydrogen Bond*; Freeman: San Francisco, 1960.
(62) Knözinger, H. In *The Hydrogen Bond. Recent Developments in Theory and Experiments*; Schuster, P., Zundel, G., Sandorfy, C., Eds.; North-Holland: Amsterdam, 1976; Vol. 3, p 1263.
(63) Cant, N. W.; Little, L. H. *Nature* **1966**, *211*, 69.
(64) Cant, N. W.; Little, L. H. *Can. J. Chem.* **1965**, *43*, 1252.
(65) Cant, N. W.; Little, L. H. *Can. J. Chem.* **1964**, *42*, 802.
(66) Cant, N. W.; Little, L. H. *Can. J. Chem.* **1967**, *45*, 3055.
(67) Cant, N. W.; Little, L. H. *Can. J. Chem.* **1968**, *46*, 1373.
(68) Tsiganenko, A. A.; Babaeva, M. A. *Opt. Spectrosc.* **1983**, *54*, 665.
(69) Clydon, M. F.; Sheppard, N. *J. Chem. Soc., Chem. Commun.* **1969**, 1431.
(70) Pelmenschikov, A. G.; van Santen, R. A.; Jänchen, J.; Meijer, E. *J. Phys. Chem.* **1993**, *97*, 11071.
(71) Pelmenschikov, A. G.; van Wolput, J. H. M. C.; Jänchen, J.; van Santen, R. A. *J. Phys. Chem.*, submitted.
(72) Pelmenschikov, A. G.; Santen, R. A. v. *J. Phys. Chem.* **1993**, *97*, 10678.
(73) Curthoys, G.; Davydov, V. Y.; Kiselev, A. V.; Kiselev, S. A.; Kusnetsov, B. U. *J. Colloid Sci.* **1974**, *48*, 58.
(74) Rouxhet, P. G.; Sempels, R. E. *J. Chem. Soc., Faraday Trans. I* **1974**, *70*, 2021.
(75) Paukshtis, E. A.; Yurchenko, E. N. *React. Kinet. Catal. Lett.* **1981**, *16*, 131.
(76) Kubelkova, L.; Beran, S.; Lercher, J. *ZEOLITES* **1989**, *9*, 539.
(77) Wang, P.-K.; Ansermat, J.-P.; Rudaz, S. L.; Wang, Z.; Shore, S.; Slichter, C. P.; Sinfield, J. H. *Science* **1986**, *234*, 35.
(78) Engelhardt, G.; Michel, D. *High-resolution solid-state NMR of silicates and zeolites*; Wiley: Chichester, 1987.
(79) Pfeifer, H. *NMR: Basic Princ. Prog.* **1994**, *31*, 31.
(80) Fraissard, J.; Ito, T. *ZEOLITES* **1988**, *8*, 350.
(81) Chen, R.; Springuel-Huet, M. A.; Fraissard, J. *Stud. Surf. Sci. Catal.* **1991**, *65*, 219.
(82) Mastikin, V. M.; Mudrakowsky, I. L.; Filimonova, S. V. *ZEOLITES* **1990**, *10*, 593.
(83) Haase, F.; Sauer, J. *J. Phys. Chem.* **1994**, *98*, 3083.
(84) Chalasinski, G.; Gutowski, M. *Chem. Rev.* **1988**, *88*, 943.
(85) van Lenthe, J. H.; van Duijneveldt-van de Rijdt, J. G. C. M.; van Duijneveldt, F. B. In *Ab initio Methods in Quantum Chemistry-II*, Advances in Chemical Physics, Vol. 69; Lawley, K. P., Ed.; John Wiley & Sons Ltd.: New York, 1987; p 521.
(86) Hobza, P.; Sauer, J.; Morgeneyer, C.; Hurych, J.; Zahradník, R. *J. Phys. Chem.* **1981**, *85*, 4061.
(87) Sauer, J.; Zahradník, R. *Int. J. Quantum Chem.* **1984**, *26*, 793.
(88) Hehre, W. J.; Radom, L.; Schleyer, P. v. R.; Pople, J. A. *Ab initio Molecular Orbital Theory*; Wiley: New York, 1986.
(89) Boys, S. F.; Bernardi, F. *Mol. Phys.* **1970**, *19*, 553.
(90) Gutowski, M.; van Duijneveldt-van de Rijdt, J. G. C. M.; van Lenthe, J. H.; van Duijneveldt, F. B. *J. Chem. Phys.* **1993**, *98*, 4728.
(91) Davidson, E. R.; Chakravorty, S. J. *Chem. Phys. Lett.* **1994**, *217*, 48.
(92) Jeziorski, B.; Kolos, W. In *Molecular Interactions*; Ratajczak, H., Orville-Thomas, W., Eds.; Wiley: New York, 1982; Vol. 3, p 1.
(93) Buckingham, A. D. In *Intermolecular Interactions: From Diatomics to Biopolymers*; Pullman, B., Ed.; Wiley: New York, 1978; Vol. 1, p 1.
(94) Claviere, P. In *Intermolecular Interactions: From Diatomics to Biopolymers*; Pullman, B., Ed.; Wiley: New York, 1978; p 69.
(95) Fogarasi, G.; Pulay, P. In *Vibrational Spectra and Structure*; During, J., Ed.; Elsevier: Amsterdam, 1985; Vol. 14, p 125.
(96) Pulay, P.; Fogarasi, G.; Pongor, G.; Boggs, J. E.; Vargha, A. *J. Am. Chem. Soc.* **1983**, *195*, 7037.
(97) Handy, N. C.; Gaw, J. F.; Simandiras, E. D. *J. Chem. Soc., Faraday Trans. II* **1987**, *83*(9), 1577.
(98) Ugliengo, P.; Saunders, V. R.; Garrone, E. *J. Phys. Chem.* **1990**, *94*, 2260.
(99) Ugliengo, P.; Garrone, E. *J. Mol. Catal.* **1989**, *54*, 439.
(100) Viruela-Martin, P.; Zicovich-Wilson, C. M.; Corma, A. *J. Phys. Chem.* **1993**, *97*, 13713.
(101) Hobza, P.; Sauer, J. *Theoret. Chim. Acta* **1984**, *65*, 279.
(102) Sauer, J.; Hobza, P. *Theoret. Chim. Acta* **1984**, *65*, 291.
(103) Sauer, J. *Z. Chem.* **1985**, *25*, 254.
(104) Parr, R. G.; Yang, W. *Density-Functional Theory of Atoms and Molecules*; Oxford University Press: New York, 1989.
(105) Trickey, S. B., Ed. *Advances in Quantum Chemistry-Density Functional Theory of Many-Fermion Systems*; Academic Press, Inc.: San Diego, 1990; Vol. 21.
(106) Labanowski, J. K., Andzelm, J. W., Eds. *Density Functional Methods in Chemistry*; Springer Verlag, Inc.: New York, 1991.
(107) Frisch, M. J.; Trucks, G. W.; Head-Gordon, M.; Gill, P. M. W.; Wong, M. W.; Foresman, J. B.; Johnson, B. G.; Schlegel, H. B.; Robb, M. A.; Replogle, E. S.; Gomperts, R.; Andres, J. L.; Raghavachari, K.; Binkley, J. S.; Gonzalez, C.; Martin, R. L.; Fox, D. J.; DeFrees, D. J. Baker, J.; Stewart, J. J. P.; Pople, J. A. *GAUSSIAN 92*; Gaussian, Inc.: Pittsburgh, PA, 1992.
(108) Amos, R. D.; Alberts, I. L.; Andrews, J. S.; Colwell, S. M.; Handy, N. C.; Jayatilaka, D.; Knowles, P. J.; Kobayashi, R.; Koga, N.; Laidig, K. E.; Maslen, P. E.; Murray, C. W.; Rice, J. E.; Sanz, J.; Simandiras, E. D.; Stone, A. J.; Su, M.-D. *CADPAC5: The Cambridge Analytical Derivatives Package*; University of Cambridge: Cambridge, U.K., 1992.
(109) Ahlrichs, R.; Bär, M.; Brode, S.; Ehrig, M.; Haase, F.; Häser, M.; Horn, H.; Kölmel, C.; Schäfer, A.; Schiffer, H.; Weis, R. *TURBOMOLE*; Universität Karlsruhe: Karlsruhe, 1992.
(110) Vosko, S. H.; Wilk, L.; Nusair, M. *Can. J. Phys.* **1980**, *58*, 1200.
(111) von Barth, U.; Hedin, L. *J. Phys. C: Solid State Phys.* **1972**, *5*, 1629.
(112) Becke, A. D. *Phys. Rev. A* **1988**, *28*, 3098.
(113) Perdew, J. P. *Phys. Rev. B: Condens. Matter* **1986**, *33*, 8822.
(114) Ziegler, T. *Chem. Rev.* **1991**, *91*, 651.
(115) Sosa, C.; Andzelm, J.; Elkin, B. C.; Wimmer, E.; Dobbs, K. D.; Dixon, D. A. *J. Phys. Chem.* **1992**, *96*, 6630.
(116) Velde, G. T.; Baerends, E. J. *Chem. Phys.* **1993**, *177*, 399.
(117) Neyman, K. M.; Rösch, N. *Chem. Phys.* **1993**, *177*, 561.
(118) Sim, F.; St. Amant, A.; Papai, I.; Salahub, D. R. *J. Am. Chem. Soc.* **1992**, *114*, 4391.
(119) Holme, T. A.; Truong, T. N. *Chem. Phys. Lett.* **1993**, *215*, 53.
(120) Sana, M.; Leroy, G.; Wilante, C. *Organometallics* **1992**, *11*, 781.
(121) Salahub, D. 8th International Congress of Quantum Chemistry, Prague 1994, Invited lecture.
(122) Pisani, C.; Dovesi, R. *Int. J. Quantum Chem.* **1980**, *17*, 501.
(123) Dovesi, R.; Pisani, C.; Roetti, C.; Saunders, V. R. *Phys. Rev. B: Condens. Matter* **1983**, *28*, 5781.
(124) Pisani, C.; Dovesi, R.; Roetti, C. *Hartree-Fock ab initio Treatment of Crystalline Systems*, Lecture Notes in Chemistry, Vol. 48; Springer-Verlag: Berlin, 1988.
(125) Dovesi, R.; Pisani, C.; Roetti, C.; Causà, M.; Saunders, V. R. *QCPE*, Program No. 577; Indiana University: Bloomington, IN, 1988.

(126) Dovesi, R.; Saunders, V. R.; Roetti, C. *CRYSTAL92, User Manual*; Gruppo di Chimica Teorica, Universitá di Torino and SERC Laboratory: Daresburgy, 1992.
(127) Vetrivel, R.; Catlow, C. R. A.; Colbourn, E. A. *J. Phys. Chem.* **1989**, *93*, 4594.
(128) Dupuis, M.; Farazdel, A.; Karna, S. P.; Maluendes, S. A. *MOTECC: Modern Techniques in Computational Chemistry*; Clementi, E., Ed.; Escom: Leiden, 1991.
(129) Guest, M. F.; Kendrick, J. *GAMESS User Manual*; Daresbury Laboratory: Warrington, U.K., 1985.
(130) Pisani, C. *Phys. Rev. B: Condens. Matter* **1978**, *17*, 3143.
(131) Pisani, C.; Dovesi, R.; Nada, R.; Kantorovich, L. N. *J. Chem. Phys.* **1990**, *92*, 7448.
(132) Pisani, C.; Dovesi, R.; Nada, R.; Tamiro, S. *Surf. Sci.* **1989**, *216*, 489.
(133) Pisani, C.; Orlando, R.; Nada, R. In *Cluster Models for Surface and Bulk Phenomena*, NATO ASI Series B, Vol. 283; Pacchioni, G., Bagus, P. S., Parmigiani, F., Eds.; Plenum Press: New York, 1992; p 515.
(134) Pisani, C.; Orlando, R.; Nada, R. In *Quantum Mechanical Cluster Calculations in Solid State Studies*; Grimes, R. W., Catlow, C. R. A., Shluger, A. L., Eds.; World Scientific Publishing Co. Pte. Ltd: Singapore, 1992; p 117.
(135) Pisani, C. *J. Mol. Catal.* **1993**, *82*, 229.
(136) Whitten, J. L.; Pakkanen, T. A. *Phys. Rev. B: Condens. Matter* **1980**, *21*, 4357.
(137) Whitten, J. L. *Phys. Rev. B: Condens. Matter* **1981**, *24*, 1810.
(138) Whitten, J. L. *Chem. Phys.* **1993**, *177*, 387.
(139) Harding, J. H.; Harker, A. H.; Keegstra, P. B.; Pandey, R.; Vail, J. M.; Woodward, C. *Physica* **1985**, *131B*, 151.
(140) Vail, J. M.; Pandey, R.; Kunz, A. B. *Rev. Solid State Sci.* **1991**, *5*, 181.
(141) Sauer, J. In *Cluster Models for Surface and Bulk Phenomena*, NATO ASI Series B, Vol. 283; Pacchioni, G., Bagus, P. S., Parmigiani, F., Eds.; Plenum Press: New York, 1992; p 533.
(142) Hermann, K. In *Cluster Models for Surface and Bulk Phenomena*, NATO ASI Series B, Vol. 283; Pacchioni, G., Bagus, P. S., Parmigiani, F., Eds.; Plenum Press: New York, 1992; p 209.
(143) Greatbanks, S. P.; Sherwood, P.; Hillier, I. H. *J. Phys. Chem.* **1994**, *98*, 8134.
(144) Teunissen, E. H.; Jansen, A. P. J.; van Santen, R. A.; Orlando, R.; Dovesi, R. *J. Chem. Phys.*, in press.
(145) BIOSYM Technologies, I. *Catalysis and Sorption Project Software, Embed Module*; BIOSYM Technologies, Inc.: San Diego, 1994.
(146) Allavena, M.; Seiti, K.; Kassab, E.; Ferenczy, G.; Angyan, J. G. *Chem. Phys. Lett.* **1990**, *168*, 461.
(147) D'Arco, P.; Causà, M.; Roetti, C.; Silvi, B. *Phys. Rev. B: Condens. Matter* **1993**, *47*, 3522.
(148) Causà, M.; Dovesi, R.; Roetti, C. *Phys. Rev. B: Condens. Matter* **1991**, *43*, 11937.
(149) Harrison, N. M.; Saunders, V. R.; Aprá, E.; Causà, M.; Dovesi, R. *Phys. Rev. B: Condens. Matter* **1992**, *4*, L261.
(150) McCarthy, M. I.; Hess, A. C. *J. Chem. Phys.* **1992**, *96*, 6010.
(151) Scamehorn, C. A.; Hess, A. C.; McCarthy, M. I. *J. Chem. Phys.* **1993**, *99*, 2786.
(152) Colle, R.; Salvetti, D. *Theoret. Chim. Acta* **1975**, *37*, 329.
(153) Perdew, J. P. *Phys. Rev. B: Condens. Matter* **1986**, *34*, 7406.
(154) Causà, M.; Zupan, A. *Chem. Phys. Lett.* **1994**, *220*, 145.
(155) Causà, M., to be published.
(156) Pisani, C.; Corà, F.; Orlando, R.; Nada, R. *Surf. Sci.* **1993**, *282*, 185.
(157) Colbourn, E. A. *Surf. Sci. Rep.* **1993**, *15*, 8.
(158) Garrone, E.; Zecchina, A.; Stone, F. S. *Phil. Mag.* **1980**, *42B*, 683.
(159) Levine, J. D.; Mark, P. *Phys. Rev.* **1966**, *144*, 751.
(160) Causà, M.; Ricca, F. *Surf. Sci.* **1993**, *298*, 251.
(161) Thiel, P. A.; Madey, T. E. *Surf. Sci. Rep.* **1987**, *7*, 211.
(162) Sauer, J. *Chem. Rev.* **1989**, *89*, 199.
(163) Gropen, O.; Almlof, J.; Wahlgren, U. In *Cluster Models for Surface and Bulk Phenomena*, NATO ASI Series B, Vol. 283; Pacchioni, G., Bagus, P. S., Parmigiani, F., Eds.; Plenum Press: New York, 1992; p 453.
(164) Rösch, N. In *Cluster Models for Surface and Bulk Phenomena*, NATO ASI Series B, Vol. 283; Pacchioni, G., Bagus, P. S., Parmigiani, F., Eds.; Plenum Press: New York, 1992; p 251.
(165) Whitten, J. L. In *Cluster Models for Surface and Bulk Phenomena*, NATO ASI Series B, Vol. 283; Pacchioni, G., Bagus, P. S., Parmigiani, F., Eds.; Plenum Press: New York, 1992; p 375.
(166) Hermann, K.; Bagus, P. S.; Nelin, C. J. *Phys. Rev. B: Condens. Matter* **1987**, *35*, 9467.
(167) Langreth, D. C.; Mehl, M. J. *Phys. Rev. B: Condens. Matter* **1983**, *28*, 1909.
(168) Hu, C. D.; Langreth, D. C. *Phys. Scr.* **1985**, *32*, 391.
(169) Siegbahn, P. E. M.; Nygren, M. A.; Wahlgren, U. In *Cluster Models for Surface and Bulk Phenomena*, NATO ASI Series B, Vol. 283; Pacchioni, G., Bagus, P. S., Parmigiani, F., Eds.; Plenum Press: New York, 1992; p 267.
(170) Schüle, J.; Siegbahn, P.; Wahlgren, U. *J. Chem. Phys.* **1988**, *89*, 6982.
(171) Cremaschi, P.; Whitten, J. L. *Phys. Rev. Lett.* **1981**, *46*, 1242.
(172) Cremaschi, P.; Whitten, J. L. *Surf. Sci.* **1985**, *149*, 273.
(173) Cremaschi, P.; Whitten, J. L. *Theoret. Chim. Acta* **1981**, *72*, 485.
(174) Madhaven, P. V.; Whitten, J. L. *J. Chem. Phys.* **1982**, *77*, 2673.
(175) Whitten, J. L.; Fischer, C. R. *Phys. Rev. B: Condens. Matter* **1984**, *30*, 6821.
(176) Yang, H.; Whitten, J. L. J. *Chem. Phys.* **1988**, *89*, 5329.
(177) Yang, H.; Whitten, J. L. J. *Chem. Phys.* **1993**, *98*, 5039.
(178) Yang, H.; Whitten, J. L. *Surf. Sci.* **1989**, *223*, 131.
(179) Chattopadhyay, A.; Yang, H.; Whitten, J. L. *J. Phys. Chem.* **1990**, *94*, 6379.
(180) Yang, H.; Whitten, J. L. *Surf. Sci.* **1991**, *255*, 193.
(181) Yang, H.; Whitten, J. L. *J. Am. Chem. Soc.* **1991**, *113*, 6442.
(182) Jing, Z.; Whitten, J. L. *Surf. Sci.* **1991**, *250*, 147.
(183) Yang, H.; Whitten, J. L. *J. Chem. Phys.* **1989**, *91*, 126.
(184) Yang, H.; Whitten, J. L. *J. Chem. Phys.* **1992**, *96*, 5529.
(185) Yang, H.; Whitten, J. L. *Surf. Sci.* **1993**, *289*, 30.
(186) Yang, H.; Whitten, J. L. R. R.; Thomas, R.; Markunas, R. *Surf. Sci.* **1992**, *277*, L95.
(187) Kassab, E.; Seiti, K.; Allavena, M. *J. Phys. Chem.* **1991**, *95*, 9425.
(188) Geerlings, P.; Tariel, N.; Botrel, A.; Lissillour, R.; Mortier, W. J. *J. Phys. Chem.* **1984**, *88*, 5752.
(189) Datka, J.; Geerlings, P.; Mortier, W.; Jacobs, P. *J. Phys. Chem.* **1985**, *89*, 3483.
(190) Datka, J. *J. Phys. Chem.* **1985**, *89*, 3488.
(191) Zhidomirov, G. M.; Kazansky, V. B. *Adv. Catal.* **1986**, *34*, 131.
(192) Illas, F.; Roset, L.; Ricart, J. M.; Rubio, J. *J. Comput. Chem.* **1993**, *14*, 1534.
(193) Gibbs, G. V.; Meagher, E. P.; Newton, M. D.; Swanson, D. K. In *Structure and Bonding in Crystals*; O'Keefe, M., Navrotsky, A., Eds.; Academic: New York, 1981; Vol. 1, p 195.
(194) Gibbs, G. V. *Am. Mineral.* **1982**, *67*, 421.
(195) Mezey, P. G. In *Catalytic Materials: Relationship Between Structure and Reactivity*, ACS Symposium Series 248; Whyte, T. E. J., Betta, A. D., Derouane, E. G., Baker, R. T. K., Eds.; American Chemical Society: Washington, DC, 1984; p 145.
(196) Bleiber, A.; Sauer, J. 1994, in preparation.
(197) Dyke, T. R.; Mack, K. M.; Muenter, J. S. *J. Chem. Phys.* **1977**, *66*, 498.
(198) Fredin, L.; Nelander, B.; Ribbegard, G. *J. Chem. Phys.* **1977**, *66*, 4065.
(199) Nelander, B. *J. Chem. Phys.* **1980**, *72*, 77.
(200) Nelander, B. *J. Chem. Phys.* **1988**, *88*, 5254.
(201) Page, R. H.; Frey, J. G.; Shen, Y.-R.; Lee, Y. T. *Chem. Phys. Lett.* **1984**, *106*, 373.
(202) Mortier, W. J.; Sauer, J.; Lercher, J. A.; Noller, H. *J. Phys. Chem.* **1984**, *88*, 905.
(203) Murray, C. W.; Laming, G. J.; Handy, N. C.; Amos, R. D. *Chem. Phys. Lett.* **1992**, *199*, 551.
(204) Sauer, J.; Ahlrichs, R. *J. Chem. Phys.* **1990**, *93*, 2575.
(205) Stave, M. S.; Nicholas, J. B. *J. Phys. Chem.* **1993**, *97*, 9630.
(206) Ugliengo, P.; Bleiber, A.; Garrone, E.; Sauer, J.; Ferrari, A. M. *Chem. Phys. Lett.* **1992**, *191*, 537.
(207) Phillips, J. C. *Rev. Mod. Phys.* **1970**, *42*, 317.
(208) Causà, M.; Dovesi, R.; Pisani, C.; Roetti, C. *Phys. Rev. B: Solid State Phys.* **1986**, *33*, 1308.
(209) Causà, M.; Dovesi, R.; Pisani, C.; Roetti, C. *Surf. Sci.* **1986**, *175*, 551.
(210) Tanabe, K.; Misono, M.; Ono, Y.; Hattori, H. *New Solid Acids and Bases*, Studies in Surface Science and Catalysis, Vol. 51; Elsevier: Amsterdam, 1989.
(211) Coluccia, S.; Segall, R. L.; Tench, A. J. *J. Chem. Soc., Faraday Trans. I* **1979**, *75*, 289.
(212) Zecchina, A.; Lofthouse, M. G.; Stone, F. S. *J. Chem. Soc., Faraday Trans. I* **1975**, *71*, 1476.
(213) Ito, T.; Tashiro, T.; Kawasaki, M.; Watanabe, T.; Toi, K.; Kobayashi, H. *J. Phys. Chem.* **1991**, *95*, 4476.
(214) Zecchina, A.; Stone, F. S. *J. Catal.* **1986**, *101*, 227.
(215) Guglielminotti, E.; Coluccia, S.; Garrone, E.; Cerruti, L.; Zecchina, A. *J. Chem. Soc., Faraday Trans. I* **1979**, *75*, 96.
(216) Prutton, M.; Walker, J. A.; Welton-Cook, M. R.; Felton, R. C. *Surf. Sci.* **1979**, *89*, 95.
(217) Marchese, L.; Coluccia, S.; Martra, G.; Zecchina, A. *Surf. Sci.* **1992**, *269*, 135.
(218) Zecchina, A.; Coluccia, S.; Spoto, G.; Scarano, D.; Marchese, L. *J. Chem. Soc., Faraday Trans.* **1990**, *84*, 703.
(219) Ramis, G.; Busca, G.; Lorenzelli, V. *Mater. Chem. Phys.* **1991**, *29*, 425.
(220) Coluccia, S.; Boccuzzi, F.; Ghiotti, G. C. M. *Z. Phys. Chem. Neue Folge* **1980**, *121*, 141.
(221) Colbourn, E. A.; Mackrodt, W. C. *Surf. Sci.* **1984**, *143*, 391.
(222) Pope, S. A.; Hillier, I. H.; Guest, M. F.; Colbourn, E. A.; Kendrick, J. *Surf. Sci.* **1984**, *139*, 299.
(223) Pacchioni, G.; Cogliandro, G.; Bagus, P. S. *Surf. Sci.* **1991**, *255*, 344.
(224) He, J. W.; Estrada, C. A.; Corneille, J. S.; Wu, M. C.; Goodman, D. W. *Surf. Sci.* **1992**, *261*, 164.
(225) Paukshtis, E. A.; Yurchenko, E. N. *Usp. Khim.* **1983**, *52*, 426.
(226) Paukshtis, E. A.; Yurchenko, E. N. *Russ. Chem. Rev.* **1983**, *52*, 242.

(227) Henry, R.; Chapon, C.; Duriez, C. *J. Chem. Phys.* **1991**, *95*, 700.
(228) Furuyama, S.; Fujii, H.; Kawamura, M.; Morimoto, T. *J. Phys. Chem.* **1978**, *82*, 1028.
(229) Pacchioni, G.; Neyman, K. M.; Rösch, N. *J. Electron Spectrosc. Related Phenom.* **1994**, in press.
(230) Rösch, N.; Neyman, K. M.; Birkenhener, U. In *Adsorption on Ordered Surfaces of Ionic Solids and Thin Films*, Springer Series in Surface Science, Vol. 33; Umbach, E., Freund, H.-J., Eds.; Springer Verlag: Berlin Heidelberg, 1993; p 206.
(231) Lakhlifi, A.; Girardet, C. *Surf. Sci.* **1991**, *241*, 400.
(232) Nygren, M. A.; Pettersson, L. G. M.; Barandiaran, Z.; Seijo, L. *J. Chem. Phys.* **1994**, *100*, 2010.
(233) Barandiaran, Z.; Seijo, L. *J. Chem. Phys.* **1988**, *89*, 5739.
(234) Pacchioni, G.; Minerva, T.; Bagus, P. S. *Surf. Sci.* **1992**, *275*, 450.
(235) Scarano, D.; Spoto, G.; Bordiga, S.; Coluccia, S.; Zecchina, A. *J. Chem. Soc., Faraday Trans.* **1992**, *88*, 291.
(236) Huzimura, R.; Yanagisawa, Y.; Matsumura, K.; Yamabe, S. *Phys. Rev. B: Condens. Matter* **1990**, *41*, 3786.
(237) Matsumura, K.; Yamabe, S.; Fujioka, H.; Yanagisawa, Y.; Huzimura, R. *Phys. Rev. B: Condens. Matter* **1987**, *36*, 6145.
(238) Sawabe, K.; Koga, N.; Morokuma, K.; Iwasawa, Y. *J. Chem. Phys.* **1992**, *97*, 6871.
(239) Ito, T.; Murakami, T.; Tokuda, T. *J. Chem. Soc., Faraday Trans. I* **1983**, *79*, 913.
(240) Pacchioni, G. *Surf. Sci.* **1993**, *281*, 207.
(241) Meixner, D. L.; Arthur, D. A.; George, S. M. *Surf. Sci.* **1992**, *261*, 141.
(242) Heidberg, J.; Meine, D. *Surf. Sci. Lett.* **1992**, *279*, L175.
(243) van Hove, M. A.; Wang, S. W.; Ogletree, D. F.; Somorjai, G. A. *Adv. Quant. Chem.* **1989**, *20*, 1.
(244) Pöhlchen, M.; Staemmler, V. *J. Chem. Phys.* **1992**, *97*, 2583.
(245) Escalona Platero, E.; Coluccia, S.; Zecchina, A. *Langmuir* **1985**, *1*, 407.
(246) Escalona Platero, E.; Coluccia, S.; Zecchina, A. *Surf. Sci.* **1986**, *171*, 465.
(247) Escalona Platero, E.; Scarano, D.; Spoto, G.; Zecchina, A. *Faraday Discuss. Chem. Soc.* **1985**, *80*, 183.
(248) Klier, K. *Collect. Czech. Chem. Commun.* **1963**, *28*, 2996.
(249) Snis, A.; Strömberg, D.; Panas, I. *Surf. Sci.* **1993**, *292*, 317.
(250) Escalona Platero, E.; Fubini, B.; Zecchina, A. *Surf. Sci.* **1987**, *179*, 404.
(251) Garrone, E.; Fubini, B.; Escalona Platero, E.; Zecchina, A. *Langmuir* **1989**, *5*, 240.
(252) Kuhlenbeck, H.; Odorfer, G.; Jaeger, R.; Illing, G.; Mull, T.; Freund, H. J.; Pohlchen, M.; Staemmler, V.; Witzel, S.; Scharfschwerdt, C.; Wenneman, K.; Liedtke, T.; Neumann, M. *Phys. Rev. B: Condens. Matter* **1991**, *43*, 1969.
(253) Pettersson, L. G. M. *Theoret. Chim. Acta* **1994**, *87*, 293.
(254) Staemmler, V. In *Adsorption on Ordered Surfaces of Ionic Solids and Thin Films*, Springer Series in Surface Sciences, Vol. 33; Umbach, E., Freund, H.-J., Eds.; Springer Verlag: Berlin Heidelberg, 1993; p 169.
(255) Escalona Platero, E.; Coluccia, S.; Zecchina, A. *Langmuir* **1985**, *1*, 407.
(256) Causá, M.; Dovesi, R.; Ricca, F. *Surf. Sci.* **1993**, *280*, 1.
(257) Causá, M.; Kotomin, E.; Pisani, C.; Roetti, C. *J. Phys. C: Solid State Phys.* **1987**, *20*, 4991.
(258) Dovesi, R.; Orlando, R.; Ricca, F.; Roetti, C. *Surf. Sci.* **1987**, *186*, 267.
(259) Dovesi, R.; Roetti, C.; Causà, M.; Pisani, C. In *Proceedings of a European Conference on Structure and Reactivity of Surfaces*, Trieste/Italy 1988, Studies in Surface Science and Catalysis, Vol. 48; Morterra, C., Zecchina, A., Costa, G., Eds.; Elsevier: Amsterdam, 1989; p 385.
(260) Orlando, R.; Pisani, C.; Ruiz, E.; Sautet, P. *Surf. Sci.* **1992**, *275*, 482.
(261) McCarthy, M. I.; Hess, A. C.; Harrison, N. M.; Saunders, V. R. *J. Chem. Phys.* **1993**, *98*, 6387.
(262) Orio, L.; Bolis, V.; Fubini, B.; Morterra, C. In *Proceedings of the 7th International Meeting on Modern Ceramics Technology, Materials Science Monographs*, Montecatini, Terme/Italy 1990; Elsevier: Amsterdam, 1991; p 1789.
(263) Langel, W.; Parrinello, M. *Phys. Rev. Lett.*, in press.
(264) Car, R.; Parrinello, M. *Phys. Rev. Lett.* **1985**, *55*, 2471.
(265) Colbourn, E. A.; Mackrodt, W. C. *Surf. Sci.* **1982**, *117*, 571.
(266) Pacchioni, G.; Cogliandro, G.; Bagus, P. S. *Int. J. Quantum Chem.* **1992**, *42*, 1115.
(267) Neyman, K. M.; Rösch, N. *Surf. Sci.* **1993**, *297*, 223.
(268) Neyman, K. M.; Rösch, N. *Ber. Bunsenges. Phys. Chem.* **1992**, *96*, 1711.
(269) Neyman, K. M.; Rösch, N. *Chem. Phys.* **1992**, *168*, 267.
(270) Escalona Platero, E.; Coluccia, S.; Zecchina, A. *Surf. Sci.* **1986**, *171*, 465.
(271) Morterra, C.; Bolis, V.; Magnacca, G. *Langmuir* **1994**, *10*, 1812.
(272) Spoto, G.; Bordiga, S.; Scarano, D.; Zecchina, A. *Catal. Lett.* **1992**, *13*, 39.
(273) Vetrivel, R.; Catlow, C. R. A. In *Modelling of Structure and Reactivity in Zeolites*; Catlow, R. C. A., Ed.; Academic Press: London, 1992; p 217.
(274) Dilmukhambetov, E. E.; Lyigin, V. I.; Chadiarov, E. G. *Zh. Fiz. Khim.* **1988**, *62*, 226.
(275) Beran, S. *J. Phys. Chem.* **1983**, *87*, 55.
(276) Beran, S. *Stud. Surf. Sci. Catal.* **1984**, *18*, 99.
(277) Sauer, J.; Deininger, D. *J. Phys. Chem.* **1982**, *86*, 1327.
(278) Sauer, J.; Deininger, D. *ZEOLITES* **1982**, *2*, 114.
(279) Sauer, J.; Fiedler, K.; Schirmer, W.; Zahradník, R. In *Proceedings of the 5th International Conference on Zeolites*, Naples/Italy 1980, Vol. 5; Rees, L. C. V., Ed.; Heyden: London, 1980; p 501.
(280) Egerton, T. A.; Stone, F. S. *J. Chem. Soc., Faraday Trans. I* **1973**, *69*, 22.
(281) Bordiga, S.; Escalona Platero, E.; Otero Arean, C.; Lamberti, C.; Zecchina, A. *J. Catal.* **1992**, *137*, 179.
(282) Bordiga, S.; Scarano, D.; Spoto, G.; Zecchina, A. *Vib. Spectrosc.* **1993**, *5*, 65.
(283) Yamazaki, T.; Watanuki, I.; Ozawa, S.; Ogino, Y. *Bull. Chem. Soc. Jpn.* **1988**, *61*, 1039.
(284) Koubi, L.; Blain, M.; Cohen de Lara, E.; Leclerq, J.-M. *Chem. Phys. Lett.* **1994**, *217*, 544.
(285) Bordiga, S.; Garrone, E.; Lamberti, C.; Zecchina, A.; Garrone, E.; Otero Arean, C.; Kazansky, V. B., manuscript in preparation.
(286) Yamazaki, T.; Watanuki, I.; Ozawa, S.; Ogino, Y. Langmuir **1988**, *4*, 433.
(287) Atkinson, D.; Curthoys, G. *J. Chem. Soc., Faraday Trans. I* **1981**, *77*, 897.
(288) Cohen de Lara, E.; Seloudoux, R. *J. Chem. Soc., Faraday Trans. I* **1983**, *79*, 2271.
(289) Spoto, G.; Zecchina, A.; Bordiga, S.; Ricchiardi, G.; Martra, G. *Appl. Catal. B* **1994**, *3*, 151.
(290) Merchan, M.; Nebot-Gil, I.; Gonzáles-Luque, R.; Orti, E. *J. Chem. Phys.* **1987**, *87*, 1690.
(291) Nicholas, J. B.; Winans, R. E.; Harrison, R. J.; Iton, L. E.; Curtiss, L. A.; Hopfinger, A. J. *J. Phys. Chem.* **1992**, *96*, 7958.
(292) Luke, B. T. *J. Phys. Chem.* **1993**, *97*, 7505.
(293) Bär, M. R.; Sauer, J. *Chem. Phys. Lett.* **1994**, *226*, 405.
(294) Bronnimann, C. E.; Zeigler, R. C.; Maciel, G. E. *J. Am. Chem. Soc.* **1988**, *110*, 2023.
(295) Morrow, B. A.; Gay, I. D. *J. Phys. Chem.* **1988**, *92*, 5569.
(296) Legrand, A. P.; Hommel, H.; Taïbi, H.; Miquel, J. L.; Tougne, P. *Colloid. Surf.* **1990**, *45*, 391.
(297) Leonardelli, S.; Facchini, L.; Fretigny, C.; Tougne, P.; Legrand, A. P. *J. Am. Chem. Soc.* **1992**, *114*, 6412.
(298) Zhuralev, L. T. *Langmuir* **1987**, *3*, 316.
(299) Iler, R. K. *The Chemistry of Silica*; Wiley-Interscience: New York, 1979; Chapter 6.
(300) Ryason, P. R.; Russell, B. G. *J. Phys. Chem.* **1975**, *79*, 1276.
(301) Ugliengo, P.; Ferrari, A. M.; Garrone, E., to be published.
(302) Sauer, J.; Bleiber, A. *Catal. Today* **1988**, *3*, 485.
(303) Damrauer, R.; Simon, R.; Krempp, M. *J. Am. Chem. Soc.* **1991**, *113*, 4432.
(304) Sauer, J. *J. Phys. Chem.* **1987**, *91*, 2315.
(305) Garrone, E.; Ugliengo, P. In Proceedings *of a European Conference on Structure and Reactivity of Surfaces*, Trieste/Italy 1988, Studies in Surface Science and Catalysis, Vol. 48; Morterra, C., Zecchina, A., Costa, G., Eds.; Elsevier: Amsterdam, 1989; p 405.
(306) Mix, H.; Sauer, J.; Schröder, K.; Merkel, A. *Coll. Czech. Chem. Commun.* **1988**, *53*, 2191.
(307) Shen, J. H.; Klier, K. *J. Colloid. Interf. Sci.* **1980**, *75*, 56.
(308) Sauer, J. In *Modelling of Structure and Reactivity in Zeolites*; Catlow, C. R. A., Ed.; Academic Press: London, 1992; p 183.
(309) Gordon, M. S.; Damrauer, R.; Krempp, M. *J. Phys. Chem.* **1993**, *97*, 7820.
(310) Sauer, J.; Hobza, P.; Zahradník, R. *J. Phys. Chem.* **1980**, *84*, 3318.
(311) Hess, C. A.; McMillan, P. F.; O'Keeffe, M. *J. Phys. Chem.* **1986**, *90*, 5661.
(312) Hess, A. C.; McMillan, P. F.; O'Keeffe, M. *J. Phys. Chem.* **1987**, *91*, 1395.
(313) De Almeida, W. B.; O'Malley, P. J. *Chem. Phys. Lett.* **1991**, *178*, 483.
(314) De Almeida, W. B.; O'Malley, P. J. *J. Mol. Struct.* **1991**, *246*, 179.
(315) Sosa, C.; Ferris, K. M.; Noga, J. *J. Mol. Struct.* **1992**, *265*, 163.
(316) Pelmenschikov, A. G.; Morosi, G.; Gamba, A. *J. Phys. Chem.* **1991**, *95*, 10037.
(317) Pelmenschikov, A. G.; Morosi, G.; Gamba, A. *J. Phys. Chem.* **1992**, *96*, 2241.
(318) Pelmenschikov, A. G.; Morosi, G.; Gamba, A. *J. Phys. Chem.* **1992**, *96*, 7422.
(319) Sauer, J.; Hill, J.-R. *Chem. Phys. Lett.* **1994**, *218*, 333.
(320) Sauer, J.; Schröder, K.-P. *Z. Phys. Chem. (Leipzig)* **1985**, *266*, 379.
(321) Ferrari, A. M.; Ugliengo, P.; Garrone, E. *J. Phys. Chem.* **1993**, *97*, 2671.
(322) Hoffman, P.; Knözinger, E. *Surf. Sci.* **1987**, *188*, 181.
(323) McFarlan, A. J.; Morrow, B. A. *J. Phys. Chem.* **1991**, *95*, 5388.
(324) Fubini, B.; Bolis, V.; Cavenago, A.; Garrone, E.; Ugliengo, P. *Langmuir* **1993**, *9*, 2712.
(325) Senchenya, I. N.; Mikheikin, I. D.; Zhidomirov, G. M.; Kazansky, V. B. *Kinet. Kataliz.* **1981**, *22*, 1174.

(326) Hertl, W.; Hair, M. L. *Nature* **1969**, *223*, 1950.
(327) Fubini, B.; Bolis, V.; Cavenago, A.; Ugliengo, P. *J. Chem. Soc., Faraday Trans.* **1992**, *88*, 277.
(328) Ugliengo, P.; Saunders, V. R.; Garrone, E. *Surf. Sci.* **1989**, *224*, 498.
(329) Sauer, J.; Morgeneyer, C.; Schröder, K. P. *J. Phys. Chem.* **1984**, *88*, 6375.
(330) Flanigen, E. M.; Bennett, J. M.; Grose, R. W.; Cohen, J. P.; Patton, R. L.; Kirchner, R. M.; Smith, J. V. *Nature* **1978**, *271*, 512.
(331) Bolis, V.; Fubini, B.; Marchese, L.; Martra, G.; Costa, D. *J. Chem. Soc., Faraday Trans.* **1991**, *87*, 497.
(332) Fubini, B.; Bolis, V.; Bailes, M.; Stone, F. S. *Solid State Ionics* **1989**, *32/33*, 258.
(333) Bolis, V.; Marchese, L.; Coluccia, S.; Fubini, B. *Adsorpt. Sci. Technol.* **1988**, *5*, 239.
(334) Chakoumakos, B. C.; Gibbs, G. V. *J. Phys. Chem.* **1986**, *90*, 996.
(335) Klier, K. *J. Chem. Phys.* **1973**, *58*, 737.
(336) Klier, K.; Shen, J. H.; Zettlemoyer, A. C. *J. Phys. Chem.* **1973**, *77*, 1458.
(337) Anderson, J. H.; Wickersheim, K. A. *Surf. Sci.* **1964**, *2*, 252.
(338) Ferrari, A. M., Torino, 1990.
(339) Ugliengo, P.; Saunders, V. R.; Garrone, E. *J. Phys. Chem.* **1990**, *94*, 2260.
(340) Borello, E.; Zecchina, A.; Morterra, C. *J. Phys. Chem.* **1967**, *71*, 2938.
(341) Ugliengo, P.; Saunders, V. R.; Garrone, E. *Chem. Phys. Lett.* **1990**, *169*, 501.
(342) Busca, G.; Lamotte, J.; Lavalley, J. C.; Lorenzelli, V. *J. Am. Chem. Soc.* **1987**, *109*, 5197.
(343) Legon, A. C.; Millen, D. J. *J. Chem. Rev.* **1986**, *86*, 635.
(344) Legon, A. C.; Millen, D. J. *Acc. Chem. Res.* **1987**, *20*, 39.
(345) Ugliengo, P.; Saunders, V. R.; Garrone, E. *J. Phys. Chem.* **1989**, *93*, 5210.
(346) Bates, S.; Dwyer, J. *J. Phys. Chem.* **1993**, *97*, 5897.
(347) Beebe, T. P.; Gelin, P.; Yates, J. T. *Surf. Sci.* **1984**, *148*, 526.
(348) Ghiotti, G.; Garrone, E.; Morterra, C.; Zecchina, A. *J. Phys. Chem.* **1979**, *83*, 2863.
(349) Senchenya, I. N.; Ugliengo, P.; Garrone, E., to be published.
(350) Luque, F. J.; Orozco, M.; Illas, F.; Rubio, J. *J. Am. Chem. Soc.* **1991**, *113*, 5203.
(351) Garrone, E.; Ugliengo, P.; Ghiotti, G.; Borello, E.; Saunders, V. R. *Spectrochim. Acta* **1993**, *49A*, 1221.
(352) Kazansky, V. B. In *Structure and Reactivity of Modified Zeolites*, Studies in Surface Science and Catalysis, Vol. 18; Jacobs, P. A., Jaeger, N. I., Jiru, P., Kazansky, V. B., Schulz-Ekloff, G., Eds.; Elsevier: Amsterdam, 1984; p 61.
(353) Welsh, H. L.; Kriegler, R. T. *J. Chem. Phys.* **1969**, *50*, 1043.
(354) Cocito, G.; Cognolato, L.; Modone, E.; Sordo, B. *J. Opt. Commun.* **1988**, *9*, 1.
(355) Garrone, E.; Kazansky, V. B.; Kustov, L. M.; Sauer, J.; Senchenya, I. N.; Ugliengo, P. *J. Phys. Chem.* **1992**, *96*, 1040.
(356) De Almeida, W. B.; O'Malley, P. J. *J. Chem. Soc., Chem. Comm.* **1991**, *7*, 455.
(357) De Almeida, W. B.; O'Malley, P. J. *J. Chem. Soc., Faraday Trans.* **1993**, *2*, 983.
(358) Bordiga, S.; Ferrari, A. M.; Garrone, E.; Ugliengo, P.; Zecchina, A. In *Book of Abstracts*, EUROCAT-I, Montpellier, Vol. 2, 1993; p 962.
(359) Breneman, C. M.; Wiberg, K. B. *J. Comput. Chem.* **1990**, *11*, 361.
(360) Ugliengo, P., unpublished.
(361) Garrone, E.; Ugliengo, P. *Mater. Chem. Phys.* **1991**, *29*, 287.
(362) Garrone, E.; Ugliengo, P.; Ferrari, A. M. In *Trends in Physical Chemistry*; Council of Scientific Research Integration, Eds.; Trivandrum: India, 1992; Vol. 3, p 327.
(363) Kagiya, T.; Sumida, Y.; Watanabe, T.; Tachi, T. *Bull. Chem. Soc. Jpn.* **1971**, *44*, 923.
(364) Lias, S. G.; Bartmess, J. E.; Liebman, J. F.; Holmes, J. L.; Levin, R. D.; Mallard, W. G. *J. Phys. Chem. Ref. Data* **1988**, *17*, Supplement 1.
(365) Spitz, R. N.; Barton, J. E.; Barteau, M. A.; Staley, R. H.; Sleight, A. W. *J. Phys. Chem.* **1986**, *90*, 4067.
(366) Garrone, E.; Stone, F. S. In *Proceedings of 8th International Congress on Catalysis*, Berlin 1984, Vol. 3; DCHEMA Verlag Chemie: Weinheim, 1985; p 441.
(367) Ugliengo, P.; Ferrari, A. M.; Garrone, E., manuscript in preparation.
(368) Bassett, D. R.; Boucher, E. A.; Zettlemoyer, A. C. *J. Colloid Interface Sci.* **1970**, *34*, 3.
(369) Zecchina, A.; Bordiga, S.; Spoto, G.; Scarano, D.; Petrini, G.; Leofanti, G.; Padovan, M.; Arean, C. O. *J. Chem. Soc., Faraday Trans.* **1992**, *88*, 2959.
(370) Garrone, E.; Chiappetta, R.; Spoto, G.; Ugliengo, P.; Zecchina, A.; Fajula, F. In *Proceedings of the 9th International Zeolite Conference*, Montreal 1992; von Ballmoos, R., Higgins, J. B., Treacy, M. M. J., Eds.; Butterworth-Heinemann: Stoneham/USA, 1993; p 267.
(371) Pfeifer, H.; Freude, D.; Kärger, J. In *Studies in Surface Science and Catalysis*, Catalysis and Adsorption by Zeolites, Vol. 65; Öhlmann, G., Pfeifer, H., Fricke, R., Eds.; Elsevier: Amsterdam, 1991; p 89.
(372) Engelhardt, G.; Jerschkewitz, H.-G.; Lohse, U.; Sarv, P.; Samoson, A.; Lippmaa, E. *ZEOLITES* **1987**, *7*, 289.
(373) Fleischer, U.; Kutzelnigg, W.; Bleiber, A.; Sauer, J. *J. Am. Chem. Soc.* **1993**, 7833.
(374) Kustov, L. M.; Kazansky, V. B.; Beran, S.; Kubelkova, L.; Jiru, P. *J. Phys. Chem.* **1987**, *91*, 5247.
(375) Wakabayashi, F.; Kondo, J.; Wada, A.; Domen, K.; Hirose, C. *Catal. Lett.* **1993**, *21*, 257.
(376) Wakabayashi, F.; Kondo, J.; Wada, A.; Domen, K.; Hirose, C. *J. Phys. Chem.* **1993**, *97*, 10761.
(377) Makarova, M. A.; Ojo, A. F.; Karim, K.; Hunger, M.; Dwyer, J. *J. Phys. Chem.* **1994**, *98*, 3619.
(378) Sauer, J.; Kölmel, C. M.; Hill, J.-R.; Ahlrichs, R. *Chem. Phys. Lett.* **1989**, *164*, 193.
(379) Hill, J.-R.; Sauer, J., 1993, unpublished results.
(380) Schröder, K.-P.; Sauer, J. *J. Phys. Chem.* **1993**, *97*, 6579.
(381) Haase, F.; Sauer, J., 1994, to be published.
(382) Hill, J.-R.; Sauer, J., submitted.
(383) Sauer, J. *J. Mol. Catal.* **1989**, *54*, 312.
(384) Jacobs, P. A.; Mortier, W. J. *ZEOLITES* **1982**, *2*, 226.
(385) Mastikhin, V. M.; Mudrakovsky, I. L.; Nosov, A. V. *Bruker Rep.* **1989**, *2*, 18.
(386) Datka, J.; Boczar, M.; Rymarowicz, P. *J. Catal.* **1988**, *114*, 368.
(387) Datka, J.; Boczar, M.; Gil, B. *Langmuir* **1993**, *9*, 2496.
(388) Kawakami, H.; Yoshida, S.; Yonezawa, T. *J. Chem. Soc., Faraday Trans. II* **1984**, *80*, 205.
(389) Stuckenschmidt, E.; Kassner, D.; Joswig, W.; Baur, W. H. *Eur. J. Mineral.* **1992**, *4*, 1229.
(390) Teunissen, E. H.; van Duijneveldt, F. B.; van Santen, R. A. *J. Phys. Chem.* **1992**, *96*, 366.
(391) Kassab, E.; Fouquet, J.; Allavena, M.; Evleth, E. M. *J. Phys. Chem.* **1993**, *97*, 9034.
(392) Teunissen, E. H.; van Santen, R. A.; Jansen, A. P. J.; van Duijneveldt, F. B. *J. Phys. Chem.* **1993**, *97*, 203.
(393) Paukshtis, E. A.; Pankratev, Y. D.; Pelmenshikov, A. G.; Burgina, E. B.; Turkov, V. M.; Yurchenko, E. N.; Zhidomirov, G. M. *Kinet. Katal.* **1986**, *27*, 1440.
(394) Teunissen, E. H.; Roetti, C.; Pisani, C.; de Man, A. J. M.; Jansen, A. P. J.; Orlando, R.; van Santen, R. A.; Dovesi, R. *Modell. Simul. Mater. Sci. Eng.* **1994**, in press.
(395) Jentys, A.; Warecka, G.; Derewinski, M.; Lercher, J. A. *J. Phys. Chem.* **1989**, *93*, 4837.
(396) Marchese, L.; Chen, J.; Wright, P. A.; Thomas, J. M. *J. Phys. Chem.* **1993**, *97*, 8109.
(397) Gale, J. D.; Catlow, C. R. A.; Carruthers, J. R. *Chem. Phys. Lett.* **1993**, *216*, 155.
(398) Krossner, M.; Haase, F.; Sauer, J. Book of Abstracts, Satellite Meeting "Quantum Chemical Aspects of Heterogeneous Catalysis", Berlin, June 26–28, 1994.
(399) Vetrivel, R.; Catlow, C. R. A.; Colbourn, E. A. In *Innovation in Zeolite Materials Science*, Studies in Surface Science and Catalysis, Vol. 37; Grobet, P. J., Ed.; Elsevier: Amsterdam, 1988; p 501.
(400) Kubelkova, L.; Novakova, J.; Nedomova, K. *J. Catal.* **1990**, *124*, 441.
(401) Mirth, G.; Lercher, J. A.; Anderson, M. W.; Klinowski, J. *J. Chem. Soc., Faraday Trans.* **1990**, *86*, 3039.
(402) Haase, F.; Sauer, J., in preparation.
(403) Thamm, H. *J. Chem. Soc., Faraday Trans. I* **1989**, *85*, 1.
(404) Gorte, R. J., 1993, personal communication.
(405) Parrillo, D. J.; Gorte, R. J. *J. Phys. Chem.* **1993**, *97*, 8786.
(406) Kramer, G. J.; Santen, R. A. v.; Emeis, C. A.; Nowak, A. K. *Nature* **1993**, *363*, 529.
(407) Sauer, J. *Nature (London)* **1993**, *363*, 493.
(408) Senchenya, I. N.; Kazansky, V. B. *Catal. Lett.* **1991**, *8*, 317.
(409) Malkin, V. G.; Fleischer, U.; Sauer, J.; Kutzelnigg, W., in preparation.
(410) Haw, J. F.; Richardson, B. R.; Oshiro, I. S.; Lazo, N. D.; Speed, J. A. *J. Am. Chem. Soc.* **1989**, *111*, 2052.
(411) Kutzelnigg, W.; Fleischer, U.; Schindler, M. *NMR Basic Princ. Prog.* **1990**, *23*, 165.
(412) Senchenya, I.; Ugliengo, P.; Garrone, E., unpublished results.
(413) Sim, F.; Catlow, C. R. A.; Dupuis, M.; Watts, J. D. *J. Chem. Phys.* **1991**, 4215.
(414) Nicholas, J. B.; Winans, R. E.; Harrison, R. J.; Iton, L. E.; Curtiss, L. A.; Hopfinger, A. J. *J. Phys. Chem.* **1992**, *96*, 10247.
(415) Andrews, J.; Handy, N., 1989, personal communication.
(416) Sauer, J.; Haase, F., 1993, unpublished.
(417) Vega, A. J.; Luz, Z. *J. Phys. Chem.* **1987**, *91*, 365.
(418) Pfeifer, H.; Freude, D.; Hunger, M. *ZEOLITES* **1985**, *5*, 274.
(419) Jacobs, W. P. J. H. Thesis. *Spectroscopic Studies of the Proton-Ammonia Interaction in Zeolite Y*, University of Technology Eindhoven, 1993.
(420) Jacobs, W. P. J. H.; Haan, J. W.; van de Ven, L. J. M.; van Santen, R. A. *J. Phys. Chem.* **1993**, *97*, 10394.

(421) Sauer, J.; Kölmel, C.; Haase, F.; Ahlrichs, R. In *Proceedings of the 9th International Zeolite Conference*, Montreal 1992; von Ballmoos, R., Higgins, J. B., Treacy, M. M. J., Eds.; Butterworth-Heinemann: Stoneham/USA, 1993; p 679.
(422) Sauer, J., 1993, unpublished results.
(423) Zelenkovskii, V. M.; Zhidomirov, G. M.; Kazansky, V. B. *React. Kinet. Catal. Lett.* **1984**, *24*, 15.
(424) Sauer, J.; Schirmer, W. In *Innovation in Zeolite Materials Science*, Studies in Surface Science and Catalysis, Vol. 37; Grobet, P. J., Mortier, W. J., Vansant, E. F., Schulz-Ekloff, G., Eds.; Elsevier: Amsterdam, 1988; p 323.
(425) Sauer, J. *Acta Chim. Phys. (Szeged)* **1985**, *31*, 19.
(426) Limtrakul, J.; Hannongbua, S. *J. Mol. Struct. (Theochem)* **1993**, *280*, 139.
(427) O'Malley, P. J.; Dwyer, J. *Chem. Phys. Lett.* **1988**, *143*, 97.
(428) O'Malley, P. J.; Dwyer, J. *J. Chem. Soc., Chem. Commun.* **1987**, 72.
(429) Kogelbauer, A.; Lercher, J. A.; Steinberg, K.-H.; Rössner, F.; Schöllner, A.; Dmitriev, R. V. *ZEOLITES* **1989**, *9*, 224.
(430) Jacobs, W. P. J. H.; van Wolput, J. H. M. C.; van Santen, R. A. *ZEOLITES* **1993**, *13*, 170.
(431) Udovic, T. J.; Cavanagh, R. R.; Rush, J. J.; Wax, M. J.; Stucky, G. D.; Jones, G. A.; Corbin, D. R. *J. Phys. Chem.* **1987**, *91*, 5968.
(432) Brand, H. V.; Curtiss, L. A.; Iton, L. E. *J. Phys. Chem.* **1992**, *96*, 7725.
(433) Sauer, J.; Kölmel, C.; Teunissen, E.; Roetti, C.; Ugliengo, P. Periodic versus Cluster Ab initio Treatment of Condensed Systems; CECAM Workshop, Orsay, Paris, 1991.
(434) Jobic, H.; Czjzek, M.; Santen, R. A. v. *J. Phys. Chem.* **1992**, *96*, 1540.
(435) Parker, L. M.; Bibby, D. M.; Burns, G. R. *ZEOLITES* **1993**, *13*, 107.
(436) Serrallach, A.; Meyer, R.; Günthard, H. H. *J. Mol. Spectrosc.* **1974**, *52*, 94.
(437) Ison, A.; Gorte, R. J. *J. Catal.* **1984**, *89*, 150.
(438) Messow, U.; Quitzsch, K.; Herden, H. *ZEOLITES* **1984**, *4*, 255.
(439) Lercher, J. A., 1991, personal communication.
(440) Auroux, A.; Vedrine, J. C. *Stud. Surf. Sci. Catal.* **1985**, *20*, 311.
(441) Sauer, J. In *Recent Advances in Zeolite Science*, Studies in Surface Science and Catalysis, Vol. 52; Klinowski, J., Barrie, P. J., Eds.; Elsevier: Amsterdam, 1989; p 73.
(442) Krossner, M.; Sauer, J., 1994, unpublished results.
(443) Haase, F.; Sauer, J., 1994, unpublished results.
(444) Hill, J.-R.; Sauer, J. *J. Phys. Chem.* **1994**, *98*, 1238.
(445) Jameson, C. J.; Jameson, A. K.; Baello, B. I.; Lim, H.-M. *J. Chem. Phys.* **1994**, *100*, 5965.
(446) Jameson, C. J.; Jameson, A. K.; Lim, H.-M.; Baello, B. I. *J. Chem. Phys.* **1994**, *100*, 5977.
(447) Vigné-Maeder, F. *J. Phys. Chem.* **1994**, *98*, 4666.
(448) Pacchioni, G.; Clotet, A.; Ricart, J. M. *Surf. Sci.* **1994**, *315*, 337.
(449) Nicholas, J. B.; Hess, A. C. *J. Am. Chem. Soc.* **1994**, *116*, 5428.
(450) Haw, J. F.; Hall, M. B.; Alvarado-Swaisgood, A. E.; Munson, E. J.; Lin, Z.; Beck, L. W.; Howard, T. *J. Am. Chem. Soc.* **1994**, *116*, 7308.